Spring 2013

Effect of dense heat exchanging internals on the hydrodynamics of bubble column reactors using non-invasive measurement techniques

Mohammed Khloofh Al Mesfer

Department: Chemical and Biochemical Engineering

EFFECT OF DENSE HEAT EXCHANGING INTERNALS ON THE HYDRODYNAMICS OF BUBBLE COLUMN REACTORS USING NON-INVASIVE MEASUREMENT TECHNIQUES

by

MOHAMMED KHLOOFH AL MESFER

A DISSERTATION

Presented to the Faculty of the Graduate School of the

MISSOURI UNIVERSITY OF SCIENCE AND TECHNOLOGY

In Partial Fulfillment of the Requirements for the Degree

DOCTOR OF PHILOSOPHY

in

CHEMICAL ENGINEERING

2013

Approved by

Muthanna Al-Dahhan, Advisor
Parthasakha Neogi
Jee-Ching Wang
Serhat Hosder
Hyoung Lee

ABSTRACT

Given their efficiency and capital cost reduction, bubble/slurry bubble column reactors are the reactors of choice for Fischer-Tropsch (FT) synthesis, offering clean alternative fuels and chemicals. FT synthesis is an exothermic process that requires many heat exchanging tubes in order to remove heat efficiently and maintain the desired temperature and isothermal operating condition. The impact of the heat exchanging tubes (internals) on the hydrodynamics is not fully understood. Reliably designing and scaling up bubble column reactors requires proper understanding of hydrodynamics, as well as heat and mass transfer parameters.

The main objective of this work is to advance the understanding of the effect of internals (25% covered cross-sectional area to meet FT needs) on hydrodynamics (gas holdup distribution, 3D liquid velocity, Reynolds stresses, turbulent kinetic energy, eddy diffusivity, etc.) in bubble columns. Single-source γ-ray Computed Tomography (CT) and Radioactive Particle Tracking (RPT) were used for the first time to study the effect of dense internals and gas velocity on the phase holdup distribution and radial profiles, liquid velocity field and turbulent parameter profiles.

The main findings obtained for the first time in this study can be summarized as follows:

- The presence of internals at a given superficial gas velocity causes:
    - An increase in gas holdup and the axial centerline liquid velocity
    - A sharp decrease in turbulence parmeters
- The increase in superficial gas velocity in the presence of internals causes:
    - An increase in gas holdup, axial centerline liquid velocity and turbulent parameters.

ACKNOWLEDGMENTS

First of all, praise belongs to God (ALLAH) for his kindness and so many blessings in my life.

I express gratitude from the depth of my heart to my advisor, Professor Muthanna H. Al-Dahhan, for his supervision, advice, knowledge and support which have made this work possible. I would also like to acknowledge the members of my committee, namely, Prof. Parthasakha Neogi, Dr. Jee-Ching Wang (Department of Chemical and Biochemical Engineering), Dr. Serhat Hosder (Department of Mechanical and Aerospace Engineering) and Dr. Hyoung Lee (Department of Nuclear Engineering) for taking interest in my work and examining my dissertation.

I thank Mr. Deen for his efforts in helping me to solve the technical and mechanical problems in the experiments. I would like to thank the secretaries of the Department of Chemical and Biochemical Engineering for their constant help with paperwork. I also thank my friends and colleagues at Missouri S&T for their continued and untiring support during tough times.

I express a deep sense of appreciation to my parents, brothers and sisters for their unconditional support. Words are far from adequate to thank them, and what I can do is to keep this deep feeling in my heart forever. During the most challenging and painful years of my life, my wife, daughter and son shared both the happiness and sadness along with me, as we faced the ups and downs of our lives together. Without their encouragement and confidence, I would have failed many times due to hesitance and doubt.

TABLE OF CONTENTS

LIST OF ILLUSTRATIONS

LIST OF TABLES

NOMENCLATURE

A	specific interfacial area, cm^2/cm^3
A	radiation absorbance
c	gas holdup power-law profile constant
C	number of the counts
C_{xx}	correlation function
d	distance
$d_{P,}$	particle diameter, cm
D, D_R	column (reactor) diameter, cm
D_p	probe diameter
D_{rr}	radial turbulent diffusivity, cm^2/s
D_{zz}	axial turbulent diffusivity, cm^2/s
$D_{\theta\theta}$	azimuthal turbulent diffusivity, cm^2/s
f	frequency, Hz = 1/s
g	gravity: 980 cm/s^2
H_{dyn}	column dynamic height, cm
H_{st}	column static (gas free) height, cm
k_l	liquid thermal conductivity
I	intensity of the radiation
k	turbulent kinetic energy (TKE), cm^2/s^2
l	length, cm
m	gas holdup power-law profile exponent
N_S	number of tracer particle occurrences
N_r	number of radial positions for column discretization
N_θ	number of azimuthal positions for column discretization
N_z	number of axial positions for column discretization
P	pressure, Pa
Pe_K	Peclet number of phase K: $U_{G0}H_D/E_K$
r	radial coordinate, cm
R	column radius, cm

Re_G	Reynolds number of gas phase: $DU_G(\rho_L - \rho_G)/\mu_L$
st	wavelet filtration threshold value
t	time, s
U	superficial velocity, cm/s
u	local phase velocity, cm/s
$\overline{u_i' u_j'}$	transport of momentum due to turbulent velocity fluctuations along with direction due to instantaneous flow in the jth direction, cm^2/s
u_0	centerline liquid velocity, cm/s
$\bar{u}$	readily averaged velocity, cm/s
ut	terminal setting velocity, cm/s
u_{tran}	transition velocity
x	x coordinate, cm
X	CT spatial resolution, cm
X_v	fractions covered by internals
Y	y coordinate, cm
Y	tracer particle displacement, cm
z	z (axial) coordinate, cm

Greek Letters

ε	phase holdup
$\bar{\varepsilon}$	cross-sectional averaged phase holdup
ϕ	dimensionless radial direction, r/R
μ	viscosity, $g/(ms^2)$
υ	kinematic viscosity, cm^2/s
θ	azimuthal coordinate, degrees or radians
ρ	density, g/cm^3
$(\rho\mu)_K$	γ-ray attenuation coefficient of the K phase, cm^{-1}
σ	surface tension, g/cms
τ_{pq}	stress in the pq direction (p, q = r, θ, z), cm^2/s^2

Subscripts

0	nominal, initial, column center-line
atm	atmospheric pressure (P = 0.1 MPa)
D	detector
eff	effective
G	gas phase
K	phase denominator (G, L, S or combination)
L	liquid phase
r	in radial direction
t	turbulent
W	wall

List of Abbreviations

2D	Two Dimensional
3D	Three Dimensional
AM	Alternating Minimization Algorithm
BTL	Biomass to Liquid
CARPT	Computed Automated Radioactive Particle Tracking
CFD	Computational Fluid Dynamics
CSA	Cross-Sectional Area
CT	Computed Tomography
CTL	Coal to Liquid
DGD	Dynamic Gas Disengagement
EIA	Energy Information Administration
FT	Fischer-Tropsch
GTL	Gas to Liquid
IEO	International Energy Outlook

LED	Light-Emitting Diode
RCFDM	Recirculation and Cross Flow with Dispersion Model
RPT	Radioactive Particle Tracking

1. INTRODUCTION

Recently, concern has been rising regarding the depletion of oil reserves, climate changes and the polluting effects of fossil fuels. Worldwide oil demand continues to increase rapidly due to a growing population and increased oil consumption among developing countries. These trends have caused the failure of countries that supply oil to produce sufficient quantities to fulfill the worldwide demand, thus creating a gap between production and consumption that will continue to grow, as depicted in Figure 1.1, and further inflating prices.

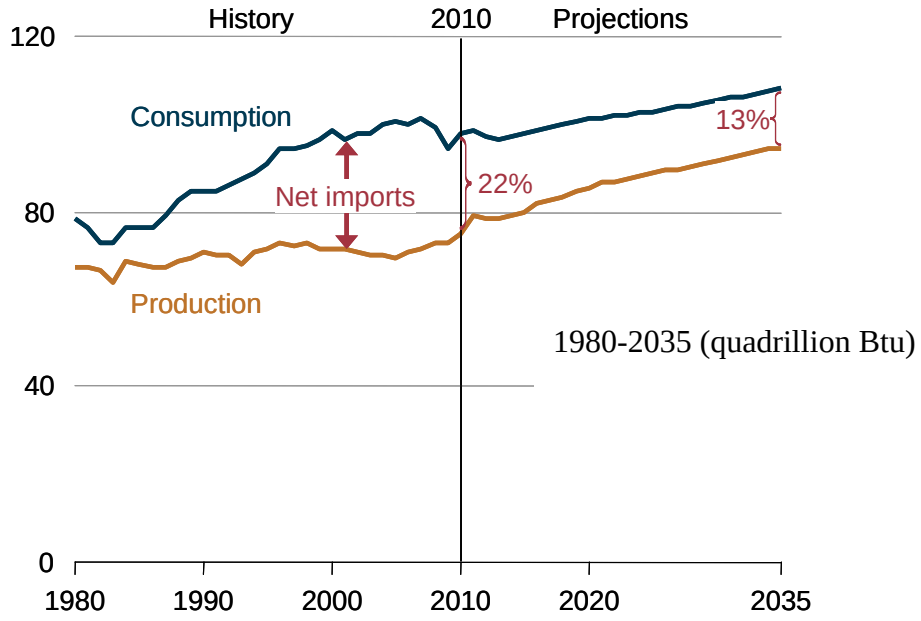

Source: U.S. Energy Information Administration (EIA), Annual Energy Outlook 2012

Figure 1.1. Total Energy Production and Consumption, 1980-2035

In addition, the effects of climate change have become more disastrous due to an increase in the concentration of carbon dioxide (CO_2) in the atmosphere. Charles T. Maxwell, the senior energy strategist of C.J Lawrence Inc., summarized these issues, stating, "Our country's leaders have three main choices: Taking over someone else's oil fields until they are depleted; carrying on until the lights go out and Americans are freezing in the dark; or changing our life style by energy conservation while heavily investing in alternative energy sources at higher cost" (Barron's, 2004). Therefore, using a mix of alternative energy sources, such as solar, wind, biomass, gas, coal, nuclear, etc., appears to be the most promising solution to fill the gap between production and consumption. While such alternatives require significant expense to set up and maintain, they unquestionably provide long-term benefits in terms of environmental health and low cost over time. Gas–to-liquid (GTL) technology has appeared as an alternative to the traditional refining of crude oil and provides an avenue for investments in natural and clean resources. GTL is a multistep process for converting natural gas through its conversion to synthesis gas (a mixture of carbon monoxide and hydrogen) into higher molecular weight hydrocarbons using the Fisher-Tropsch (FT) process, as follows:

$$n\,CO + (2n+1)H_2 \rightarrow C_2H_{2n+1} + n\,H_2O$$

Natural gas is considered one of earth's cleanest and most abundant natural resources. It also is produced as biogas via the anaerobic digestion of animal fat and municipal wastes. Furthermore, synthesis gas (Co and H_2) can be produced from biomass and from coal; these processes for producing hydrocarbons are called Biomass to Liquid (BTL) and Coal to Liquid (CTL), respectively.

During World War II, two German researchers, Franz Fischer and Hans Tropsch, motivated by their country's lack of petroleum resources but abundance of coal, invented a method by which to produce liquid fuels from coal by converting coal to syngas (Co and H_2). Called Fisher-Tropsch (FT) synthesis, it attracted the attention of many countries at that time, though more for strategic than economic reasons. Today's high price of crude oil and increasing energy demand have caused focus to shift once again to FT synthesis, which now is regarded as an environmentally friendly commercial technology.

There are typically two main FT technologies: High-temperature FT (300-350 °C) (gas-solid system), such as a fluidized bed or a circulating fluidized bed, and low-temperature FT (180-240 °C) (gas-liquid-solid system), such as a slurry bubble column with a suspended catalyst or trickled bed. Based on reaction engineering considerations and economics, the slurry bubble column reactor is considered one of the most promising reactors for long chain hydrocarbon production, which efficiently removes heat from exothermic FT synthesis.

In general, in its simplest form, that of a bubble column, this reactor is a cylindrical vessel into which gas enters through a distributor (sparger) into a liquid phase or liquid-solid particle suspension. The gas phase contains one or more reactants; the liquid phase usually contains products and/or reactants, while solids are typically catalyst particles, as shown in Figure 1.2.

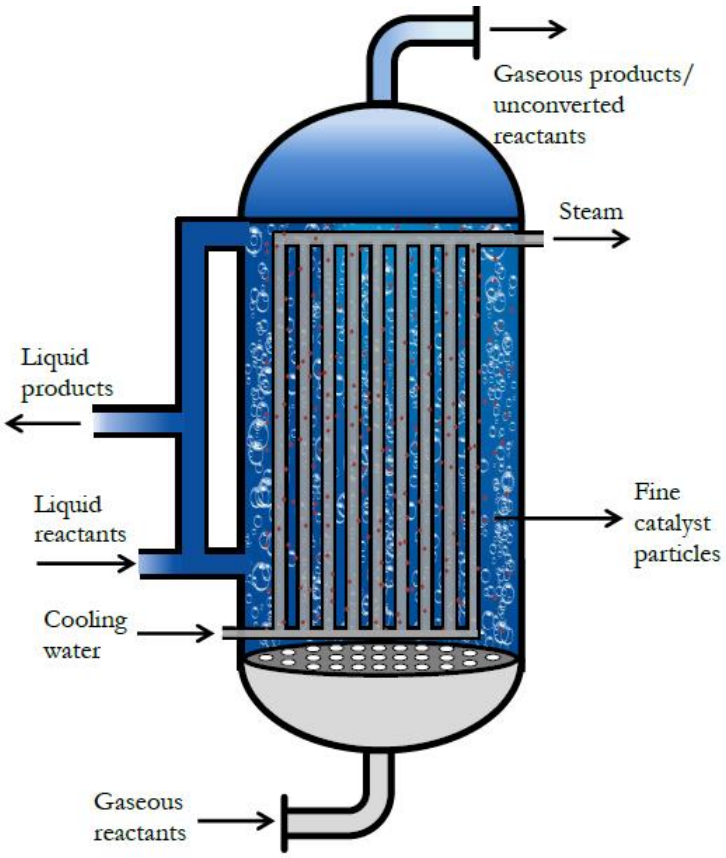

Figure 1.2. Sketch of Slurry/Bubble Column Reactor

The liquid phase usually consists of product and/or reactant, while the gas phase typically consists of reactant, and the solid particles are catalysts ranging in size from 5 to 150 μm (Krishna et al., 1997). The liquid/slurry phase flow can occur in batch form or can occur either with (co-current) or against (counter-current) the flow of the gas phase. Commonly, bubble/slurry bubble columns operate with aspect ratios of L/d_R greater than three and with a superficial gas velocity magnitude greater than the superficial liquid velocity. Bubble/slurry bubble column reactors are heated or cooled using coils or other

internal heat exchanges to promote heat transfer. As a result, the presence of internals and their configurations significantly affect the hydrodynamic behavior of the reactor.

Bubble columns as multiphase reactors are employed in a wide range of applications in both the chemical and biochemical industries. Methanol synthesis, FT, oxidation reaction, polymerization of olefin, hydrogenation reactions, alkylation reactions, cell cultures, and biological wastewater treatment are examples of reactions occurring in slurry and bubble column reactors. Their advantages over other contacting devices, including their low cost of construction and operation, lack of moving parts, easy temperature control, and good heat and mass transfer, make bubble column reactors suitable for many applications. However, their major disadvantages include a considerable degree of back-mixing of phases, scale-up and design issues due to complex interactions among phases.

Given their efficiency and capital cost reduction, bubble column reactors are the best choice for the FT process. These types of reactors usually operate at a high superficial gas velocity (0.2 - 0.4 m/s), high temperature (513 - 523 K), high pressure (3 - 5 Mpa) and high solids loading (approaching 40% by volume) (Krishna, 2000; Krishna et al., 2001). Reliably designing and scaling up bubble column reactors requires accurate hydrodynamics information, as well as heat and mass transfer parameters in the churn-turbulent regime.

1.1. MOTIVATION

Although constructing bubble column reactors is simple, some studies (Shah, 1982; Fan, 1989; Deckwer et al., 1993; Saxena, 1995; Kantarci, 2004) have reported that

the successful commercialization of such reactors requires an improved understanding of fluid dynamics and its influences. The operation of a bubble column reactor depends on its operating and design parameters, process reaction kinetics, and physical and thermodynamic properties, as detailed in Figure 1.3. All of these parameters affect the reactor's performance, design and scale-up. Obviously, the hydrodynamics and their influence on transport characteristics are complex. Therefore, considerable effort has been reported in the literature regarding the hydrodynamics of bubble columns (Devanththan, 1991; Kumar, 1994; Degaleesan, 1997; Luo et at., 1999; Wu et al., 2001; Wang et al., 2003; Ong, 2003). Unfortunately, these and many other published studies have not accounted for the presence of heat exchanger tubes or for their influence on bubble column hydrodynamics and mass and heat transfer parameters.

Many applications of bubble column reactors, such as FT and liquid phase methanol synthesis, best support a high superfical gas velocity, high pressure, high temperature, high catalyst loading and large diameter. However, only a limited number of hydrodynamic FT parameters have been investigated (Behish et al., 2000; Krishana & Sie, 2000; Krishan & Van Beten, 2003). The hydrodynamics, phase holdup distribution, velocity field and turbulent parameters have been investigated in more detail using computed tomography (CT) and computer-automated radioactive particle tracking (CARPT) in limited studies (Ong, 2003; Rados, 2003; Han, 2007; Shaikh, 2007). However, the impact of heat exchanger internals on fluid dynamics and scale-up have not been studied or understood fully.

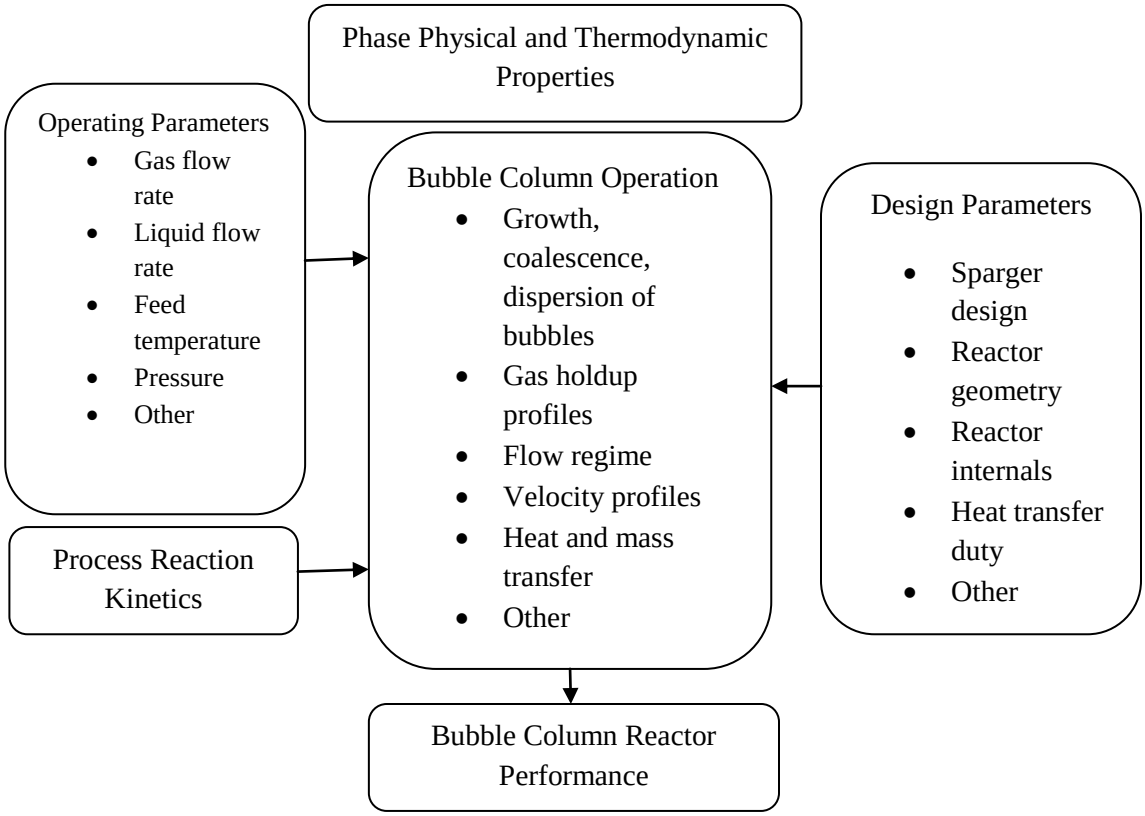

Figure 1.3. Effect of Operating Parameters, Design Parameters, Physical and Thermodynamic Properties and Kinetic on Bubble Column Reactor Operation

As noted previously, one important area of application for bubble column reactors is in the FT process, which is characterized by its environmental friendliness and commercial advantages. FT synthesis is an exothermic process that requires many heat exchanger tubes in order to remove heat efficiently and maintain the desired temperature and isothermal operating condition. Knowledge of the effect of internals and their configuration on the hydrodynamics and transport characteristics that influence reactor performance is critical to understanding the flow behavior in bubble column reactors for

proper design and scale-up. Some research studies have been conducted to identify the effect of internals and their design configuration in bubble column reactors (Fair et al., 1962; Shah et al., 1978; Saxena, 1993; Chen et al., 1999; Larachi et al., 2006; Youssef & Al-Dahhan, 2009; Yousssef, 2010; Rahman & Al-Dahhan, 2010; Jhawar, 2011; Hamed, 2012). Most of these studies focused on mass transfer, heat transfer, bubble dynamics, gas and liquid dispersion, etc. rather than detailed hydrodynamics. All of the studies indicated that the studied transport parameters could be affected by internals. However, while the bubble column reactors utilized in a wide range of industrial applications are equipped with internals, a lack of understanding of the impact of internals on hydrodynamic and transport characteristics remains. The lack of reported studies can be attributed to the following factors: 1) the flow pattern in such reactors is complex even in the absence of internals; 2) a lack of published unified geometrical standards for internals further complicates their design; 3) trade secrets cause information to be guarded instead of shared for the facilitation of research. Because the majority of these few studies have been limited to overall parameters and cross-sectional areas (CSA) occluded by internals, there exists a need to investigate the effects of internals in simulated situations of interest to industry regarding the local parameters, such as local gas holdup, liquid velocity field and turbulence parameters, to support proper industrial reactor design and scale-up.

In summary, the presence of internals and their configurations complicate the flow pattern in bubble column reactors, so investigations into bubble columns with internals have been limited. In addition, the published studies either focused on heat transfer rather than hydrodynamics or were performed at low superficial gas velocities with a small volume fraction covered by internals. Despite numerous attempts,

dependable data for the design and scale-up of bubble column reactors are not available. While all of the reported studies have indicated that internals can effect the reactor's performance, a lack of understanding of the impact of internals on hydrodynamic and transport characteristics remains. Therefore, the present study seeks to clarify the effects of vertical internals on hydrodyamics (gas holdup, liquid velocity field and turbulence parameters), the keys to bubble column reactor design and scale-up, under parameters of interest to industry (high velocities and large volume fraction covered by internals) by using non-invasive techniques, such as Computed Tomagraphy (CT) and Radioactive Particle Tracking (RPT).

This study will make a unique contribution to the literature in this field because no previous studies, to our knowloge, have investigated the effect of dense vertical internals on the local liquid velocity field, phase distribution or turbulence parameter profiles due to measurement limitations in the presence of internals. A need exists to study the effect of internals on the hydrodyamics in bubble columns in order to acquire reliable data for design and scale-up, benchmarking CFD models and advancing a proper understanding of the effect of dense internals on the studied parameters. The present study is the first to obtain and investigate a time-averaged cross-sectional distribution and radial profile of gas holdup, as well as the velocity field and turbulence parameter profiles in bubble column reactors with dense internals that mimic those in FT using advanced techniques (CT and RPT) under a wide range of superfical gas velocities. In addition, the study will provide crucial information to clarify the effect of internals on the performance of bubble column reactors and to benchmark CFD models and simulations of bubble columns with internals.

1.2. RESEARCH OBJECTIVES

The overall objective of this work is to advance the understanding of hydrodynamics in bubble columns with internals. Specifically, the goal of this work is to use advanced measurement techniques (CT and RPT) to investigate, analyze and evaluate, for the first time, the effect of internals on the following hydrodynamics in a bubble column reactor:

- The time-averaged phase holdup distribution of the phases in a dynamic air-water system, via non-invasive CT.
- The liquid velocity field and turbulence parameters (Reynolds stresses, turbulent kinetic energy, turbulent eddy diffusivities, etc.), via non-invasive RPT and a fully automated calibration device that will improve the accuracy of RPT measurements.

An air-water system will be used for simplicity, and due to more data of other studies using same system available in the literature for comparison with obtained data.

The completion of this work will enhance the understanding of the effect of hydrodynamics on the performance of bubble column reactors with dense internals and facilitate the design and scale-up of these kinds of reactors. It also will provide, for the first time, data for benchmarking computational fluid dynamics (CFD) in a gas-liquid system with intense internal tubes/rods. The obtained knowledge of the effect of internals on hydrodynamic parameters will facilitate the need for a detailed assessment of the thermal hydraulic of the core of light water nuclear reactors containing dense fuel rods to ensure safe operation, as well as to advance the development of sustainable light water nuclear reactors and small modular reactors (SMRs).

1.3. THESIS ORGANIZATION

A brief, general review of the literature on gas holdup, turbulence parameters, flow regimes and internals in bubble column reactors is provided in Section 2. Section 3 describes the measurement techniques (CT and RPT) and outlines the experimental setup of this work. Section 4 discusses the detailed results of CT, while Section 5 discusses the results of RPT. Finally, Section 6 summarizes the study and provides recommendations for future work.

2. LITERATURE REVIEW

As noted in Section 1, the operation of a bubble column reactor depends on the operating parameters, design parameters, process reaction kinetics and physical and thermodynamic properties (refer to Figure 1.3). The hydrodynamics and their influence on transport characteristics are very complex. Therefore, this issue has been the focus of many studies reported in the literature on bubble columns, with a primary concentration on design and scale-up, flow regime analysis and hydrodynamic parameters, including gas holdup, phase back-mixing, bubble characteristics and mass and heat transfer coefficients. Despite broad industrial applications of bubble column reactors equipped with internal heat exchanger tubes, most published studies have not accounted for them or their influence on bubble column hydrodynamics and mass transfer parameters. To fill the gap in the numerous studies on bubble columns that lack a consideration of the effect of internals, this study will provide a review of gas holdup, flow regime, liquid velocity field, turbulence parameters and internals.

2.1. GAS HOLDUP

Fractional gas holdup is considered an important parameter in the design of bubble column reactors. The gas holdup governs the local buoyancy, which drives the liquid circulation and turbulence; thus, these parameters govern the rate of heat and mass transfer. The gas holdup is defined as the fraction of gas in a gas-in-liquid dispersion (Deckwer, 1992) and can refer either to the overall gas holdup, which is obtained by measuring the change in the dynamic height compared to the static height of a liquid, or to the local holdup at a specific point in the reactor. A considerable number of gas holdup

studies have been reported in relation to bubble column reactors (e.g., Saxena et al., 1990; Krishna et al., 1994; Kumar et al., 1997b; Lefebvre & Guy, 1999; Bouafi et al., 2001; Degaleean et al., 2001; Forret et al., 2003; Chen et al., 2003; Ong, 2003; Shaikh & Al-Dahhan, 2005). Various techniques based on conductivity, resistivity, optical probe, nuclear (X-ray or gamma-ray) tomography, particle image velocimetry (PIV), ultrasound Doppler, etc., have been utilized over the years to determine the local gas holdup. As opposed to the other techniques, X-ray and gamma-ray computed tomography techniques are non-invasive and unhindered by the opacity of the domain. Although many studies have proposed correlations for predicting the phase holdup in a gas-liquid system (e.g., Roy et al., 1963; Akita & Yoshia, 1973; Joshi & Sharma, 1979; Reilley et al., 1984; Kawaw et al., 1992; Krishna & Ellenberger, 1996; Luo et al., 1999), they all have a limited range of applications.

Relevant studies have reported that the main variables affecting gas holdup in bubble columns include superficial gas velocity, physical liquid properties, column geometry, operation temperature and pressure, gas distributor design and internals and their configurations. In the subsections to follow, the effects of some of these variables are presented.

2.1.1. Superficial Gas Velocity. The superficial gas velocity is one of the most important variables affecting hydrodynamics. It is expressed as the volumetric flow rate divided by the total CSA of the column. The effect of gas velocity can be assumed by $\varepsilon_g \sim u_g^n$, in which n could be a function of physical material properties, column geometry, gas distributor design or flow regime (Deckwer, 1992). Not surprisingly, the majority of published studies investigated the effect of superficial gas velocity on the

overall and local gas holdup (e.g., Hills, 1974; Kumar et al., 1994; Joshi et al., 1998; Wu et al., 2001; Ong, 2003; Xue, 2004; Youssef, 2010). Although the evaluation of gas holdup was investigated using different techniques, such as CT tomography (Kummar et al., 1994; Ong, 2003) and optical probe (Xue, 2004; Youssef, 2010), the results conclusively revealed that the local gas holdup, similar to the overall gas holdup, increases as the superficial gas velocity increases. Ong (2003) reported that with an increase in the superficial gas velocity, the gas holdup profile becomes almost parabolic. He found that increased superficial gas velocity leads to a higher gas holdup value and steeper radial profile, as seen in Figure 2.1.

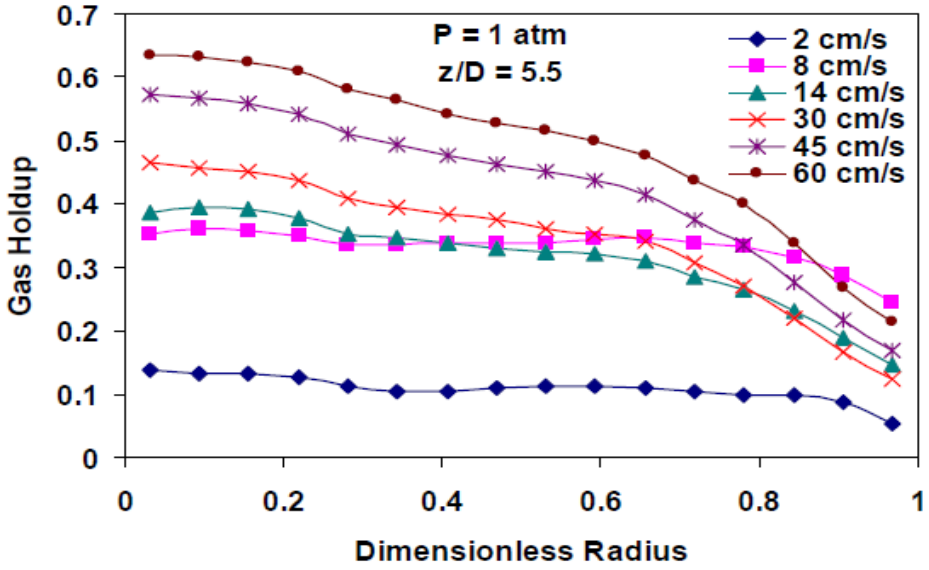

Source: Ong, 2003

Figure 2.1. Effect of Superficial Gas Velocity on Radial Gas Holdup Using Perforated Plate Distribution D4 (0.15% Open Area; d0=0.5) at z/D =5.5, P= 1 atm

In addition, the flat holdup profile was observed as long as a bubbly flow was sustained. Xue (2004) and Youssef (2010) also found similar results using the optical probe. Based on findings obtained from empty bubble columns, in a bubbly flow regime, the superficial gas velocity and radial gas holdup profile increase almost linearly, while in a churn-turbulent regime, this linear relationship decays. Small bubbles are formed in bubbly flows, and as the superficial gas velocity increases, more bubbles of similar or somewhat larger sizes are generated before passing a transition regime. On the other hand, in a churn-turbulent regime, large bubbles form due to coalescence with a steeper gas holdup profile because large bubbles move towards the column's center at a high rate.

2.1.2. Column Dimension and Gas Sparger (Distributor). The column diameter and gas distribution are two of the most important design variables for bubble column reactors. An ideal gas distributor design would uniformly distribute the gas bubbles and decrease the pressure drop. The effects of the column dimension and gas sparger have been studied comprehensively in the literature. Wilkinson et al. (1992) reported that the gas holdup was independent of the column diameter when the column diameter was larger than 15 cm, and the sparger design was found to have no effect at high pressure and when the sparger hole diameter was 1.5 mm. Similarly, Zahradnik et al. (1982) observed no effect of the sparger design when the sparger hole diameter was larger than 1.6 mm. Pino et al. (1992) reported that the effect of the column height within the ratio $3 \leq {}^{L}/_{D} \leq 12$ and the effect of the column diameters (10 and 29 cm) on the gas holdup of a forming system using the air-kerosene in semi-batch mode were insignificant. When forming occurred at high gas velocities, the height and column diameter had no

effect on the gas holdup. Luo et al. (1999) found that the effect of the column height was negligible when the column height to diameter ratio exceeded 5. Additionally, the type of distribution strongly affected the gas holdup at superficial gas velocities below 6 cm/s. Ong (2003) investigated the sparger's effect on gas holdup. The effect of the distributor on the radial gas holdup profile was insignificant deep in the churn turbulent flow regime. The sparger design significantly affected the bubbly flow regime, and the initial bubble size depended upon the sparger hole diameter; therefore, decreasing the sparger hole diameter reduces the bubble size and enhances the average gas holdup.

One may conclude based on the gas holdup studies discussed above that as superficial gas velocity increases, so does radial gas holdup. The effect of the column height on gas holdup is negligible when the column height to diameter ratio exceeds 5. In addition, the gas holdup is independent of the column diameter when the column diameter is greater than 15 cm. In the bubbly flow regime, the sparger design and its configurations produce a significant effect, while no effect of the distributor was observed deep in the churn-turbulent flow regime or when the orifice diameter exceeded 1.5 mm.

2.2. FLOW REGIMES

The demarcation of the flow regime is essential for assessing the bubble column reactor's performance. Based on the literature, the investigated parameters (e.g., gas holdup, liquid recirculation, etc.) strongly depend on the flow regime. The flow regimes in bubble column reactors are categorized into four types, including bubbly (homogenous), slug, churn-turbulent (heterogonous) and annular flow regimes. Figure

2.2 shows the first three types of flow regimes, which are commonly observed in bubble columns.

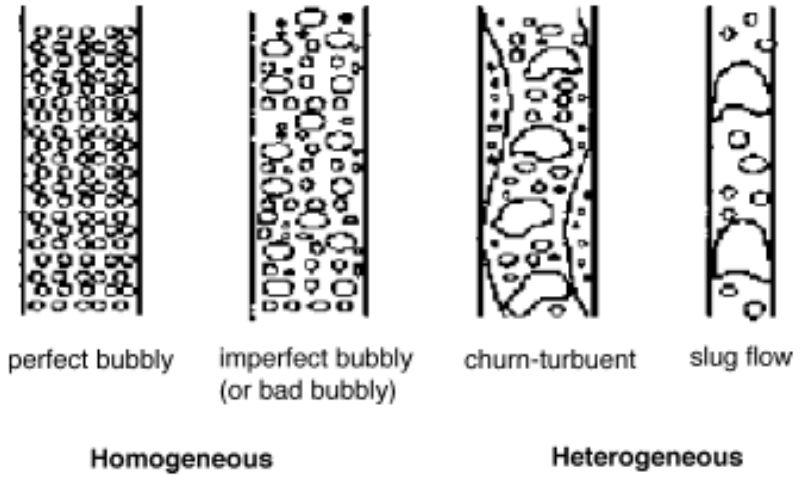

Source: Kantarci et al., 2005

Figure 2.2. Various Flow Regimes in Bubble Column Reactors

A slug flow can be observed only in association with small diameters at high gas velocities; thus, it is infrequently found in industry. Conversely, bubbly and churn-turbulent flow regimes are frequently encountered in columns of industrial interest. Therefore, they have been investigated heavily.

A bubbly flow regime usually occurs at low to moderate gas velocities and is characterized by uniformly sized bubbles, which are strongly a function of the type and design of the gas distributor, as well as its liquid properties. In this regime, the bubbles

rise vertically at an almost constant rate without coalescence and then break up. Due to uniformity in the homogenous regime, liquid phase recirculation is insignificant. The bubbly regime has the advantage of a large interfacial area, which is attractive in mass transfer. Despite this fact and the completely different hydrodynamic characteristics between bubbly and churn-turbulent flow regimes, the interest for industry applications is to operate the bubble column under churn-turbulent flow regimes.

The churn-turbulent flow (heterogeneous) regime occurs at high superficial gas velocities and generally is characterized by small and large bubbles rising at high velocities. These bubbles coalesce and break up, leading to enhanced bubble size distribution and intense liquid turbulence. In churn-turbulent regimes, a significant variation in the radial gas holdup can be observed because large bubbles form due to coalescence and move towards the column's center at a high rate; thus, the gas holdup in the center is greater than at the wall. The bouncy forces resulting from this non-uniform gas holdup distribution cause large-scale liquid recirculation in this flow regime. Therefore, mass and heat transfer in churn-turbulent regimes are more pronounced than in bubbly regimes.

The bubbly, churn-turbulent and slug flow regimes have different transition regions. The transition from a bubbly to a churn-turbulent or slug flow regime depends on system parameters such as gas velocity, column diameter, distributor design, the presence of solids, physical properties of the phase, etc. The boundaries associated with the transition regions for bubble columns are presented in Figure 2.3.

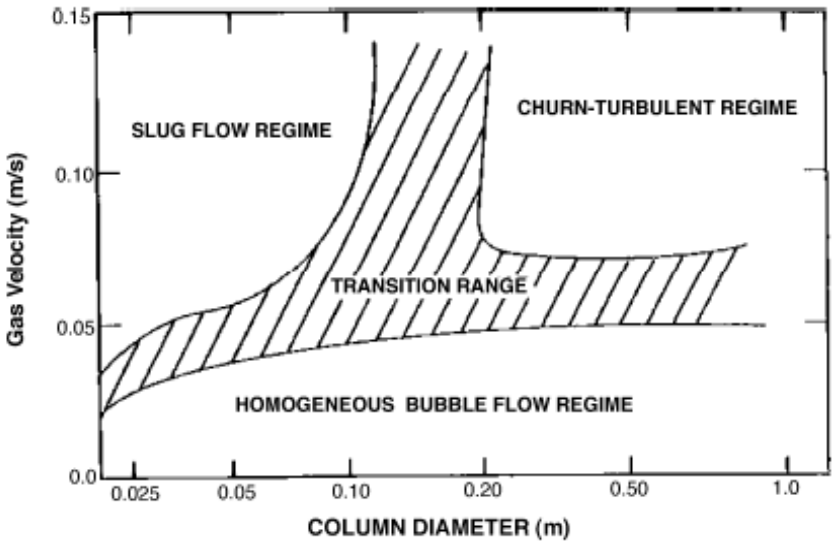

Source: (Kantraci et al., 2005)

Figure 2.3. Flow Regime Map for Bubble Column

As noted previously, bubbly flow regimes and churn-turbulent flow regimes have completely different hydrodynamic characteristics. Therefore, identifying the flow regimes in bubble and slurry bubble columns is very important because most applications in these reactors can be classified and maintained according to the flow regimes, such as biochemical processes in bubbly flow regimes and highly exothermic processes in churn-turbulent regimes. Therefore, numerous studies have focused on detecting the flow regime in bubble and slurry bubble columns under different system and operating conditions. Some studies were based on visual observations, which is conceivable when the column is clear. Different techniques have been used to classify flow regimes. Among studies using advanced measurement techniques, Krishna et al. (1991) studied the effect of operating pressures ranging from 0.1 MPa to 2 MPa on flow regime transitions in a

column 6 m in diameter using several gases (air, nitrogen, carbon monoxide, argon, helium and sulphur dioxide) and de-ionized water. The dynamic gas disengagement (DGD) technique was performed in a column 0.19 m in diameter using several different liquids (water, turpentine, mono-ethylene glycol and n-butanol) to characterize the hydrodynamics in the churn-turbulent regime. Krishna et al. (1991) reported that the gas holdup varied linearly with the superficial gas velocity in the homogeneous flow regime more so than in the heterogeneous flow regime. A pressure increase delayed the transition to the heterogeneous flow regime. The ratio of superficial gas velocity U_g to obtained gas holdup ε_g ($\frac{U_g}{\varepsilon_g}$), called the swarm rise velocity, was used to determine the transition velocity (U_{trans}) between homogenous and heterogeneous flow regimes. In homogenous flow regimes, the swarm rise velocity was found to be constant. When the gas velocity increased beyond $U_g = U_{trans}$, the swarm rise velocity increased and no longer remained constant due to the presence of different-sized bubbles. The U_{trans} was very sensitive to gas density and liquid phase properties. DGD illustrated that in churn-turbulent regimes, there are large and small bubbles; the large bubbles rise rapidly through the center of the column, while the small bubbles follow the liquid and take longer to distribute. This phenomenon causes the radial gas holdup profile to be parabolic.

Chen et al. (1994) studied flow structures in bubble columns using particle image velocimetry (PIV). They observed the following three regimes: 1) dispersed bubble flow, 2) vertical-spiral flow, and 3) turbulent flow. In this study, churn-turbulent regimes were divided into two categories, vertical-spiral flow and turbulent flow, because they have different flow structures. In dispersed bubble flow, bubble streams rise straight up with a

uniform bubble size distribution. With an increase in the superficial gas velocity, bubbles form a central bubble stream, which moves in a spiral motion as the liquid moves vertically. Tiny bubbles move up and down in the region between the central bubble stream and the column wall. In the turbulent flow regime, the coalescence of the bubbles creates large bubbles that move in a discrete manner.

Hyndman et al. (1997) studied the transition from bubbly to churn-turbulent flow in a 0.12 m in diameter column with an air-water system using steady-state holdup and pressure fluctuation data. In addition, DGD was used to characterize the hydrodynamics in the churn-turbulent flow regime. They found that the transition velocity, U_{trans}, and obtained gas holdup, ε_g, between bubbly and churn-turbulent flow regimes were 0.0375 m/s and 0.137 m/s, respectively. DGD displayed two phases, I (large bubbles) and II (small bubbles). Phase II was characterized by a linear relationship between holdup and pressure and slower bubble motions with a uniform distribution. Furthermore, the behavior of the small bubbles in the churn-turbulent regime changed insignificantly with the superficial gas velocity. The large bubbles, however, were evacuated from the column, and their behavior changed significantly with the gas velocity.

Vial et al. (2000) applied the new diagnostic 'simple' method based on a theoretical analysis of the autocorrelation function (ACF) of the time series in order to identify the flow regime transition in bubble columns and external loop airlift reactors. The experiments were conducted in a column 0.10 m in diameter and 2 m in height with two spargers (a multiple-orifice and a single-orifice nozzle). The ACF was applied to the following equations depending upon the existing flow regimes:

$$\frac{C_{xx}(\tau)}{C_{xx}(0)} = \exp\left(-\frac{\tau}{\tau_0}\right) \qquad \text{for a homogenous regime}$$

or

$$\frac{C_{xx}(\tau)}{C_{xx}(0)} = \cos(2\pi\, f_0\tau)\, \exp\left(-\frac{\tau}{\tau_0}\right) \quad \text{for a heterogeneous regime}$$

where C_{xx}, τ ,τ_0 and f_0 are the correlation function, time lag, characteristic time and frequency, respectively. These equations were used to analyze the experimental ACF curves for yielding τ_0 and f_0 near the wall. The characteristic time, τ_0 , was constant in the bubble column and airlift reactors in both homogenous and heterogeneous flow regimes, but there was a factor of 6 between τ_0 in the bubbly and churn-turbulent flow regimes. In the transition region between the regimes, an increase in τ_0 was observed.

Shaikh and Al-Dahhan (2005) used gamma-ray CT, which is designed to quantitatively determine the time-averaged phase holdup distribution, to identify the flow regime transition in a bubble column by analyzing the shape of the obtained radial gas holdup profiles. The experiments were carried out in a stainless steel column with a 0.16 m diameter and a height of 2.5 m at superficial gas velocities ranging from 1 to 30 cm/s and under ambient conditions. They found that the bubbly flow regime yielded flatter radial gas holdup profiles, while the churn-turbulent flow regime yielded parabolic profiles. A sudden change in shape at intermediate gas velocities was observed, and the transition velocity was calculated using the change in slope of the cross-sectional gas holdup with the superficial gas velocity curve and the drift flux plot. The investigators found the calculated transition velocity at the same point where the profile shape suddenly changed. Then, the steepness parameter was applied based on the following equation proposed by Luo and Svendensen (1992):

$$\frac{\varepsilon_G}{\bar{\varepsilon_G}} = \left(\frac{n+2}{n+2-2c}\right)\left(1 - c\left(\frac{r}{R}\right)^n\right) \qquad (1)$$

Where ε^{-}_{G} represents the cross-sectional average gas holdup, $\frac{r}{R}$ is the dimensionless radial position, n is the steepness parameter and c indicates the gas holdup near the wall. Shaikh and Al-Dahhan (2005) found that n was large in the bubbly flow and small in the churn-turbulent flow regimes, and the steepness parameter curve changed suddenly around the transition point, as seen in Figure 2.4.

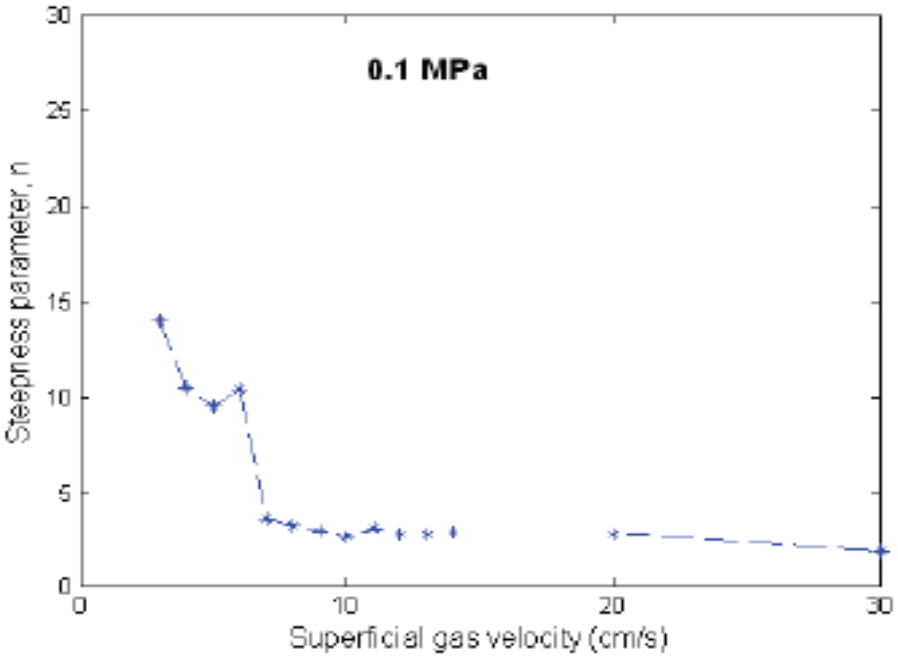

Source: Shaikh & Al-Dahhan, 2005

Figure 2.4. Evolution of Steepness Parameter with Superficial Gas Velocity in Air-Therminol LT System

In summary, although many studies have been conducted to identify the regime boundaries under different operating conditions using different methods, definite flow regime maps have not been reported. In addition, these studies have not addressed

industrial conditions or the effect of heat exchanger tubes, which are required for many bubble and slurry bubble column applications.

2.3. VELOCITY FIELD AND TURBULENCE PARAMETER PROFILES

Though some studies have investigated mixing and velocity profiles in bubble and slurry bubble column reactors, the behaviors of fluid hydrodynamics are not yet fully understood due to their complexity. A deeper knowledge of the scale dependency of hydrodynamic and transport parameters would facilitate the design and scale-up of these reactors. As noted previously, one of the most important parameters is gas holdup, which governs the circulation of the turbulent liquid. This circulation can affect mixing, as well as heat and mass transfer, and therefore reactor performance. Most studies conducted in this area have been performed at superficial gas velocities up to12 cm/s due to the limitations of the measurement techniques utilized. Velocity measurement techniques such as optical probe, laser Doppler anemometry (LDA), heat pulse anemometry (HPA), hot film anemometry (HFA) and particle image velocimetry (PIV) are limited to low gas velocities. These techniques, along with their limitations and capabilities, have been discussed by Degaleesan (1997) and therefore will not be reported here.

In recent years, a computer-automated radioactive particle tracking (CARPT) technique was developed to allow deep insight into the local flow characteristics in multiphase reactors regardless of the operating conditions. Using this technique, one can monitor the composite radioactive particle (Sc^{46} or Co^{60}), which was made to simulate a solid's density, shape and size for solids tracking or its buoyant density for liquid tracking, with a set of sodium iodide detectors located strategically around the column. A

series of studies have been performed on bubble and slurry bubble column reactors using CARPT techniques. Devantahan et al. (1990) used CARPT to investigate liquid recirculation and turbulence in a column with an internal diameter of 0.292 m in an air–water system at 0.105 m/s. This study is considered the first application of CARPT for tracing the flow of liquid in a bubble column. The investigators observed that a single recirculation cell ascended along the column's center and descended near the wall. In addition, two recirculation cells were observed at a gas velocity of less than 0.05 m/s. At the entry region, the liquid rose near the wall and descended at the center of the column, and it reversed itself in the upper free-surface zone. The inversion (transition) point occurred at r/R=0.72 (01025 m), and the average Reynolds stress radial profile was similar to the Reynolds stress profile for a single phase through a pipe.

Degaleesan (1997) investigated liquid velocities and turbulence parameters in 0.14, 0.19 and 0.44m columns with different distributors in an air-water system. Asymmetry was observed near the distribution zone, and this asymmetry varied with each distributor's unique design, being strongly affected by the smallest holes in the distributors. For the distributor with the smallest holes (0.33mm), two stagnant circulation cells were observed close to the distributor at a gas velocity of 0.2 m/s; when the gas velocity increased, the cells disappeared. The turbulent stresses were symmetrical about the axis of the column, and they did not vary significantly with the axial position in the fully developed region. The normal axial stress was two or three times larger than the radial and azimuthally normal stresses. Based on obtained data, the recirculation and cross flow with dispersion model (RCFDM) was developed to describe the mixing of liquids in bubble columns. Degaleesan et al. (2002) applied the wavelet-based filtering

algorithm to obtain accurate turbulence parameters. This technique successfully reduced the noise in the obtained data by 80-90%.

Chen et al. (1999) performed CARPT measurements in a 0.44 m in diameter column with and without internals using both air-drake oil and air-water systems to investigate the velocity field and turbulence parameters. They found that the liquid flow ascended in the center and descended near the wall. This observation aligns with the results reported in other studies (e.g., Hills, 1974; Menzel et al., 1990; Devanathan et al., 1990; Mudde et al., 1997). The axial velocity inversion point occurred at r/R = 0.68 for the air-water system and at r/R=0.6 and 0.57 for the air-drake oil system without and with internals, respectively. In the following subsection, the effect of internals on the fluid dynamics in bubble column reactors will be discussed. The normal stress in the air-water system was higher than in the air-drake oil system, while the normal radial stress in the air-drake oil system was lower than in the air-water system due to the increased viscosity of drake oil. The shear stress was close to zero in the center and near the wall for all systems.

Wu and Al-Dahhan (2001) developed the following correlation for predicting the axial liquid velocity profile in bubble columns based on CARPT data:

$$\frac{V_L(r)}{V_{L0}} = 1 - 2.65 * n^{0.44} * c(\frac{r}{R})^{2.65*n^{0.44*C}} \quad (2)$$

Where n and c are parameters of the gas holdup radial profile calculated using the correlations proposed by Wu et al. (2001):

$$n = 2.188 \times 10^{3} {Re_G}^{-0.598} {Fr_g}^{0.146} {Mo_L}^{-0.004} \quad (3)$$

$$c = 4.32 \times 10^{-2} {Re_G}^{0.2492} \quad (4)$$

The developed correlation agrees with data reported in the literature, as shown in Figure 2.5. This correlation can be applied to the solid velocity radial profile due to similarities between bubble and slurry bubble column reactors.

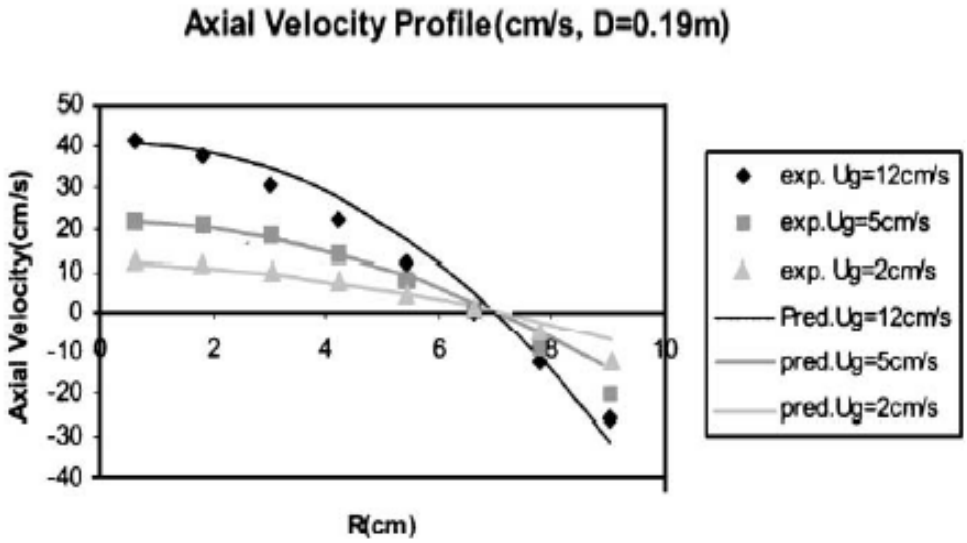

Source: Wu and Al-Dahhan (2001)

Figure 2.5. Comparison of the Correlation Predictions with Experimental Data of Degaleesan (1997)

Ong (2003) used CARPT to investigate velocity field and turbulence parameters in a 0.162 m inner diameter stainless steel column with four different gas distributors at a high superficial gas velocity and at high pressure using an air-water system. She found that the recirculation of the axial liquid increased with an increase in the superficial gas velocity and pressure, while the turbulent normal stresses and thus the turbulent kinetic energy (TKE) and the eddy diffusivities decreased with an increase in pressure. The axial

normal stress was at least two times higher than the radial and azimuthal normal stresses, thus confirming the results obtained by Degaleesan (1997). At 1 and 4 atm, liquid recirculation was independent of the distribution design. Ong modified the empirical correlation developed by Zehner (1983) to account for the effect of pressure on the centerline velocity, as follows:

$$u_{0,pred} = 0.737 g^{1/3} {D_c}^{1/3} {U_g}^{1/3} \left(\frac{\rho_g}{\rho_{g,atm}}\right)^{0.128} \quad (5)$$

where $\rho_{g,atm}$ is the gas density at atmosphere conditions. This modified correlation is valid for a column with a 0.162 m diameter, a range of pressure from 1-10 atm and a range of U_g from 30-45 cm/s.

Rados (2003) performed CARPT measurements in a 16.15 cm in diameter stainless steel slurry bubble column at high pressure using an air-water-glass bead (150 μm) system to study the effect of the superficial gas velocity, pressure, sparger design and solids loading on the solids velocity and solids turbulence parameter profiles. He found that the superficial gas velocity and operating pressure were the primary parameters affecting the velocity field and the turbulence parameter profiles. At 30 cm/s, the effect of the sparger's design on the solids velocity and solids turbulence parameter profiles was negligible; this finding held true in the two-phase (air-water) system. A small effect was observed when the solids loading was increased from 9.1% vol. to 17.8 % vol. at atmosphere conditions.

Shaikh (2007) used CARPT to study the effect of various operating conditions on the radial profile of the solids axial velocity and turbulence parameters using an air-Therminol-glass bead (150 μm) system at room temperature. A comparison of the results

of the air-Therminol-glass bead system and the air-water-glass bead system (Rados, 2003) revealed that the former system had a higher solids axial velocity and shear stress than the latter due to each phase's physical properties. When the operating pressure increased, so did the solids axial velocity and the radial-axial shear stress. The solids axial velocity and shear stress, as well as the negative velocity close the wall of the column, decreased as the solids loading increased, while the TKE and normal stresses increased as the solids loading increased due to an increase in bubbles.

Han (2007) investigated the liquid/solids velocity field and turbulence parameter profile in a 16.15 cm in diameter stainless steel column reactor using air-C_9C_{11}, an air-C_9C_{11}-FT catalyst and an air-Therminol-FT catalyst. At a superficial gas velocity of 30 cm/s, 1.0 MPa and solids loading of 25% vol., the effect of two liquids, including C_9C_{11} and Therminol, on the solids axial velocity, TKE, as well as the effect of the stresses, was mostly the same in the air-C_9C_{11}-FT catalyst and air-Therminol-FT catalyst systems. The effect of two different solids, FT and glass beads (Shaikh, 2007), on the radial profiles of the solids velocity and turbulence parameters was compared. They had similar effects on the radial profile of the axial solids velocity, in the range of $r/R > 0.4$, while the magnitude of the axial velocity of the glass beads was 25% higher than the axial velocity of the FT catalyst close to the core of the column ($r/R < 0.4$). Larger differences arose in the value of the radial profiles of the TKE, Reynolds stress and axial normal stress upon moving closer to the column's wall. An increase in the time-averaged axial velocities, TKE and other turbulence parameters was noted when the superficial gas velocity increased.

These studies contributed significantly to the understanding of flow behavior in bubble and slurry bubble column reactors. However, most industrial applications of these reactors are equipped with internals, including heat exchanger tubes, baffles, perforated plates and vibrating springs, in order to maintain isothermal operation and to control the mixing. The majority of the cited studies performed in bubble and slurry bubble column reactors did not account for any effect of the internals. In order to facilitate the successful design and scale-up of bubble column reactors, the effect of internals must be considered carefully. Therefore, internals and their effect on hydrodynamics in bubble column reactors will be discussed in the next section.

2.4. INTERNALS

Bubble column reactors are applied widely in a variety of chemical and biochemical industrial processes, such as oxidation, alkylation, hydrogenation, methanol synthesis, the Fischer-Tropsch (FT) process, and biological waste water treatment. Most of the reactions in bubble column reactors are exothermic, which require heat exchange mechanisms for removing the generated heat to maintain the desired temperature and isothermal operating conditions. Heat can be transferred through various indirect methods, such as with cooling or heating mechanisms or external heat exchangers, or through the wall of a column reactor, as shown in Figure 2.6 (Schluter et al., 1995). In most current applications, bubble column reactors are operated at high gas throughputs, high temperature and pressure, and high solids loading; thus, longitudinal flow tube bundles are appropriate (Schluter et al., 1995). For example, the heat produced by the reaction and the operating pressure during FT synthesis is about 210 kJ/mol and 12-15

bars, respectively, thus requiring intensive heat exchanger tubes (internals) that cover approximately 25% of the CSA of the reactor in order to maintain the desired temperature. Although most bubble column reactors are equipped with internals, a lack of understanding persists regarding the impact of internals on the hydrodynamic and transport characteristics. Furthermore, the lack of published, unified geometrical standards for internals further complicates their design.

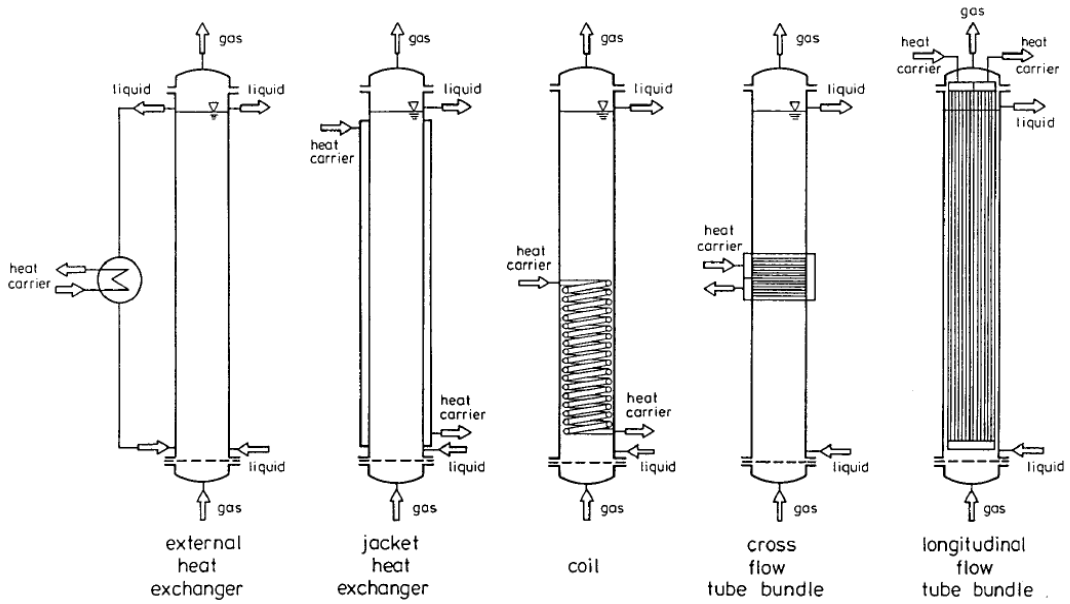

Source: Schluter et al., 1995

Figure 2.6. Indirect Heat Transfers in Bubble Column Reactors

Some attempts have been made to understand the impact of horizontal internals (perforated plates or tube bindles placed across the flow direction) or vertical internals, which are our focus in this work, on reactor performance and heat and mass transfer in

bubble and slurry bubble column reactors. Among these attempts, Yamashita (1987) studied the effect of vertical pipe and rod internals made from vinyl chloride resin and iron with different overall gas holdup arrangements. He used three column diameters, each with a different-sized single orifice nozzle as a gas distributor. The superficial gas velocities in his study ranged from 1.66 to 35.3 cm/s for the three bubble columns. He reported that the overall gas holdup was not affected by the arrangement of the vertical tubes but was sensitive to the number of internals and their outer diameter.

Saxena et al. (1992) studied the effect of internal tubes in a Pyrex glass column with a diameter of 0.305 and 19 mm in diameter internals, increasing the size and configuration of 5, 7 and 37 tubes of different blockings (1.9, 2.7 and 14.3%, respectively) of the column's total CSA for air-water and air-water-glass bead systems. They found that the gas holdup was higher for 37 tubes than for 7 tubes, and the gas holdup depended upon the geometrical configuration of the tube bundles. Saxena and Rao (1993) estimated the gas holdup in a 0.305 m in diameter slurry bubble column with 37 internals for a nitrogen-Therminol-magnetite system at different ranges of temperatures, gas velocities and solids concentrations. They reported that at a constant superficial nitrogen velocity, the gas holdup increased as the temperature increased, while the increased solids concentration had an insignificant effect on the gas holdup at higher temperatures.

Pradhan et al. (1993) studied the effect of helical coil and straight tubes (vertical internals) with internals of different diameters and with different volume fractions covered by internals X_v on gas holdup and bubble characteristics in an air-aqueous CMC solution system. They reported that the shape and size of the bubbles were affected

significantly by the diameter of the internals, and the presence of internals helped to break the bubbles down into smaller sizes. The average gas holdup increased with increases in the gas velocity and the volume fraction covered by internals X_v for each type of internals. Furthermore, helical coil internals achieved a higher gas holdup than vertical internals due to the space available among the internals, which allows the bubbles to escape directly, as is the case with straight tubes, or breaks them into smaller sizes, as is the case with coil internals.

Chen et al. (1999) investigated the effect of internals covering 5% of the column's total CSA on the gas holdup, liquid velocity, and turbulence parameters in a 44 cm in diameter column using CT and CARPT techniques for two systems, air-water and air-drake oil, both with and without internals. The study revealed that the gas holdup in the column with internals was slightly higher than in the column without internals. No significant difference was found in the velocity of liquid recirculation with or without internals, and the stagnation point moved further towards the center of the column when internals were present. At a high superficial gas velocity (10 cm/s), the turbulent stresses and eddy diffusivities were lower with internals present because of the reduced length of the turbulence scales.

De et al. (1999) studied the gas holdup in two-phase systems with different volume fractions covered by helical coils and straight internals X_v. Three different aqueous solutions, including Sodium sulphate, Butanol and Glycerine solutions with different concentrations were used as the liquid phases in this experiment. The investigators found that the gas holdup increased as the superficial gas velocities and volume fraction covered by internals X_v increased. The helical coil internals helped

reduce the size of the bubbles more so than the straight internals. Therefore, the gas holdup had a higher value with coil internals. Figure 2.7 illustrates the effect of superficial gas velocities and type of internals with different X_v on the overall gas holdup in an air-Glycerine-1 system. In addition, the average gas holdup obtained using the Butanol solution was higher than that obtained using either the Sodium sulphate or Glycerine solutions.

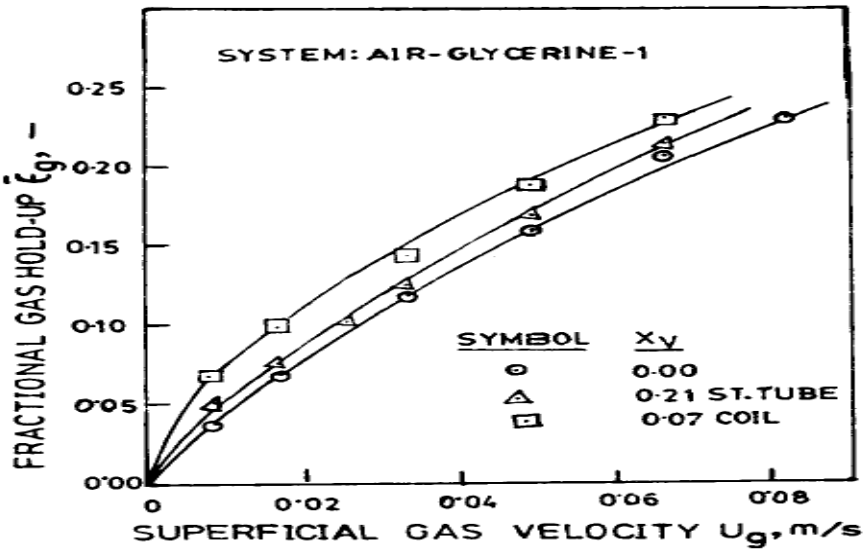

Source: De et al., 1999

Figure 2.7. Effect of Superficial Gas Velocity on Gas Holdup

Forret et al. (2003) studied liquid dispersion in a 1 m in diameter bubble column with and without internals in an air-water system. They reported that internals enhanced large-scale recirculation (Figure 2.8) and decreased the fluctuating velocity, which increased the axial liquid velocity in the center of the bed. Furthermore, the inversion

point occurred at x= 0.7 both with and without internals. To predict the effect of internals on liquid mixing, a two-dimensional (2D) model was developed. Because of the large-scale recirculation, the axial dispersion model (1D ADM) is not appropriate for use with bubble columns with internals.

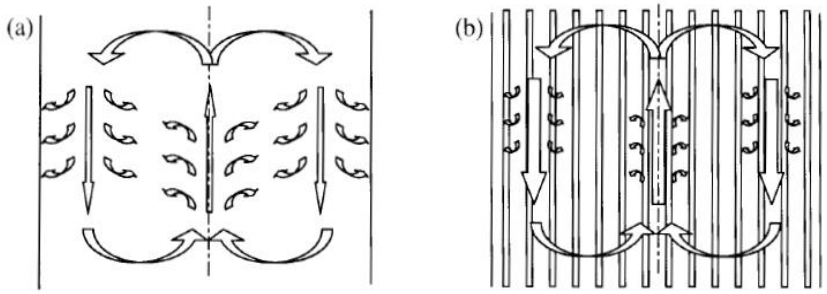

a. Without Internals b. With Internals

Source: Forret et al., 2003

Figure 2.8. Liquid Recirculation in Bubble Columns

Youssef and Al-Dahhan (2009) and Youssef (2010) studied the effect of internals on the gas holdup, gas-liquid interfacial area, bubble chord length and bubble velocity distribution in a bubble column with an 8 in diameter in an air-water system. They observed no significant effect with internals covering 5% of the cross-sectional area (CSA) at a superficial gas velocity of 20 cm/s. For the case in which internals covered 22% of the column's CSA, the overall gas holdup increased 18%, and the bubble chord length and the bubble velocity decreased due to enhanced bubble breakup. The mean velocity with which the bubbles rose when the internals covered 22% of the CSA decreased by 11% and 15% compared to the case in which internals covered 5% of the

CSA and the case in which no internals were present, respectively. Youssef (2010) used a basic liquid tracer technique to assess the impact of internals on liquid mixing in a column with an 18 in diameter. He reported that the presence of internals enhanced the liquid phase mixing, and dense internals increased the dimensionless variance. At the center of the column, no significant difference in the bubble velocity probability distribution was found between the column without internals and the column with 25% internals coverage.

Balamurugan et al. (2010) investigated the effect of internals on the gas holdup in bubble columns using vertical and vibrating helical spring internals of different diameters and thicknesses. The percentage of gas holdup obtained in the case of the bubble column with vibrating helical spring internals was 135% higher than that obtained in the case without internals. Because the spring internals helped to break large bubbles into smaller bubbles, which spend more time in the bed of the column, the gas holdup was higher than in columns either with or without vertical internals. In addition, the material, geometry and properties of the internals played a remarkable role in enhancing the gas holdup.

Jhawar (2011) used a fast response probe to illustrate the effect of the configuration of the internals on local heat transfer and hydrodynamics in a 0.15 m ID bubble column for an air-water system. Two types of internals, a circular tube bundle (A) and a concentric baffle (B1: close to distributor; B2: in fully developed region), and their combination (AB2), were used in this work. The heat transfer coefficient, gas holdup and liquid velocity increased with an increase in the superficial gas velocity due to generated turbulence. At the column’s center, the heat coefficient and bubble holdup obtained with A and AB2 internals were higher than in the column without internals. However, no

significant difference in the heat transfer coefficient was observed between B1 internals and the hollow column. The gas holdup obtained with B1 was lower than that obtained without internals because of the location of internal B1 in the distributor region, which helped the bubbles to coalesce. At the wall region (r/R=0.624), reverse gas holdup and heat transfer coefficient trends were observed. The heat transfer coefficient at the stagnation point was estimated by the correlation presented by Li and Prakash (2002) to obtain the local liquid velocity:

$$\frac{h_{st}D_p}{k_L} = a_s\,(Pr)^{0.4}\left(\frac{V_L D_p}{v_L}\right)^{0.5} \qquad (6)$$

Where h_{st} , D_p , k_L , v_L, Pr and V_L represent the heat transfer coefficient at the stagnation point, probe diameter, liquid thermal conductivity, liquid kinematic viscosity, Prandtl number and superficial liquid velocity, respectively. Jhawar and Prakash (2011) suggested that the value of a_s be set at 0.7. At the center of the column, the A and AB2 internals enhanced the line liquid velocity, while no significant difference was found with B1 compared to the hollow column. The location of internals has a significant effect on local heat transfer and hydrodynamics.

Most recently, a study of the effect of vertical cooling internals occupying up to ~25% of the total CSA of the column on the hydrodynamics and gas mixing in bubble column reactors was conducted by Hamed (2012). In this investigation, two column diameters were used, including an 8 in inside diameter with a gas velocity ranging from 5 to 45cm/s and an 18 in inside diameter with a gas velocity ranging from 20 to 45cm/s. An air-tab water system was used in all experiments; the air's superficial velocity was calculated based on the free CSA available for flow in the column. Hamed used the 4-

point optical probe and gas tracer techniques to take the measurements. Additionally, in this study, he attempted to develop and validate models that can simulate the radial gas velocity profile and axial gas mixing in the presence and absence of internals. He reported that the presence of internals increases in the center-line gas velocity, significantly decreasing axial gas mixing. On the other hand, an increase in the column diameter enhances gas circulation and increases axial gas mixing.

Computational fluid dynamics (CFD) simulations have been applied to simulate the local characteristics of hydrodynamics in bubble column reactors in both fully three- and two-dimensional systems using different approaches. Recently, CFD has become one of the most important alternative methods by which to obtain information regarding flow dynamics based on the Navier-Stokes equations, offering more safety and a much lower cost than other techniques once it is validated. Although hollow bubble columns have been investigated extensively using CFD (e.g., van Baten et al., 2002; Rampure et al., 2003; Ekambara et al., 2005; Joshi & Majumder, 2011), studies of bubble columns equipped with internals remain rare. One of the very few published studies was conducted by Larachi et al. (2006), who simulated 3-D computational fluid dynamics (CFD) for five pilot-scale configurations of internals, including an empty vessel and a vessel with uniform and non-uniform fillings of internals, as shown in Figure 2.9, to estimate the flow behavior in a bubble column. The occluded CSA ranged from 2 - 16.2%, with a 1.6 to 30 bubble diameter to gap ratio. CFD simulations indicated that the internals and their configurations affected the liquid flow structures and sharply decreased the liquid kinetic turbulent energy (Figure 2.10). In addition, the largest turbulent eddy was sensitive to the gap length scale.

(a) Empty Vessel (b) Dense Arrangement of Vessels (c) Sparse Arrangement of Internals

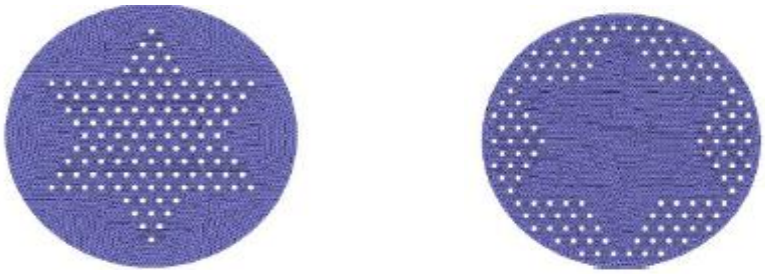

(d) Star Arrangement – Wall Clearance (e) Star Arrangement – Core Clearance

Source: Larachi et al., 2006

Figure 2.9. Configuration of Internals Used for the 3-D CFD Simulation

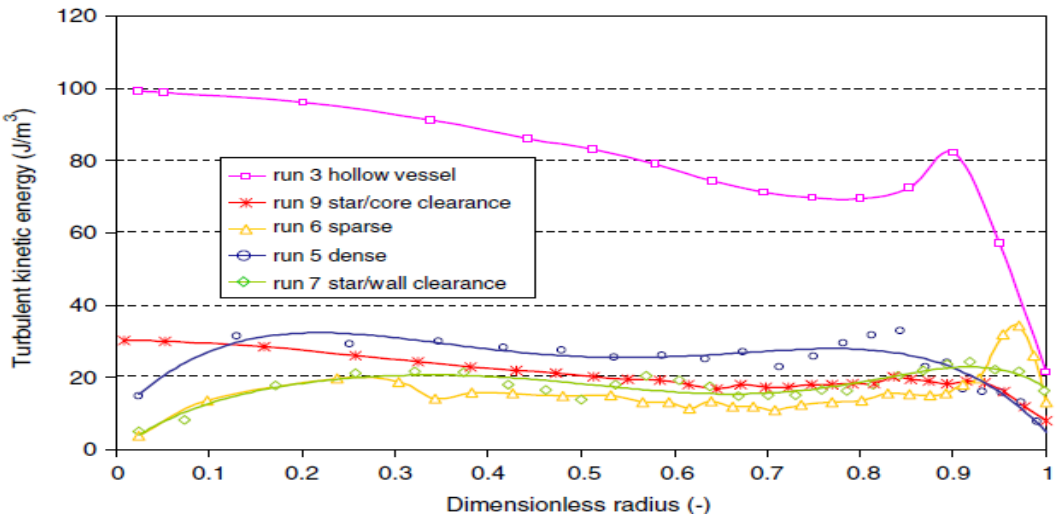

Source: Larachi et al., 2006

Figure 2.10. Comparison between the Time- and Azimuthally Averaged Profiles of Liquid Turbulent Kinetic Energy for Different Internals Configurations Using CFD Simulation

Boutet et al. (2010) used CFD to simulate the hydrodynamic/thermal coupling phenomenon in a 15.1 cm in diameter column with a bundle of two U-shaped internals, each of them being 2.67 cm in diameter at a gas velocity of 0.343 m/s. An appropriate model was defined to investigate the impact of internals on the hydrodynamics for air-Sylthem XLT. Cooling tubes bound the turbulence length scale and increased the turbulent energy dissipation rate. The local eddy length scale decreased in the presence of internals. In addition, heat removal can be affected significantly by the position of the heat exchanger tubes in bubble column reactors.

Because internals and their configurations complicate the flow pattern in bubble column reactors, studies on bubble columns with internals are limited. In addition, the available studies either have focused on heat transfer rather than hydrodynamics or were performed at low superficial gas velocities with a small volume fraction covered by internals. While all relevant studies have found that a reactor's performance can be affected by internals, a lack of understanding of the impact of internals on the hydrodynamic and transport characteristics remains. Therefore, the present study seeks to clarify the effects of vertical internals on the hydrodyamics (gas holdup, liquid velocity field and turbulence parameters) within parameters of interest to industry (high velocities and large volume fraction covered by internals) by using non-invasive techniques, such as Computed Tomography (CT) and Radioactive Particle Tracking (RPT).

3. EXPERIMENTAL SETUP AND MEASUREMENT TECHNIQUES

3.1. INTRODUCTION

As noted in Section 2, extensive studies have been conducted on the hydrodynamics in bubble and slurry bubble column reactors using various techniques. Computed tomography (CT) and computer-automated radioactive particle tracking (CARPT) have been utilized in many studies to investigate the phase holdup, velocity field and turbulence parameter profiles in gas-liquid (G-L) bubble column and gas-liquid-solid (G-L-S) slurry bubble column reactors. Most of these studies have not accounted for the effect of internals on the hydrodynamics, although many applications of bubble/slurry bubble column reactors are equipped with heat exchanger tubes. For example, one of the most popular applications of these kinds of reactors is Fischer-Tropsch (FT) synthesis, which requires large numbers of heat exchanger tubes in order to maintain the desired temperature. No doubt, these studies have enhanced our understanding of the flow behaviors in bubble/slurry bubble column reactors, but the impact of internals on hydrodynamics still needs to be quantified so that reliable data are available to design and scale-up these kinds of reactors. Due to the significant effect of internals indicated by the few reported studies on local flow characteristics, as well as the lack of understanding of this effect, the objective of the current study is to use non-invasive techniques, such as gamma ray Computed Tomography (CT) and Radioactive Particle Tracking (RPT), to investigate the effect of internals on the flow behavior of a bubble column.

In this section, CT and RPT are discussed as advanced, non-invasive measurement techniques for the local gas holdup, velocity field and turbulence

parameters. A brief description of the experimental setup also is provided. Other techniques, such as four-point optical probe for validating the obtained data, are discussed in Appendix B.

3.2. EXPERIMENTAL SETUP

The experiments were conducted in a Plexiglas column with an inner diameter of 5.5 in (0.14 m) and a height of 6 ft (1.82 m). A schematic diagram of the setup used in this study is shown in Figure 3.1. Compressed air supplied from an industrial compressor, which can deliver compressed air of 735 CFM capacity at pressures up to 200 Psig, was used as the gas phase and introduced through a distributor at the bottom after passing through appropriate filtering, while softened tap water was used as the liquid phase. Two rotameters (Brooks Instrument) with different scales were connected in parallel to cover a wide range of flow rates (160 to 3200 SCFH). The column was designed without any ports or connections on the wall because these create non-symmetry, which complicates the CT and RPT data reconstructions. The experiments were conducted batchwise with respect to the liquid but with a continuous flow of gas at ambient temperature and pressure. In all experiments, the dynamic height of the bed was kept constant at 55 in ($z/D \sim 10$) above the gas distributor by varying the static height of the bed. The gas distributor (sparger) made from stainless steel had 121 holes, each 1.32 mm in diameter, arranged in a triangular pitch, with a total free area of 1.09% (Figure 3.2).

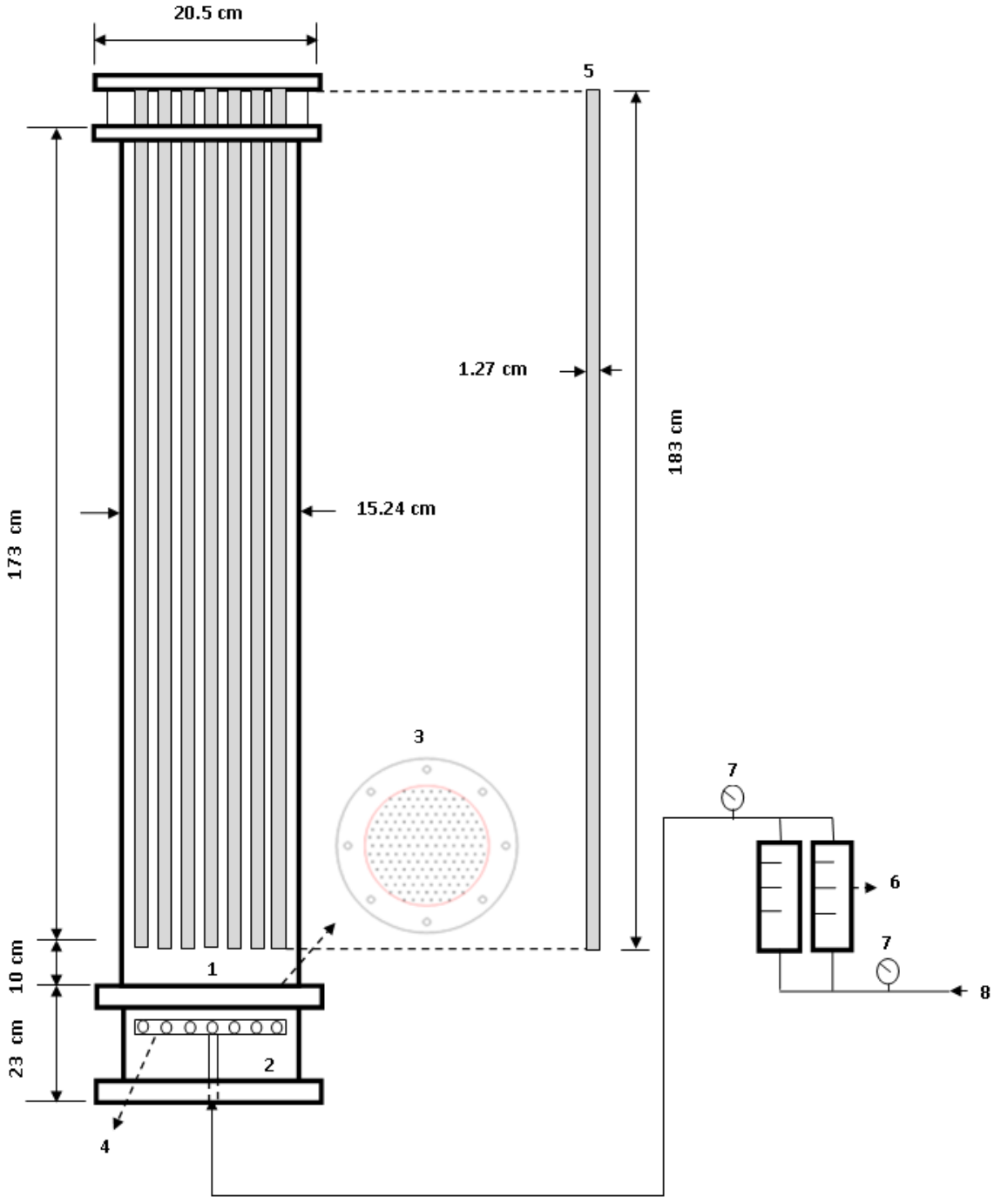

1. Plexiglas column 2. Plenum 3. Distributor 4. Sparger 5. Internal (Heat Exchanging Tube) 6. Rotameter 7. Pressure Gauge 8. Compressed and Filtered Air Inlet

Figure 3.1. Schematic Diagram of the Bubble Column Setup

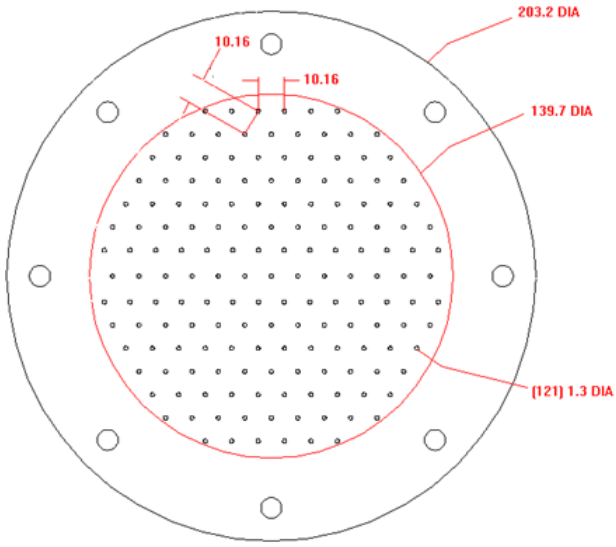

(a) Schematic Diagram of Gas Distributor (b) Photo of Distributor

Figure 3.2. Gas Distributor

To investigate the impact of internals (heat exchanging tubes) on hydrodynamics in bubble column rectors, vertical Plexiglas and stainless steel rods with 0.5 in outer diameters with the same configurations were used in the CT experiments. Plexiglas attenuation is low, and we initially were not sure whether the CT could identify the locations of the internals; therefore, stainless steel internals were manufactured and examined at selected conditions as shown in Appendix A. Only Plexiglas internals (hollow with closed ends) were used for the RPT experiments. Thirty rods, which covered 25% of the total CSA simulating the percentage used for the FT process, were placed in a triangular pitch of 0.84 in (2.14 cm), as shown in Figure 3.3. The internals were secured inside the column by three honeycomb plates to reduce the vibration and make them more stable, as seen in Figure 3.4.

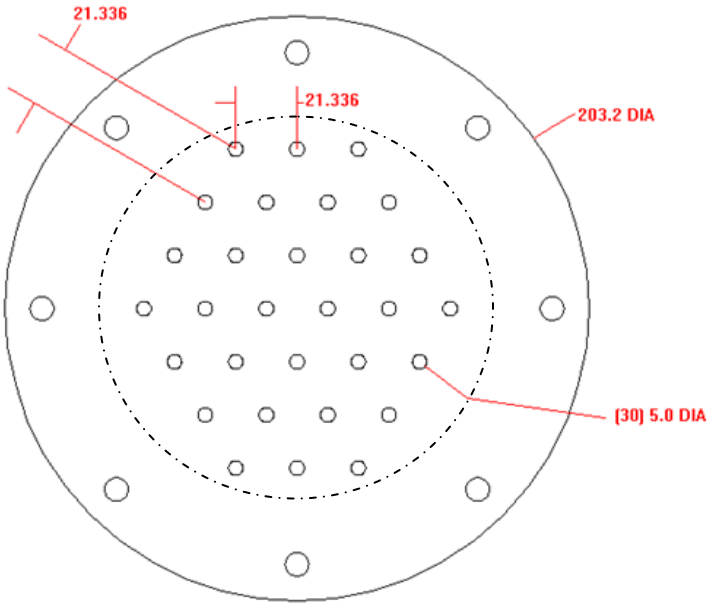

a) Schematic Diagram of Internals Configuration

b) 6” Bubble Column Equipped with Stainless Steel Internals

c) Plexiglas Internals

Figure 3.3. Internals

The experiments were conducted over a wide range of superficial gas velocities (5 cm/s - 45 cm/s) based on the total and free CSA of the column in order to compare fairly the effect of internals; this range of velocities covers the homogenous and heterogeneous flow regimes. The time-averaged cross–sectional gas holdup, velocity field and turbulence parameters in bubble columns without internals were measured to benchmark the gas holdup, velocity field and turbulence parameters of the bubble column with internals.

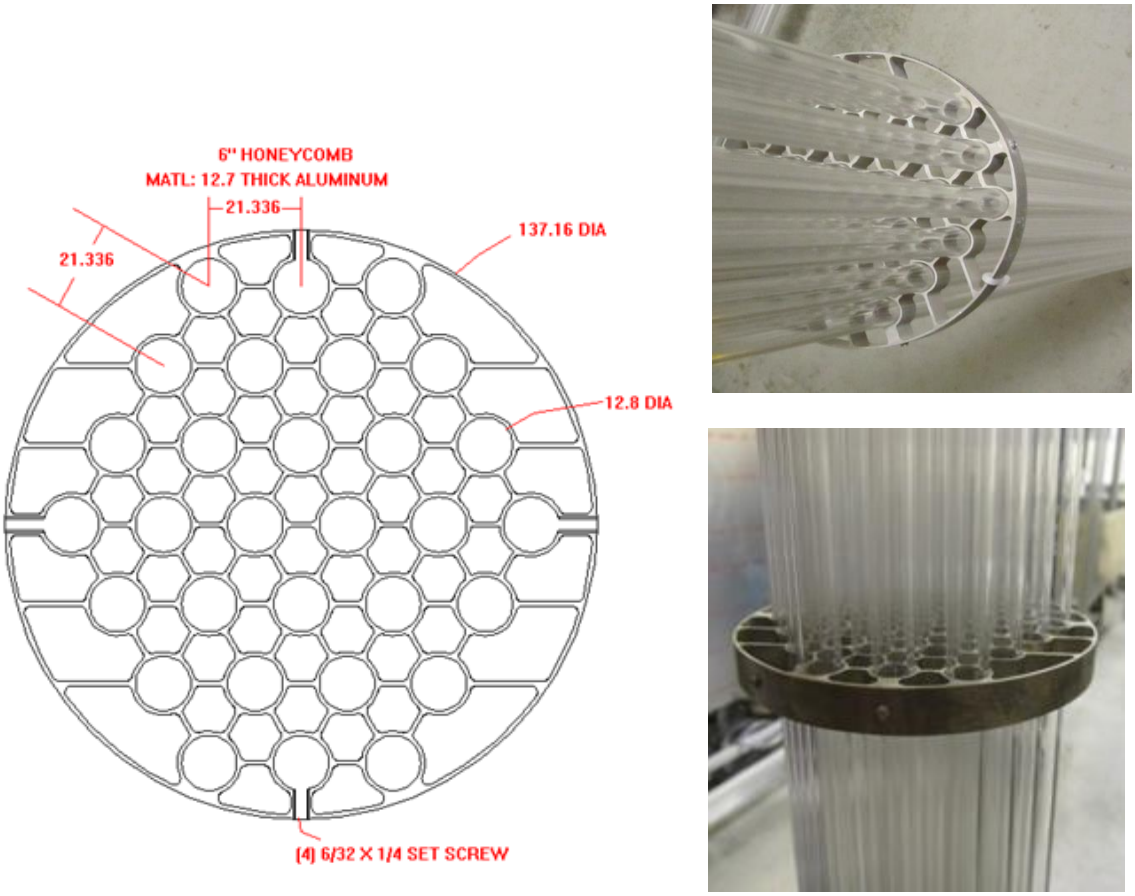

Figure 3.4. Schematic Diagram and Photo of Honeycomb

3.3. GAMMA RAY COMPUTED TOMOGRAPHY (CT) TECHNIQUE

To investigate the effect of dense internals and superficial gas velocity on the radial gas holdup profiles and cross-sectional distribution, computed tomography (CT) was employed ***for the first time*** with dense internals . Brief descriptions of CT and its experimental conditions are provided in Sections 3.3.1 and 3.3.2, respectively. A detailed description of the technique can be found elsewhere (Varma, 2008).

3.3.1. CT. In general, CT, a powerful technique for generating cross-sectional views of an object, has been applied extensively in the medical field for radiology diagnostics. Over the past two decades, CT has emerged in the field of engineering for industrial applications to image the phase distribution in multiphase processes (Kumar et al., 1997). Single- and dual–source γ-ray CT techniques have been used in various multiphase flow systems to measure the cross-sectional phase holdup distribution (Seville et al., 1986; Kumar, 1994; Roy, 2001; Ong, 2003; Rados, 2003; Bhusarapu, 2005; Luo, 2005; Han, 2007; Shaikh, 2007, Varma, 2008). As the use of single-source CT requires additional information to reconstruct three-phase holdup distribution, Varma (2008) successfully developed and validated for the first time a dual-energy, dual-source computer tomography (DE-DSCT) technique for imaging two- and dynamic three-phase holdup for a given system. He fabricated and assembled the hardware for the DSCT scanner. He also introduced the use of the alternating minimization (AM) and the expectation maximization (EM) algorithms for imaging holdup phases. The AM algorithm images were found to be more reliable than the EM algorithm images. This technique can be used as dual-source computer tomography (DSCT) for imaging dynamic three-phase holdup or single-source CT for imaging two-phase holdup or three-phase holdup when the solid phase is stationary. A more detailed description of the

technique and algorithms can be found elsewhere (Varma, 2008). In the absence of DE-DSCT, the CT/overall gas holdup method proposed by Rados (2003) can be implemented to calculate the phase holdup profiles in a dynamic three-phase system using a single gamma-ray source. A detailed description of the method is available elsewhere (Rados, 2003; Rados et al., 2005). Additional details regarding the single-source γ-ray CT technique and its software can also be found in Kumar (1994). Figure 3.5 illustrates a schematic diagram of the dual/single-source γ-ray CT technique.

The CT unit, which was developed by Varma (2008) with support from the Department of Energy (DOE) is currently available in the professor Al-Dahhan's laboratory at the Missouri University of Science and Technology (Missouri S&T). Actually it consists of two independent gamma ray sources, encapsulated Cesium (C^{137}) and Cobalt (Co^{60}), with initial strengths of ~ 250 mCi and 50 mCi, respectively (dual-source CT), as well as two arrays of 15 NaI scintillation detectors located opposite each source for imaging three phases, as shown in Figure 3.6. The sources and detectors are built on a rotary plate that moves them together 360° around the studied object, providing 197 views in each scan and 21 projections in each view. The plate can be moved up or down by a step motor to scan the object at different axial positions. Each detector consists of a cylindrical NaI crystal measuring 2" in both diameter and length, a photomultiplier and electronics. The NaI crystal absorbs fallen gamma radiation and releases it as light photons that hit the photocathode of the photomultiplier tubes (PMT). The released electrons are multiplied by a series of dynodes and sent as anode current pulses at the output. During dynamic CT experiments, the data obtained reflects the time-averaged attenuation values, which are related to phase holdup distribution in a given system. In

this work, the Cesium (Cs^{137}) source had an approximate activity of 200 mCi at the time of the experiments, and five detectors were used to reconstruct the gas holdup distribution.

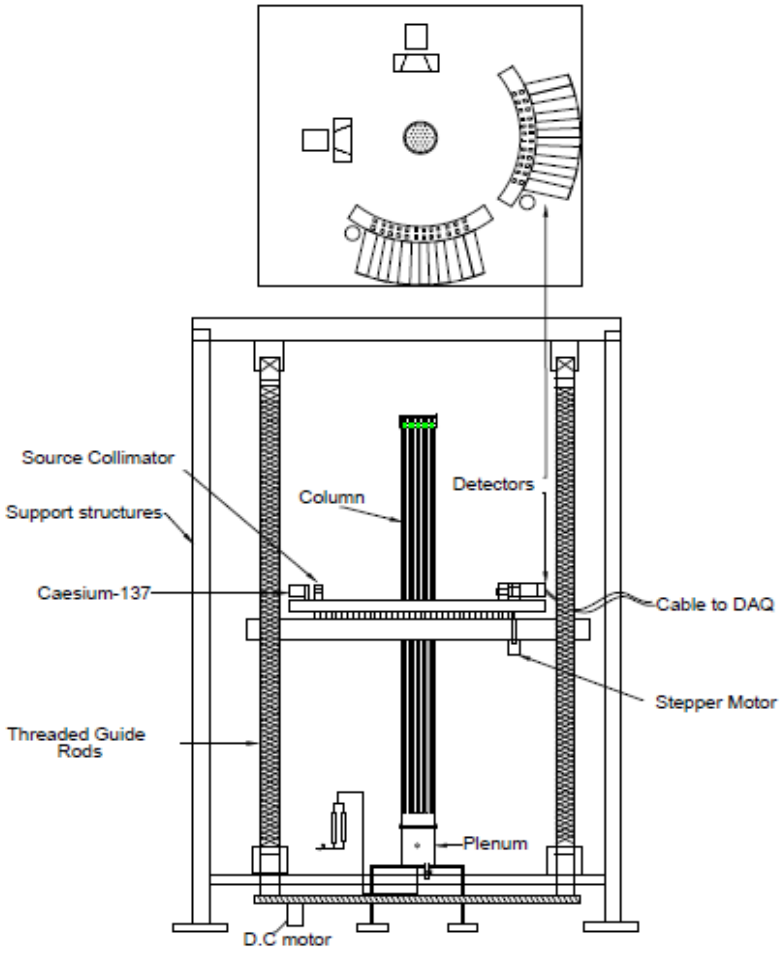

Figure 3.5. Schematic Diagram of Single-Source CT Unit

Cesium (Cs^{137}) has a half-life of 30.23 years and decays by pure β-decay, producing Barium-137, which creates all the γ-ray emissions with energy of 662 KeV. The CT scan sampling rate was 60 samples at 10 Hz, which took approximately 7.2 seconds to finish a

projection and 8.25 hours to finish a comprehensive scan. In this work, CT experiments were performed only under a two-phase condition either with a bubble column without internals or with a bubble column with internals considered an integral part of the reactor. In addition, the internals represented either a stationary solid phase or a gas-liquid-solid phase; in this case, holdup distributions were reconstructed using dual-source scans because single-source CT scans cannot adequately reconstruct three-phase holdup distributions.

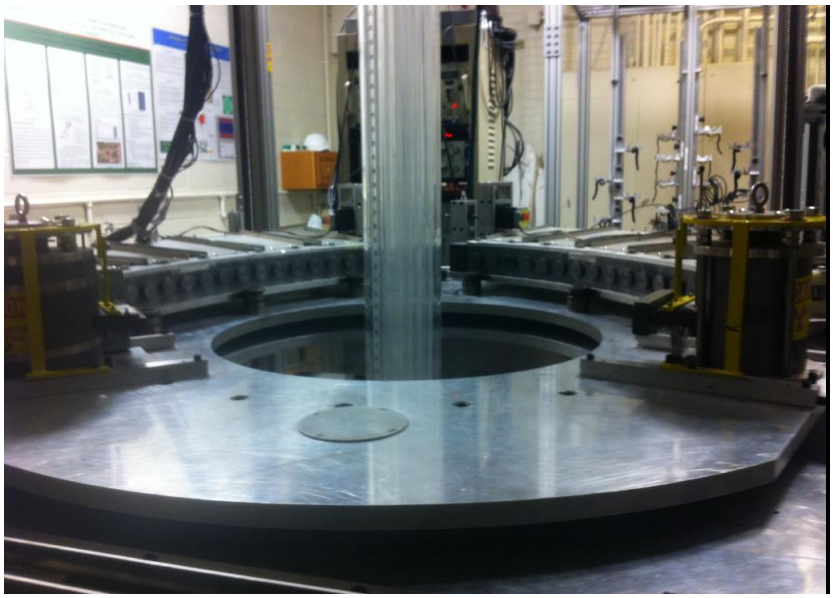

Figure 3.6. CT Setup Available in Our Lab for the 6" BCR with Internals

3.3.2. CT Experimental Conditions. All CT experiments were conducted in the Plexiglas bubble column introduced above under a wide range of gas velocities (from 5 cm/s to 45cm/s). In all of the experiments, the dynamic bed height remained constant at

1.4 m from the gas distributor. All CT scans were acquired at 80 cm (L/D = 5.8) above the gas distributor in a fully developed region. To achieve a fair comparison, the dynamic bed height and the axial scan position were kept constant in all cases, both with and without internals. Stainless steel and Plexiglas internals with diameters of 0.5 in each were used to study the impact of the internal materials type on the gas holdup distribution profiles and also to assess the method of reconstruction with internals. All of the experiments were conducted using an air-water system at atmospheric pressure and temperature. In the investigation, superficial gas velocities based on both the free area and the CSA of the column were applied to reveal their influences on the gas holdup distribution.

3.3.3. CT Reconstruction Algorithm. The reconstruction algorithm proposed by O'Sullivan and Benac (2007) and used by Varma et al. (2007) and Varma (2008) was implemented to reconstruct the cross-sectional distribution of relative attenuation in a two-phase system either with or without internals. O'Sullivan and Benac (2007) proposed an alternating minimization (AM) algorithm based on turning a maximum likelihood problem into a double minimization of I-divergence introduced by Csiszar (1991). I-divergence is a measure of inconsistency between two functions, a(y) and b(y) (Csiszar, 1991), which is given as:

$$I(a\backslash\backslash b) = \sum_{y\in Y} a(y)\, ln\left[\frac{a(y)}{b(y)}\right] - \sum_{y\in Y}[a(y) - b(y)] \qquad (7)$$

where Y is a finite dimensional space.

The function a(y) is taken to be the measured data, while b(y) is taken to be a nonlinear model (Bhusarapu, 2005). Let q(y:μ) be defined based on Beer Lamert's law for the transmission of photons (Varma, 2008), as follows:

$$q(y:\mu) = I_0(y)exp[-\sum_{x\in X} b(y|x)\mu(x)] \quad (8)$$

Where $I_0(y)$ is the incident intensity, $b(y|x)$ is the length of projection y in pixel x, $q(y:\mu)$ represents the transmission of photons and is a function of the attenuation and b(y) represents a Poisson random number d(y). Equation (7) can be rewritten as

$$I(d\backslash\backslash q(y:\mu)) = \sum_{y\in Y}\left\{d(y)\ln\left[\frac{d(y)}{q(y:\mu)}\right] - [d(y) - q(y:\mu)]\right\} \quad (9)$$

The algorithm minimizes the left term in Eq. (9) with respect to the attenuation (μ). More details and mathematical proofs regarding the AM algorithm are available elsewhere (O'Sullivan & Benace, 2001; Bhusarapu, 2005; O'Sullivan & Benace, 2007; Varma et al., 2007; Varma, 2008). In this work, the AM algorithm was used to reconstruct images that represent attenuation of the gas-liquid system. For local holdup/attenuation measurements using computed tomography (CT), the bubble column's cross-section was divided into n × m square pixels (as shown in Figure 3.7). Because this work was performed under two conditions (gas-liquid system), the ij^{th} pixel was made of the gas and liquid only with the attenuation coefficients μ_g and μ_l and thicknesses l_g and l_l. When using a single gamma radiation source, the pixel attenuation $A_{g-l,ij}$ over the path l_{ij} equals:

$$A_{g-l,ij} = \mu_g l_{g,ij} + \mu_l l_{l,ij} \quad (10)$$

The holdup summation equals unity; $\varepsilon_{l,ij} = 1 - \varepsilon_{g,ij}$ (11)

Equation (10) can be written as follows:

$$A_{g-l,ij} = \left[\mu_g \varepsilon_{g,ij} + \mu_l(1 - \varepsilon_{g,ij})\right]L_{ij} \quad (12)$$

Where

$$L_{ij} = l_{g,ij} + l_{l,ij}\ ,\ l_{g,ij} = \varepsilon_{g.ij}\, L_{ij}\ , and\ l_{l,ij} = (1 - \varepsilon_{g,ij}\ )L_{ij} \quad (13)$$

The density of gas ρ_g is << the density of liquid ρ_l , so the attenuation of the gas phase is negligible. Hence, the gas holdup in pixel ij can be written as follows:

$$\varepsilon_{g,ij} = 1 - \frac{A_{g-l,ij}}{A_{l,ij}} \tag{14}$$

where $A_{l,ij} = \mu_l L_{ij}$ (15)

To measure the phase cross-sectional distribution, the following scans were taken:

- With internals considered an integral part of the reactor:
    - Scanning the empty column with internals as a reference CT scan at the same column length used in normal operation.
    - Scanning normal gas-liquid operation under the desired conditions for obtaining $A_{g-l,ij}$.
    - Scanning the column filled with liquid and with internals at the same column length used in normal operations for obtaining $A_{l,ij}$.
- Without internals:
    - Scanning the empty column as a reference CT scan at the same column length used in normal operation.
    - Scanning normal gas-liquid operation under desired conditions for obtaining$A_{g-l,ij}$.
    - Scanning the column filled with liquid at the same column length used in normal operations for obtaining $A_{l,ij}$.

Equation (14) enables the calculation of the gas holdup profiles in a gas-liquid system with or without internals considered as an integral part of the reactor. The same

procedure for data processing was followed in the cases both with and without internals. Data processing has been discussed in detail elsewhere (Kumar et al.1995; Rados, 2003), so it will not be discussed here. When considering internals as a solid phase, this equation is not valid; instead, two independent gamma ray sources are necessary.

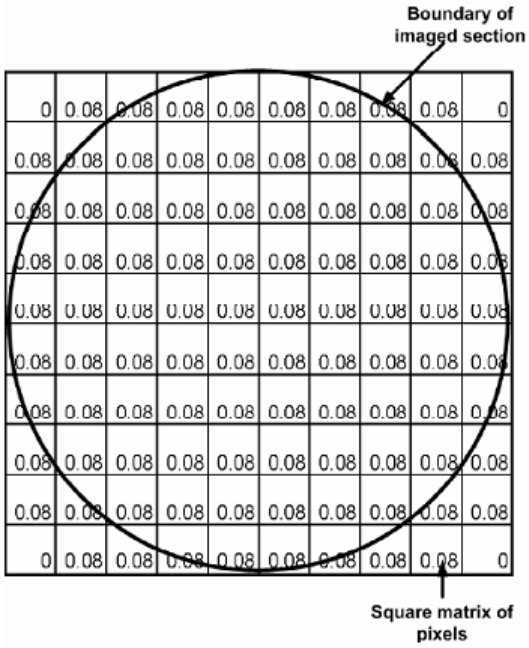

Figure 3.7. Discretization of Domain Cross-Section

3.4. RADIOACTIVE PARTICLE TRACKING (RPT) FACILITY

In the present study, radioactive particle tracking (RPT) was used to investigate ***for the first time*** the effect of dense internals and the superficial gas velocity on liquid velocity field and turbulence parameter profiles (occurrence, Reynolds stress and eddy diffusivity profiles). In the following sections, a brief description of RPT and selected conditions are presented.

3.4.1. RPT. RPT is a powerful technique for mapping the Lagrangian trajectory of a particular phase in a given system by tracking a single radioactive particle, which should match the density of the studied phase, with the aid of an array of scintillation detectors located strategically around the system. From the lagrangian trajectory, vital information can be extracted in the form of velocity field, turbulence parameters, residence time distribution, stagnant zones, and many others.

Computer-automated radioactive particle tracking (CARPT) has been used extensively to track flow patterns in complex, multiphase systems. It was first implemented by Kondukov et al. (1964), who used six scintillation detectors to study the motion of solids in a fluidized bed. In 1987, the second generation of CARPT was introduced, boasting a faster data acquisition system created by Moslemian (1987) to investigate solids velocity fields and turbulence parameters in fluidized beds. Then, the third generations of CARPT were developed by Devanathan (1991), who first used CARPT to study the liquid phase motion in a bubble column reactor, and Yang (1991), respectively. Furthermore, a series of studies successfully used RPT (e.g., Chen, 1999; Roy, 2000; Rados, 2003; Ong, 2003; Luo, 2005; Han, 2007; Shaikh, 2007; Varma, 2008). Rados (2003), Han (2007) and Shaikh (2007) advanced the application of CARPT to a high-pressure system. Recently, Vesvikar (2006), with the help of the team from the Oak

Ridge National Laboratory (ORNL), developed the fifth generation of RPT and the multiple radioactive particles tracking technique, which can track up to eight different radioactive particles simultaneously..

RPT experiments typically consist of the following two steps: 1) RPT calibration (static experiment under experimental conditions), and 2) the RPT experiment (dynamic experiment). During in-situ calibration, a single radioactive particle is placed at several known locations, and each NaI scintillation detector reserves intensity counts, which depend upon the distance between the radioactive particle and the detector, at each calibration location. From the calibration step, a count-distance map can be obtained, which will be used in the subsequent step to obtain the location of the tracer particle. During the experimental run (dynamic experiment), the radioactive particle moves freely inside the reactor to track the studied phase motion. The data obtained from the calibration and actual experiments can be used to map the trajectory of the tracer radioactive particle. The success of this process strongly depends on the success of particle preparation.

3.4.2. Preparation of the Particle. As previously noted, the reliability of the collected data depends on the quality of the preparation of the composite particle. In this study, Cobalt-60 with an activity of about 400μCi and a 600 micron diameter was used in all RPT experiments. Cobalt has a half-life of 5.28 years and presents two photo-peaks, one at 1.18 MeV and one at 1.34 MeV. Cobalt has a high density, 8.9 g/cm^3, so it was encapsulated with air in a polypropylene ball with a 2.3 mm outer diameter to obtain a composite particle density similar to the water density, as shown in Figure 3.8.

a) Microscopic Picture of a Cobalt Particle (600 micron diameter)

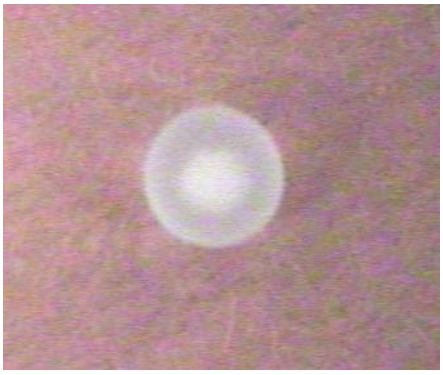

b) Picture of a Polypropylene Ball (2.38 mm)

c) Picture of a Hollow Polypropylene Ball

d) Picture of Cobalt Particle into a Polypropylene Ball

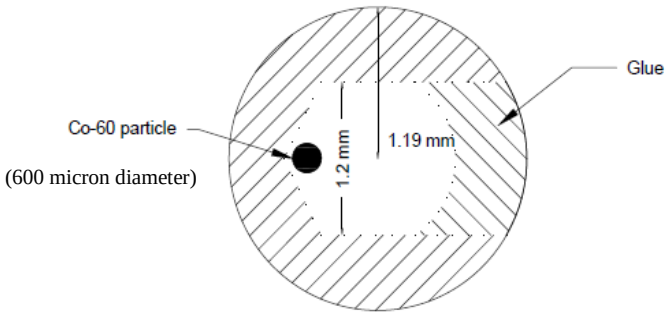

e) Schematic of Composite Particle

Figure 3.8. Cobalt Particle and Polypropylene Ball

This density was checked by measuring its terminal settling velocity in tap water in a 3 ft long tube:

$$\rho_p = \frac{18\mu_w U_t}{D_p g} + \rho_w \quad (16)$$

Where U_t, D_p, ρ_w, μ_w, g and ρ_p are the terminal setting velocity, diameter of the particle, water density, water viscosity, acceleration of gravity and density of the composite particle, respectively. The particle was coated with a thin film of paint to guarantee its wetting during the experimental run. In addition, the density of the composite particle can be increased or decreased slightly by coating the particle with spray paint or spray glue. Based on Equation 1, the density of the composite particle was approximately 0.998 g/ cm^3, and its settling velocity was less than approximately 0.05 cm/s.

3.4.3. RPT Setup. The new RPT setup was built in our laboratory at Missouri S&T. This setup included a fully automatic calibration device (r, z, and θ) and a single processing and data acquisition system, as seen in Figure 3.9. Twenty-eight NaI scintillation detectors were used, which were held on four vertical supports at equal distances around the column. Each support had 7 detectors placed at different axial levels. Each detector consisted of a cylindrical NaI crystal (2 in x 2 in), a photomultiplier and electronics.

a. Radioactive Particle Tracking RPT Setup

b. Calibration Plate and Device

Figure 3.9. RPT Setup and Calibration Device

Figure 3.10 and Table 3.1 illustrate the position and configuration of the detector. The detectors were placed on 14 axial levels with two detectors on each level facing each other. The detectors were horizontally leveled using a leveling device and dual-laser–equipped aluminum dummy detectors facing each other. The detectors were aligned in the axial and azimuthal directions using the laser-equipped aluminum dummy detector.

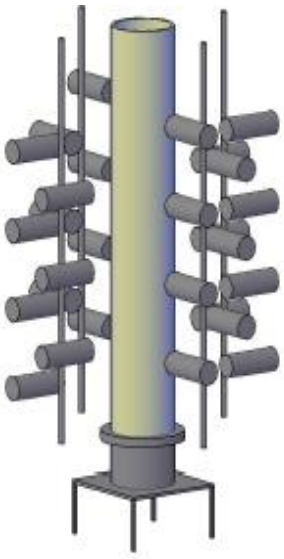

a. Angle View

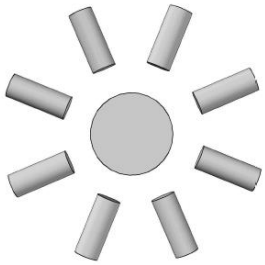

b. Top View

Figure 3.10. Schematic Diagram of the Detectors for RPT Technique

Table 3.1. Coordinates of the RPT Detectors

Detector #	r, cm	Θ,^{0}	Z, cm	Detector #	r, cm	Θ,^{0}	Z, cm
1	12.7	115	30	15	12.7	295	30
2	12.7	70	44	16	12.7	250	44
3	12.7	115	58	17	12.7	295	58
4	12.7	70	72	18	12.7	250	72
5	12.7	115	86	19	12.7	295	86
6	12.7	70	100	20	12.7	250	100
7	12.7	115	114	21	12.7	295	114
8	12.7	25	37	22	12.7	205	37
9	12.7	340	51	23	12.7	160	51
10	12.7	25	65	24	12.7	205	65
11	12.7	340	79	25	12.7	160	79
12	12.7	25	93	26	12.7	205	93
13	12.7	340	107	27	12.7	160	107
14	12.7	25	121	28	12.7	205	121

Figure 3.11 shows the laser-equipped aluminum dummy detector that was used. The detectors were arranged to cover the fully developed flow region, which was 30 cm to 145 cm from the distributor.

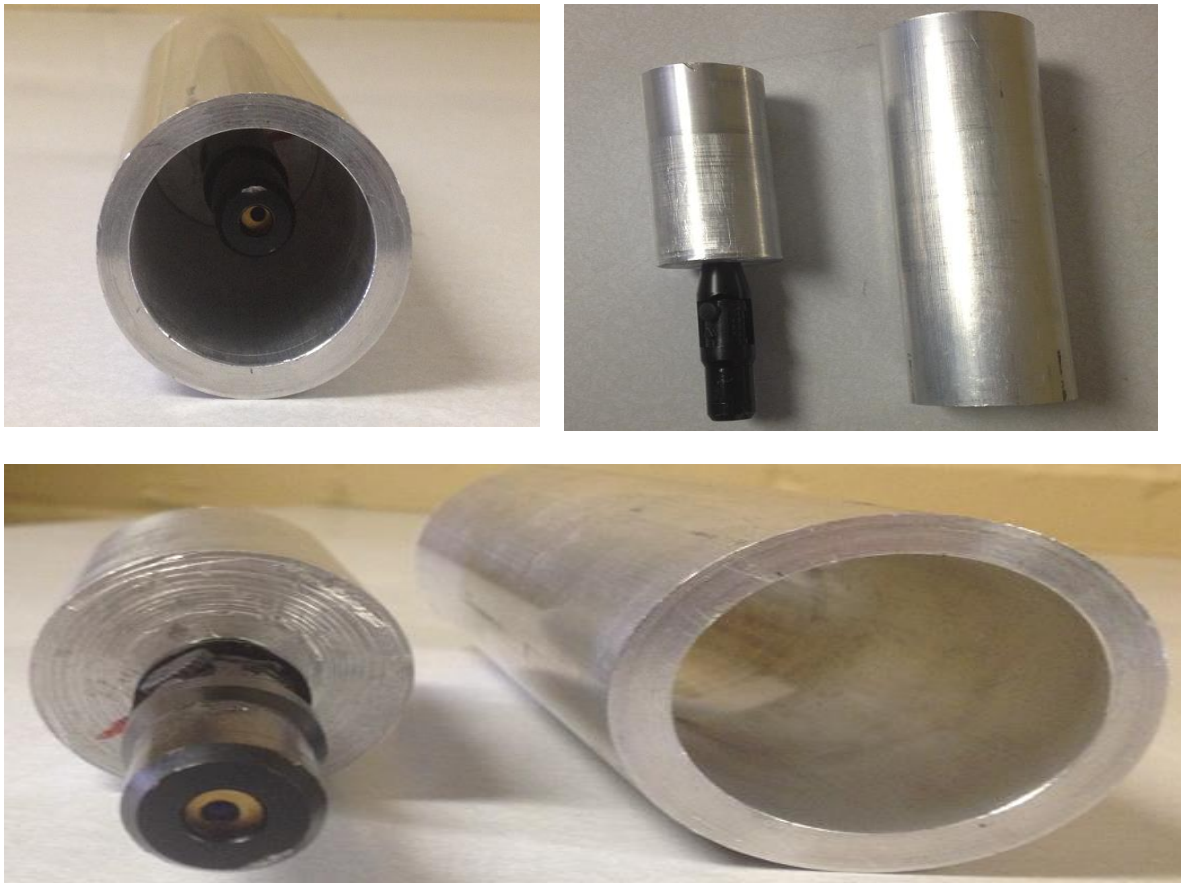

Figure 3.11. Photo of Laser-Equipped Aluminum Dummy Detector

3.4.4. RPT Experiment Conditions. All RPT experiments were conducted in the Plexiglas bubble column introduced previously. In addition, the dynamic bed height was maintained constant at 1.4 m from the gas distributor in all experiments, and mesh covered the air exit to prevent the loss of radioactive particles. Superficial gas velocities of 8, 20 and 45 cm/s were selected to obtain the overall map of the flow dynamics in the studied system. The 8 cm/s value was selected to prevent maldistributions; this value most likely occurs at the beginning of the churn-turbulent regime based on previous studies (Krishna et al., 1991; Rados, 2003; Shaikh, 2007) identifying the transition region. While a superficial gas velocity of 20 cm/s occurs at the fully developed turbulent region (Rados, 2003). The 45 cm/s value was selected because industrial processes operate at a high superficial gas velocity. Additionally, a sampling frequency of 50 Hz was selected for sample collection. To study the effect of internals on the field velocity and turbulence parameters, the hollow Plexiglas internals with a 0.31 cm wall thickness and closed ends were used to reduce the attenuation of the internal materials. The internals were secured by many honeycomb plats to prevent them from vibrating.

3.4.5. Calibration. A fully automated calibration device was developed and implemented, as shown in Figures 3.12 and 3.13. The first version of this automatic calibration devise was developed by Luo (2007). The second version was developed at Missouri S&T and manufactured by Pat Harkins (St. Louis, MO, Harkins Specialties, L.L.C.). The device can automatically move a calibration rod with a composite particle attached to its tip to several hundred or thousand known locations inside the column. The three available rods, each with a length of 3 ft, can be connected as needed to create a long calibration rod. The movements of the motors are computerized and integrated with

the data acquisition program; thus, the counts received by each detector are recorded automatically along with the data acquisition. Luo (2005) provided a description of this type of automated calibration device.

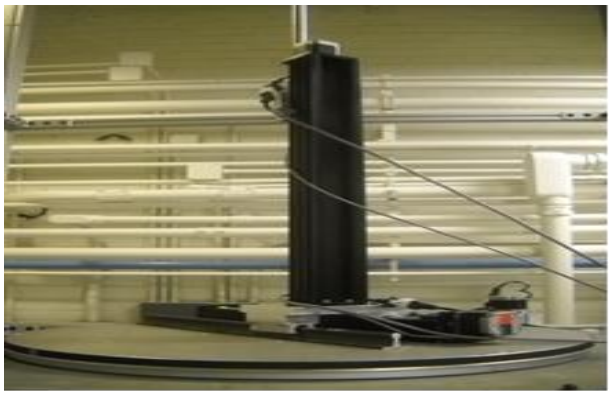

(a) Calibration Plate

(b) Photo of Calibration Device (inside)

(c) Photo of Calibration Device (outside)

Figure 3.12. Calibration Device and RPT Setup

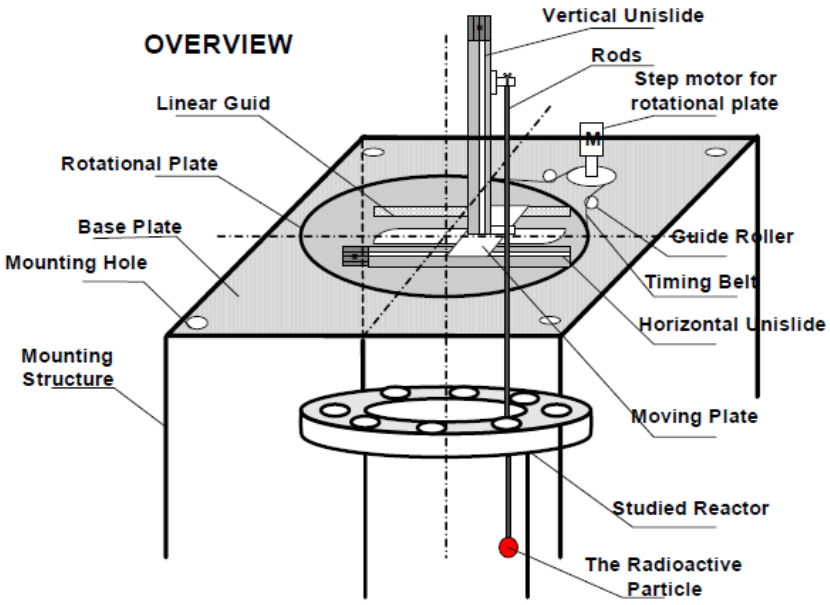

Source: Luo, 2007

Figure 3.13. Schematic Diagram of the Calibration Device

The intensity of radiation (counts) received by the detectors is a function of the distance between the radioactive particle and the detector, the medium path between the particle and the detector, and the solid angle. Therefore, the calibration experiment was conducted under the same operating conditions as the actual experiment, and the detector and the column wall were kept as close as possible to reduce the effect of the solid angle.

The calibration was performed for 1,960 known locations, which were selected to cover the fully developed region. The locations were distributed uniformly among 40 levels, with increments of Δz =2.54 cm along the axial detraction and 49 locations at each calibration level.

Hence, the relationship between the intensity of radiation (counts) and the location of the particle was obtained for all detectors. The particle was allowed to move freely into the column, acquiring data at a sample frequency of 50 Hz over 12 hours to assure that it visited each compartment of column.

3.4.6. RPT Reconstruction Algorithm. The reconstruction procedure used in this work is described only briefly here as more detail is available in Deglessan (1997), Rados (2003) and the RPT manual (2009). First, the calibration curve of the tracer particle is fitted using beta-spline fitting, and the beta-spline coefficients are obtained for each detector. The distance of the tracer particle to all detectors can be evaluated from the recorded counts during a real particle tracking experiment based on beta-spline coefficients. The relationship generated by the calibration data and the counts obtained by tracking were used to reconstruct the instantaneous position of the particle, which was accomplished using the reconstruction algorithm of Degaleesan (1997) and Rados (2003). Thus, the liquid velocity, turbulence parameters and others could be calculated after removing the background noise in the Lagrangian trajectories by using a discrete wavelet transformation (DWT) threshold filtration analysis developed by Degaleesan (1997). The velocity field, turbulence parameters and eddy diffusivities were calculated according to Degaleesan (1997) and Rados (2003) after removing the white noise from the particle trajectory data. The associated results, as well as more detail regarding the data reconstruction and processing procedures, are discussed in Section 5.

4. COMPUTED TOPOGRAPHIC STUDY OF GAS HOLDUP DISTRIBUTION

One of the main objectives of this work is to evaluate the effect of superficial gas velocity and dense internals on the gas holdup and its distribution. The overall gas holdup, cross-sectional distribution of gas holdup and the time-averaged gas holdup radial profiles are discussed in this section. The effects of the superficial gas velocity based on the total cross-sectional area (CSA) of the column, as well as the effect of internals on the overall gas holdup, are discussed in the first subsection, as is an estimation of the effect of the superficial gas velocity based on the free CSA of the column. Then, the effect of superficial gas velocity and internals on the time-averaged gas holdup radial profile and its cross-sectional distribution using CT is discussed. The time-averaged cross–sectional gas holdup in bubble columns without internals was measured to benchmark the gas holdup of the bubble column with internals.

4.1. OVERALL GAS HOLDUP

The overall (average) gas holdup was obtained by measuring the change in the bed height (Equation 17):

$$\varepsilon_g = \frac{H_{dynamic\ bed\ height} - H_{static\ bed\ height}}{H_{dynamic\ bed\ height}} \tag{17}$$

Figure 4.1 illustrates the effect of the internals and superficial gas velocities based on both the total and free CSA of the column on the overall gas holdup in the air-water system.

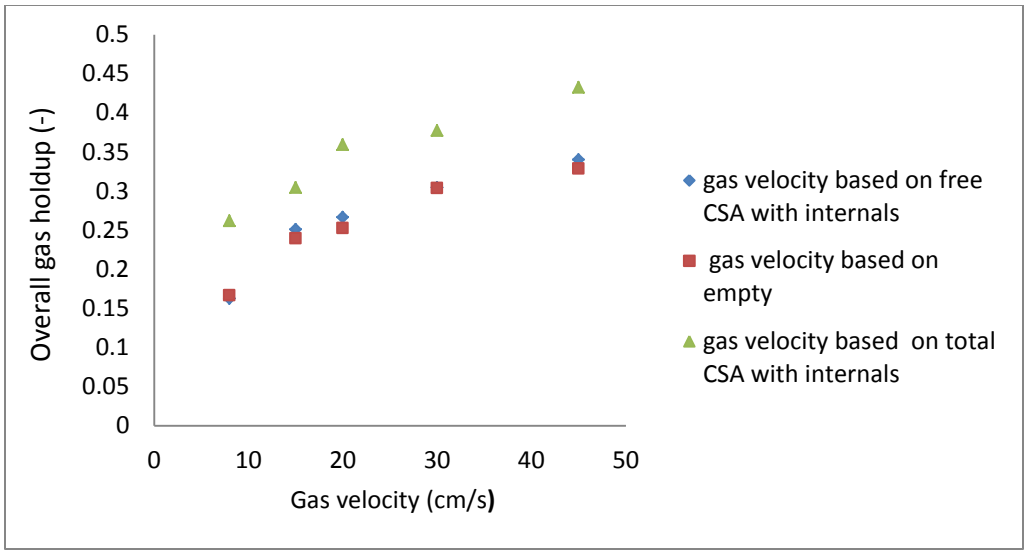

Figure 4.1. Effect of Internals and Superficial Gas Velocity on Overall Gas Holdup in Air–Water System

The overall gas holdup acted as a function of the superficial gas velocity both with and without internals; in both the total and the free CSA, the overall gas holdup increased with an increase in the superficial gas velocity. No significant effect on the overall gas holdup was observed with or without internals in the case of superficial gas velocity based on the free CSA. For example, at 45cm/s, the overall gas holdup with internals was 0.34, while for an empty column, it was 0.33. This finding can be attributed to the fact that a smaller mass of gas was introduced to the column with internals compared to that without internals to maintain the same gas velocity because internals decrease the area available for the flow. On the other hand, a significant effect was observed after applying the superficial gas velocity based on the total CSA of the column; for instance, the increase in the magnitude value of overall gas holdup with and without internals was approximately 38% and 21% at 8 and 45 cm/s, respectively, based on the

total CSA. This also occurred because the same mass of gas was introduced to the column with internals compared to that without internals, where a smaller CSA was available for the flow, which yielded a higher actual gas velocity inside the column. These results agree with all previous reported studies (e.g., De et al., 1999; Youssef, 2010; Jhawer, 2011).

To distinguish between the superficial gas velocities based on the total CSA (Case 1) and that based on the free CSA (Case 2), the flow rate was altered between the two cases. In Case 1, the gas velocity was multiplied by the total CSA of the column, and in Case 2, it was multiplied by the free CSA of the column (total CSA of column – total CSA of all internals). Therefore, the mass flow rate in Case 2 was lower than that in the case of the empty column and in Case 1, but the velocities remained the same. The superficial gas velocities based on the free CSA were used in order to assess whether the findings obtained in bubble columns without internals could be extrapolated to and used for the bubble columns with internals at the same gas velocity based on the free CSA. Most of the reported studies on bubble column reactors equipped with internals were performed under superficial gas velocities based on the total CSA. In this case, the same mass flow of gas was introduced to the columns with and without internals; hence, less CSA was available for the flow in the column with internals, causing the actual gas velocity to be higher than that in the column without internals.

4.2. LOCAL GAS HOLDUP

4.2.1 Reproducibility of CT Measurements. Before beginning a CT measurement, one of the most important factors to consider is the reproducibility of the experiments. CT measurements were repeated on two different batches of tap water on different days to demonstrate reproducibility. The results, which correspond to a superficial gas velocity of 30 cm/s, appear in Figure 4.2.

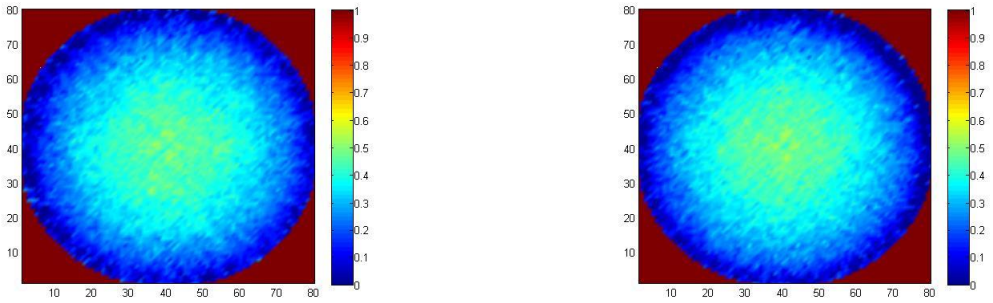

run # 1 run# 2

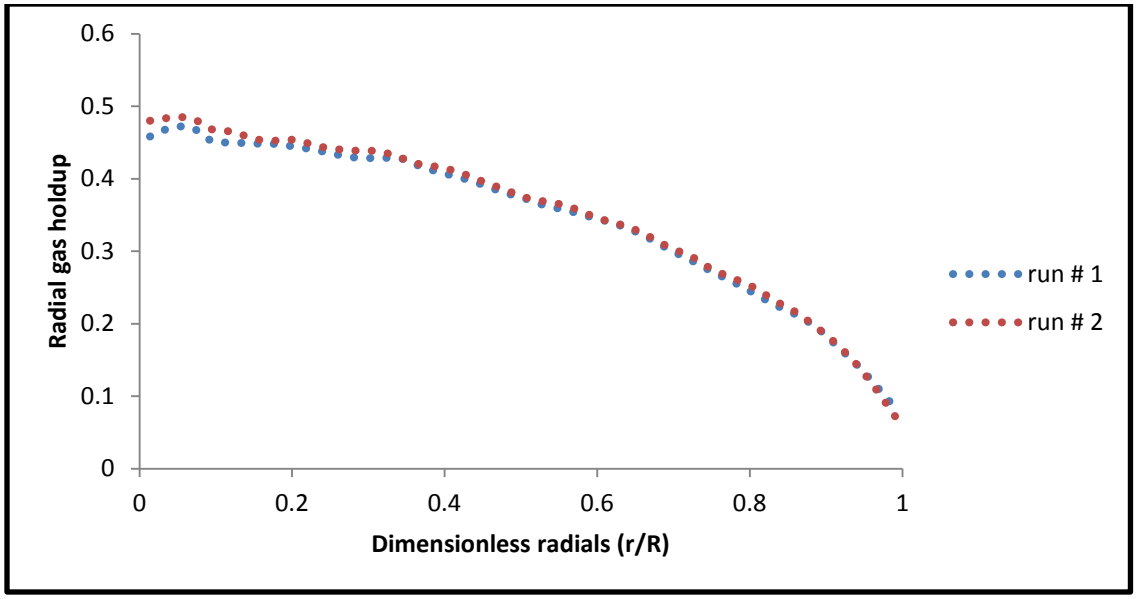

Figure 4.2. Reproducibility of Radial Gas Holdup Profiles and Its Cross-Sectional Distributions at Superficial Gas Velocity of 30 cm/s Using Two Different Batches of Water on Two Different Days

The results illustrated in Figure 4.2 indicate very good agreement among radial holdup profiles. At most radial positions, the radial gas holdup values were identical. The few differences were acceptable because they fell within ± 2% error. Accordingly, the error bars are not indicated on the data points in the following figures because they occurred within the acceptable range.

In addition, in order to further reduce uncertainty regarding the measurement and results, this study's findings pertaining to the shape of the gas holdup radial profiles were verified by a four-point optical probe measurement technique. The four-point optical probe has been used in many studies (e.g., Frijlink, 1987, Xue, 2003; Xue, 2004; Xue et al., 2008; Youssef, 2010; Jhawar, 2011) to study bubble behavior, such as local gas holdup, bubble velocity, specific interfacial area and bubble chord length. Details regarding the four-point optical probe have been discussed by Xue (2004). The four-point optical probe was used in this work to compare the CT results. In this case the gas holdup values in the pixels of the same line of measurement as the optical probe were taken. Measurements were taken at several points at appropriate increments to ensure that these points covered a variety of areas among the internals and matched the CT increments.

Figure 4.3 indicates that the radial gas holdup profile shapes and trends obtained using CT match those obtained using the four-point optical probe. As noted previously, published studies that investigated the effect of internals on the radial gas holdup profile did not report the shape of the profile because of a lack of point measurements taken along the radius or diameter of the column, e.g., only three or four points were measured to investigate the effect of dense internals.

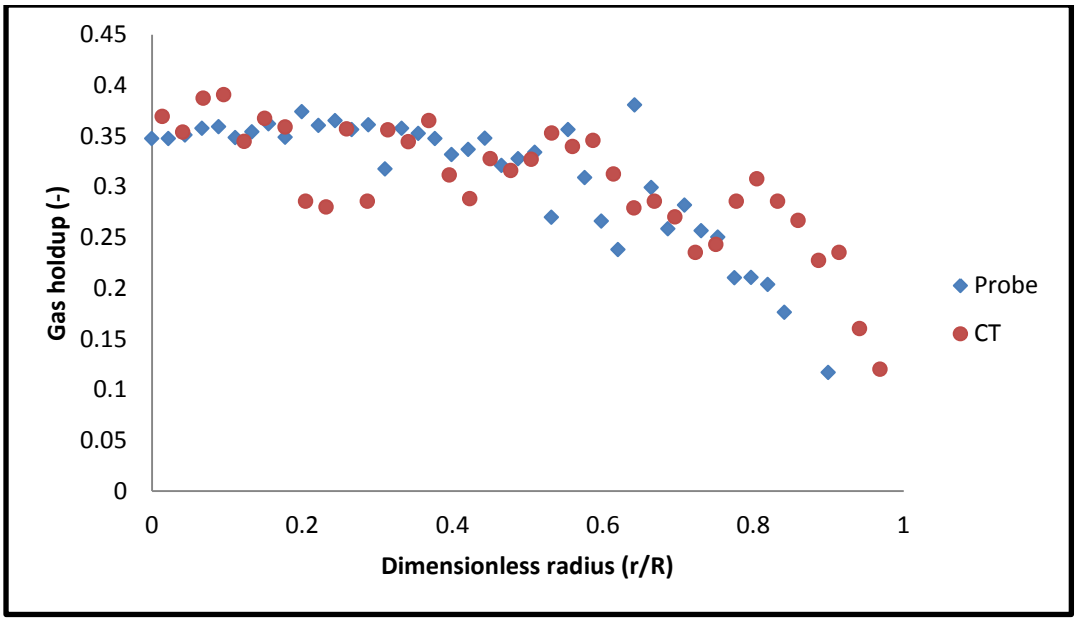

a) 8 cm/s

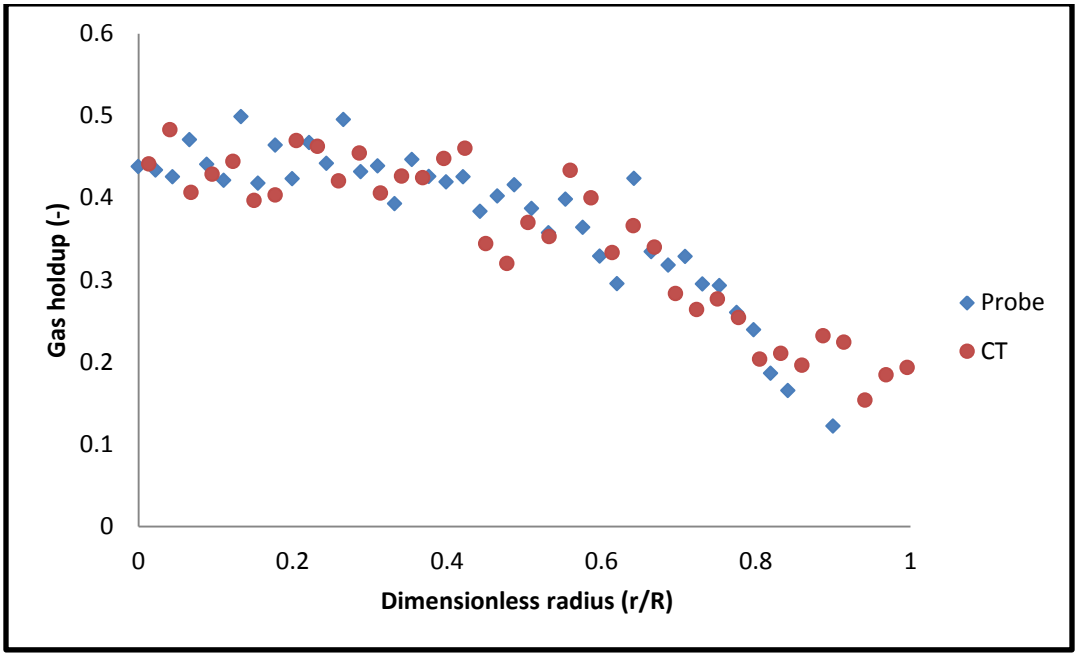

b) 20 cm/s

Figure 4.3. Comparison of Local Gas Holdup Obtained by the Four-Point Optical Probe (Courtesy of Moses, 2012) and CT

4.2.2. Cross-Sectional Gas Holdup Distribution without Internals. Figure 4.4 illustrates the cross-sectional, time–averaged gas holdup distribution in the air-water system at different superficial gas velocities, offering an idea of how gas is distributed through the column. The color variation indicates the change in the gas holdup magnitude value. Red indicates a higher gas holdup value, while blue indicates a lower value. The gas holdup increases with an increase in the superficial gas velocity. These images show approximate symmetry in the gas holdup distribution, a finding consistent with previous studies (Kumar, 1994; Chen et al., 1998; Ong, 2003; Rados, 2003). Figure 4.5 displays the probability density functions of the gas holdup distribution values in the pixel cells. Such a gas holdup distribution PDF characterizes the gas holdup variation values along the pixel cells at different superficial gas velocities. The variation in the corresponding mean, variance and standard deviation, which were directly calculated by MATLAB functions, increased with an increase in superficial gas velocity from bubbly flow regime toward churn turbulent flow regime. The maximum variance of gas holdup was found to be less than 1.8%, while the standard deviation varied less than 13%.

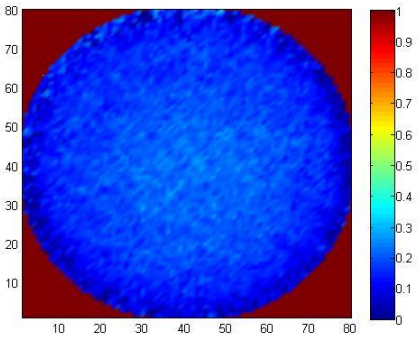

a) 5 cm/s

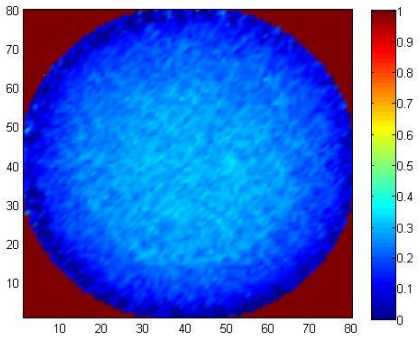

b) 8 cm/s

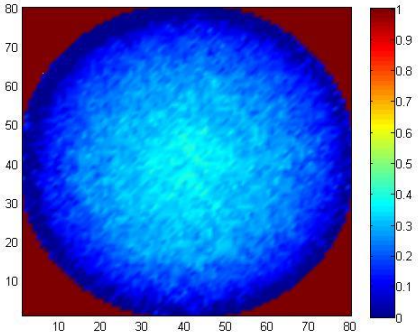

c) 15 cm/s

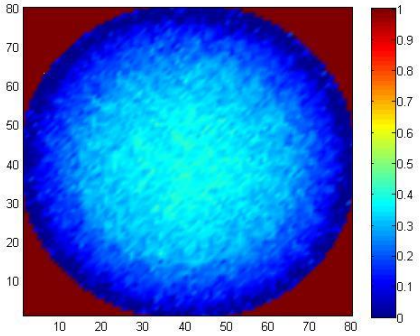

d) 20 cm/s

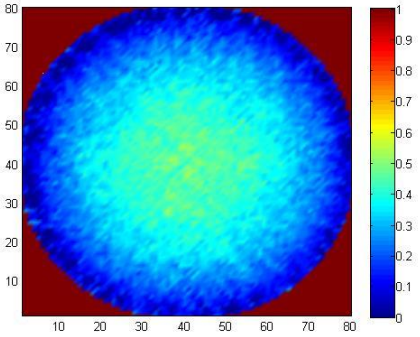

e) 30 cm/s

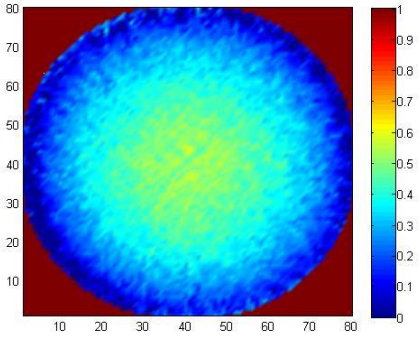

f) 45 cm/s

Figure 4.4. Cross-Sectional Gas Holdup Distribution at Various Superficial Gas Velocities

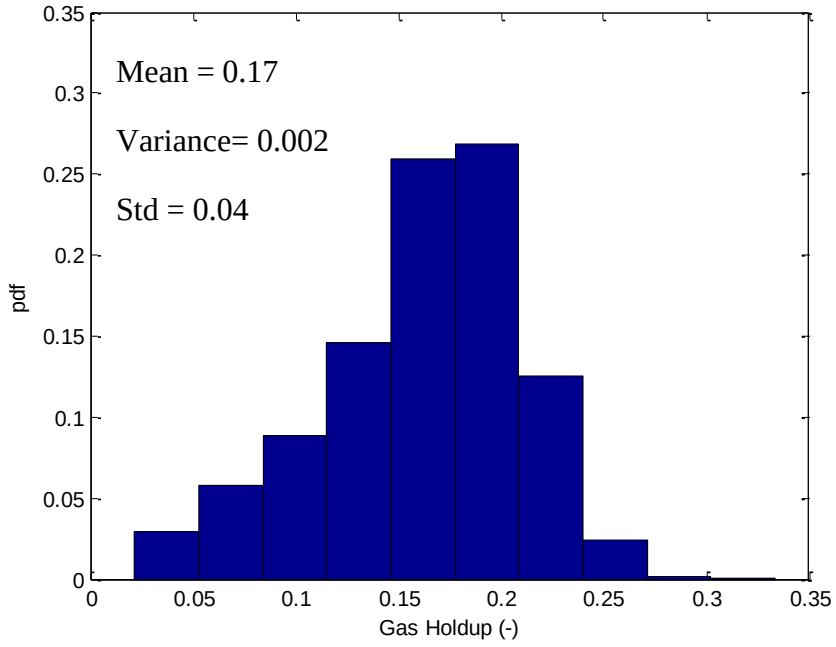

(a) 5cm/s

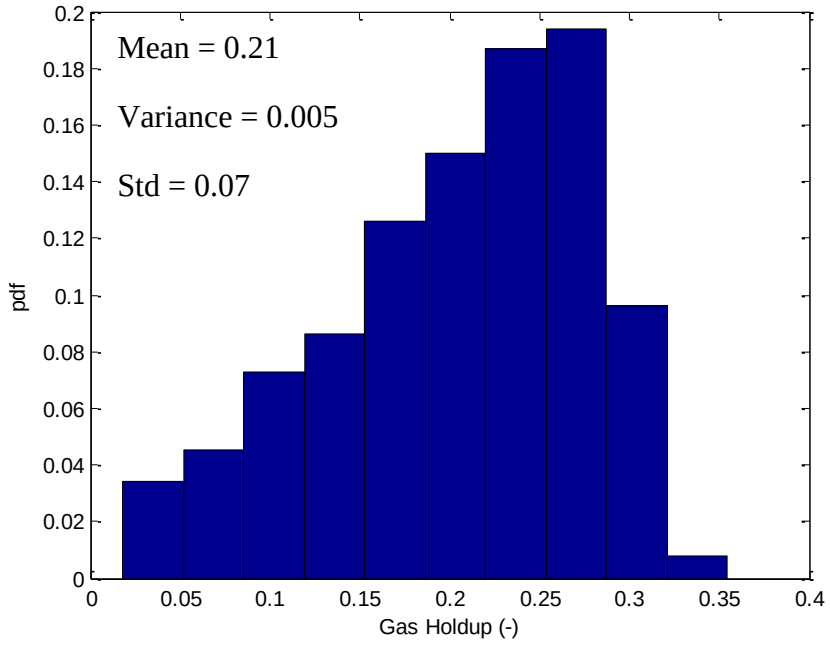

(b) 8 cm/s

Figure 4.5. Probability Density Functions of the Values of Gas Holdup in the Pixel Cells

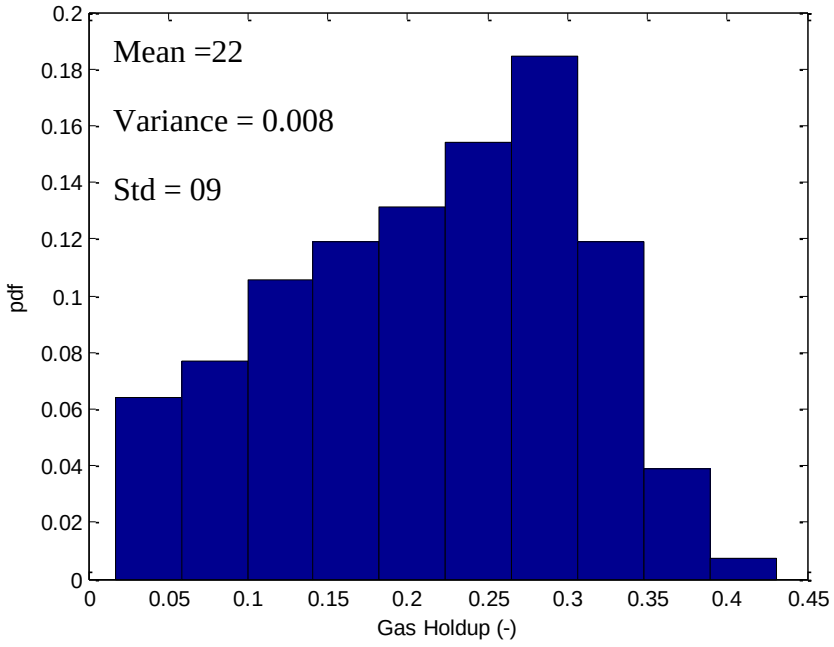

(c) 15 cm/s

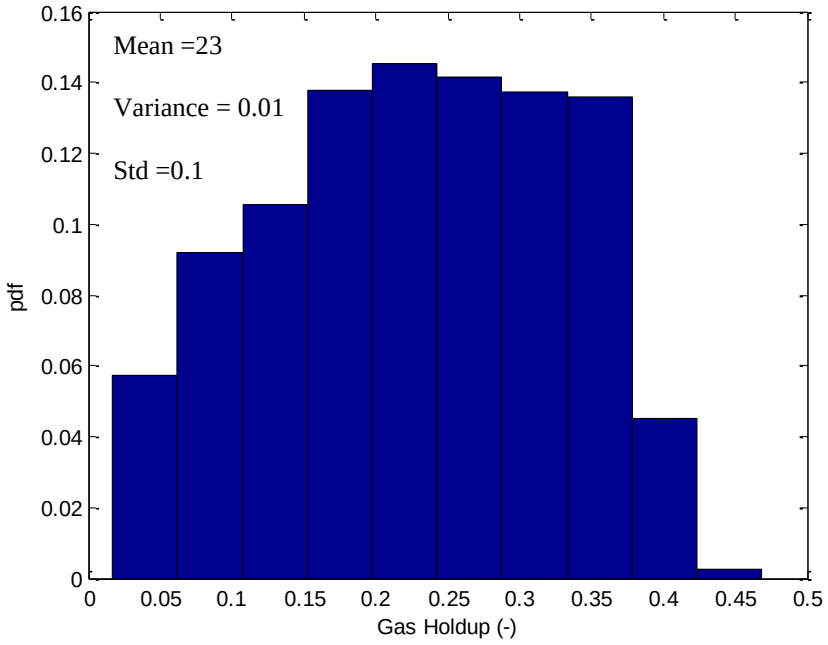

(d) 20 cm/s

Figure 4.5. Probability Density Functions of the Values of Gas Holdup in the Pixel Cells (cont).

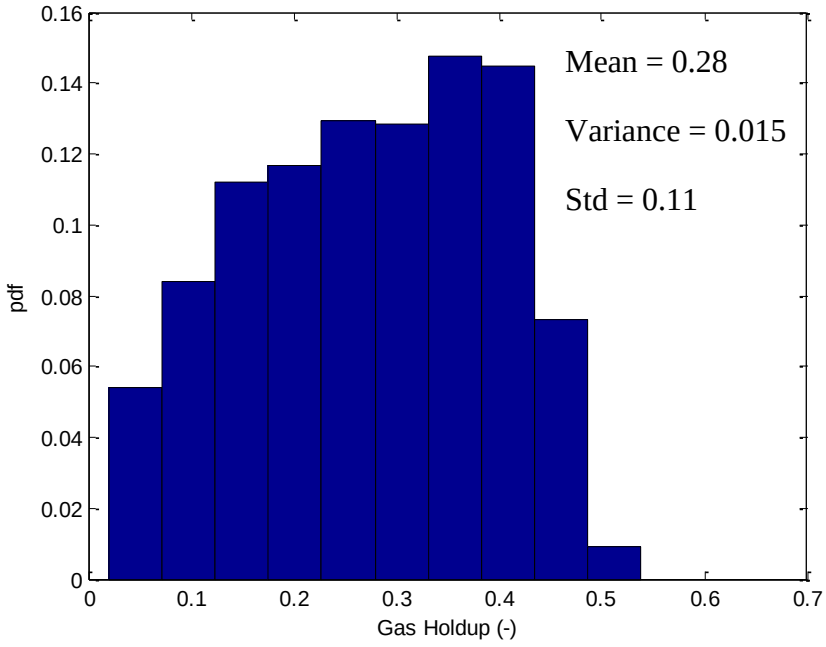

(e) 30 cm/s

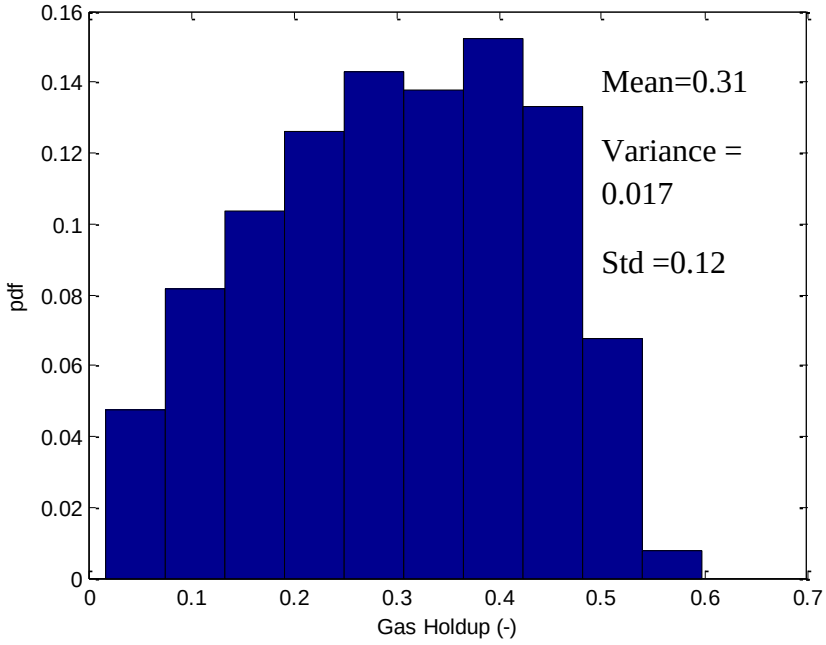

(f) 45 cm/s

Figure 4.5. Probability Density Functions of the Values of Gas Holdup in the Pixel Cells (cont.)

Table 4.1 compares the mean value gas holdup distribution and the average radial gas holdup, $\bar{\varepsilon}_g$. The difference between the mean and average radial gas holdup was found to increase somewhat with an increase in superficial gas velocity. Such a small difference and variation reflect axisymmetric flow in the bubble column reactor.

Table 4.1. Comparison of the Mean Gas Holdup Value with the Average Radial Gas Holdup

Superficial gas velocity, cm/s	Mean	$\bar{\varepsilon}_g$
5	0.17	0.18
8	0.21	0.23
15	0.22	0.25
20	0.23	0.28
30	0.28	0.34
45	0.31	0.38

4.2.3. Effect of Superficial Gas Velocity on Time-Averaged Gas Holdup Radial Profile without Internals. The effect of the superficial gas velocity on the time-averaged gas holdup radial profile at different superficial gas velocities was investigated. All CT scans were acquired at one fixed axial position (5.8 d_c) in the fully developed region. With an increase in the superficial gas velocity, the magnitude value of the gas holdup increased along the radial position, the gas holdup magnitude value was about 0.22 at 5 cm/s and the magnitude of gas holdup increased by ~ 42%, 46% and 57.7%

when the superficial gas velocity increased from 5 cm/s to 8 cm/s, 20 cm/s, and 45 cm/s, respectively (Figure 4.6). At lower superficial gas velocities corresponding to the homogenous (bubbly) flow regimes, the magnitude value of the gas holdup at the region close to the wall was found to be larger than that obtained at some higher velocities. This finding qualitatively agrees with the results achieved by Kumar (1994). Figure 4.6 clearly shows that the maximum gas holdup was obtained in the center of the column and progressively decreased towards the walls. This result can be explained by the fact that gas bubbles tend to segregate at the core of the column where there is less shear stress than near the walls, which leads to gross liquid circulation throughout the column, with liquid flowing up in the center and down near the walls (Chen et al., 1999).

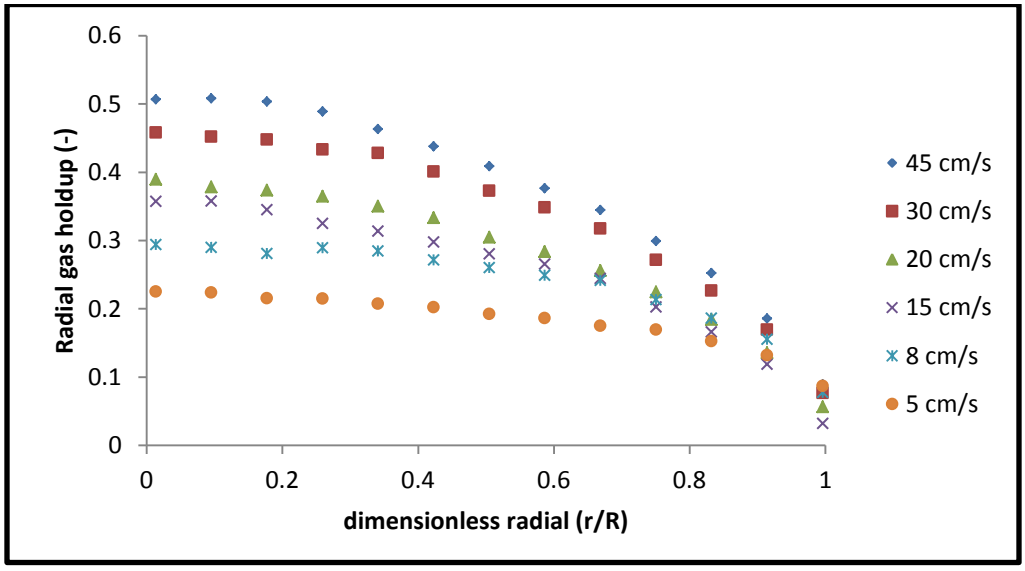

(a) Radial Gas Holdup Profiles at Different Superficial Gas Velocities

Figure 4.6. Radial Gas Holdup Profiles at Different Superficial Gas Velocities in Air-Water System (No Internals)

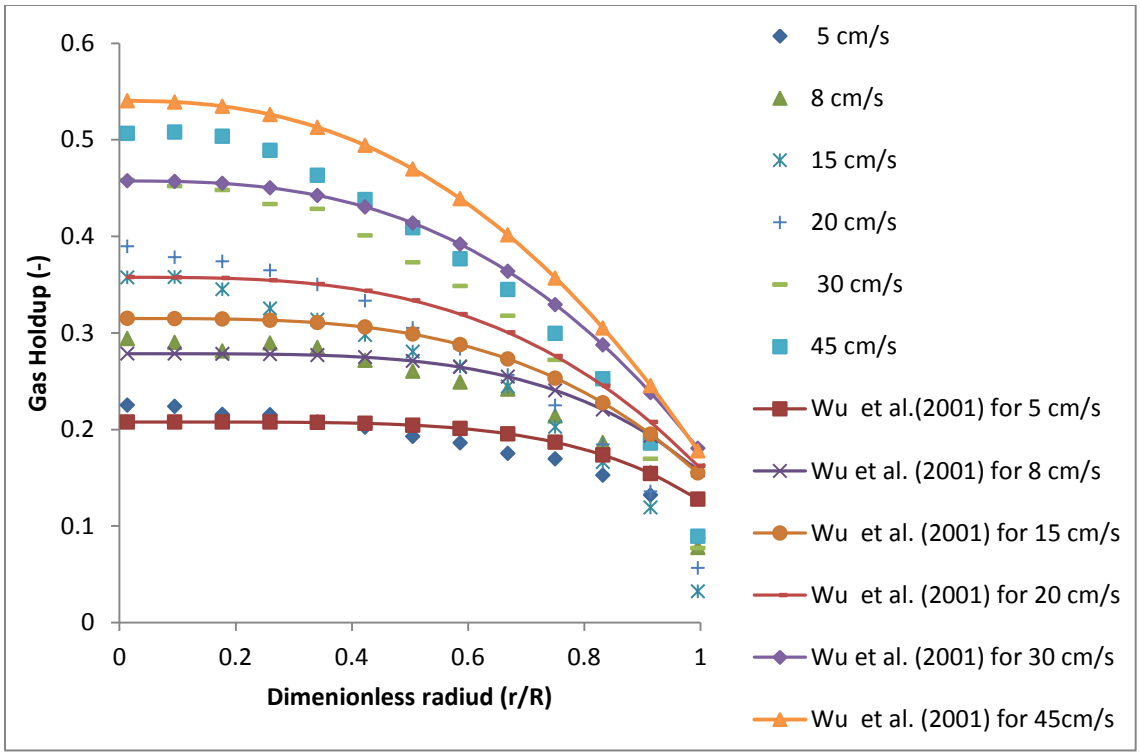

(b) Radial Gas Holdup Profiles with Fitted Steepness Parameters

Figure 4.6. Radial Gas Holdup Profiles at Different Superficial Gas Velocities in Air-Water System (No Internals) (cont.)

Figure 4.6 illustrates that when the superficial gas velocity increased, the gas holdup radial profile became steeper and more parabolic (Hills, 1974; Kumar, 1994; Joshi et al., 1998; Rados, 2003; Ong, 2003). The gas holdup radial profiles obtained from CT were compared to the correlation proposed by Luo and Svendsen (1991):

$$\varepsilon_g = \bar{\varepsilon}_g \left(\frac{n+2}{n+2-2n}\right)\left[1 - c\left(\frac{r}{R}\right)^n\right] \qquad (18)$$

where $\bar{\varepsilon}_g$, n, c and r/R are the radial averaged gas holdup, steepness parameter, wall holdup parameter and dimensionless radius, respectively.

The parameters (n,c) in Equation (18) were calculated based on correlations proposed by Wu et al. (2001) for n and c in terms of the following dimensionless groups, which are most dominant for gas holdup:

$$n = 2.188 \times 10^{3} {Re_G}^{-0.598} {Fr_g}^{0.146} {Mo_L}^{-0.004} \quad (19)$$

$$c = 4.32 \times 10^{-2} {Re_G}^{0.2492} \quad (20)$$

Figure 4.6b shows that with an increase in superficial gas velocity, the value of n decreased. For example, the value of n was 4.71, 4.0, 3.4, 3.1, 2.7 and 2.4 for 5 cm/s, 8 cm/s, 15 cm/s, 20 cm/s, 30 cm/s and 45 cm/s, respectively. The value of n was large for flat profiles (as observed at lower velocities), but small for steep profiles (as observed at higher velocities). The gas holdup profiles obtained using the values of n and c proposed by Wu et al. (2001) did not correlate well at high gas velocities or close to the wall of the column. The gas holdup values close to the column's wall were larger than those obtained from CT. However, those values correlated well using a single value of c of 0.8 (not shown in the Figure). This result can be attributed to the fact that small bubbles distribute uniformly across the column's central region at a low rate at lower velocities, while large bubbles form at higher velocities due to coalescence and move towards the column's center at a high rate. Thus, where large bubbles move, large voids form.

4.2.4. Cross-Sectional Distribution of Gas Holdup and the Time-Averaged Gas Holdup Radial Profiles in the Presence of Internals. As noted previously, it is of particular importance to understand the effect of internals on the hydrodynamics in bubble column reactors because most of their applications require them to be equipped with internals. The effect of internals (25% covered CSA) on the time–averaged gas

holdup radial profile was investigated at different superficial gas velocities based on either the total CSA or free CSA of the column. The data obtained from CT scan image processing for the time-averaged cross-sectional gas holdup distribution in an air-water system's bubble column with and without internals at different superficial gas velocities based on the total and free CSA are shown in Figure 4.7 a-r. Variation in the color for the gas holdup indicates a change in the magnitude value of gas holdup. These images clearly show that the presence of internals caused gas holdup (i.e. the color) variation, which depends upon the internals configuration and superficial gas velocity. In the presence of internals, the variation in the color shades for the gas holdup clearly increased with an increase in superficial gas velocity, especially at lower gas velocities, when considering either the gas velocity based on the total or free CSA. This increase occurred only at a high gas velocity based on the total CSA compared with the images obtained for the same range of velocities in the column without internals, which indicates a change in the magnitude value of gas holdup. These results have been confirmed by several researchers using different measurement methods (Pradhan et al., 1999; Youssef & Al-Dahhan, 2009; Balamurugan et al., 2010; Jhawar, 2011). The enhancement of gas holdup values in the presence of internals could be attributed to the fact that the internals cause the bubbles to break up into smaller bubbles with lower rise velocities and longer residence times, which increases the gas holdup. The scanned images also revealed that the time-averaged gas holdup distribution was symmetric over the cross-section at low superficial gas velocities, while asymmetric distribution occurred at higher superficial gas velocities, such as that at 45cm/s.

Figure 4.8 displays the probability density functions of the gas holdup distribution values in the pixel cells at selected superficial gas velocities based on the total and free CSA. The velocities of 5 cm/s, 8 cm/s, 20 cm/s and 45 cm/s based on the total and free CSA were selected based on the scanned images in Figure 4.8 and most likely cover the flow regimes observed in a bubble column. The variation in the corresponding mean, variance and standard deviation increases with an increase in the superficial gas velocity, as shown in Figure 4.8. The presence of internals results in an increase in variation of the values of the mean, variance and standard deviation compared to that obtained in an empty column without internals. As mentioned previously, the values of these variations reflect axisymmetric flow. The standard deviation at 45 cm/s based on the total CSA was found to be 15%, while the standard deviation at 5 cm/s based on the total CSA was 6%, which reflects the axisymmetric gas holdup distribution at this velocity. In addition, the difference between the mean values and the average radial gas holdup ($\bar{\varepsilon}_g$) values reveals the axisymmetric distribution of gas holdup, as seen in Table 4.2. The difference between the mean and the average gas holdup was 18% at 45 cm/s and 11% at 8 cm/s. Such a small difference reflects axisymmetric distribution of the flow. The probability density function of the gas holdup distribution value in the pixel cells clearly indicates some difference compared to gas holdup radial profiles in the presence of internals for both gas velocities based on free and total CSA, while with averaging, some of the differences even out, as seen with radial profiles at higher gas velocities.

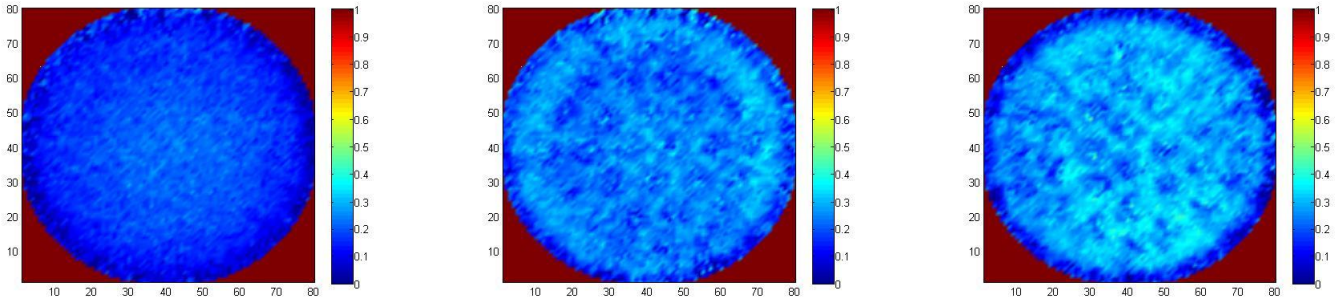

a) 5 cm/s without internals b) 5 cm/s based on free CSA c) 5 cm/s based on total CSA

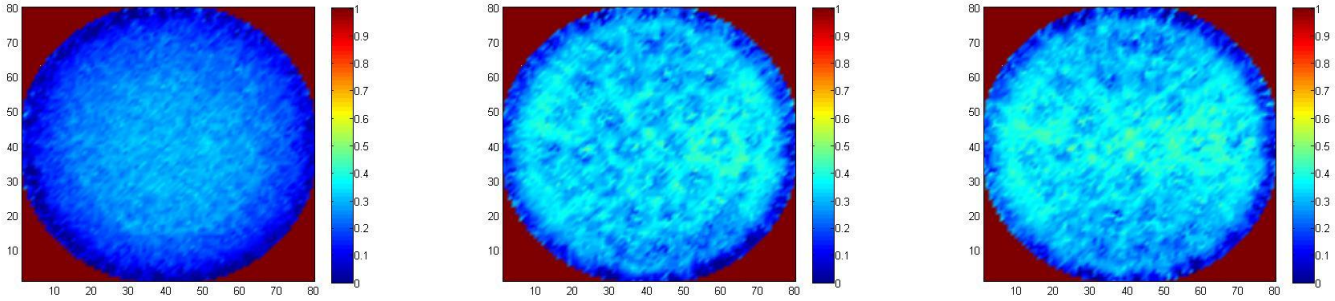

d) 8 cm/s without internals e) 8 cm/s based on free CSA f) 8 cm/s based on total CSA

Figure 4.7. Cross-Sectional Gas Holdup Distributions at Various Gas Velocities Based on Total and Free CSA for Bubble Column with and without Internals

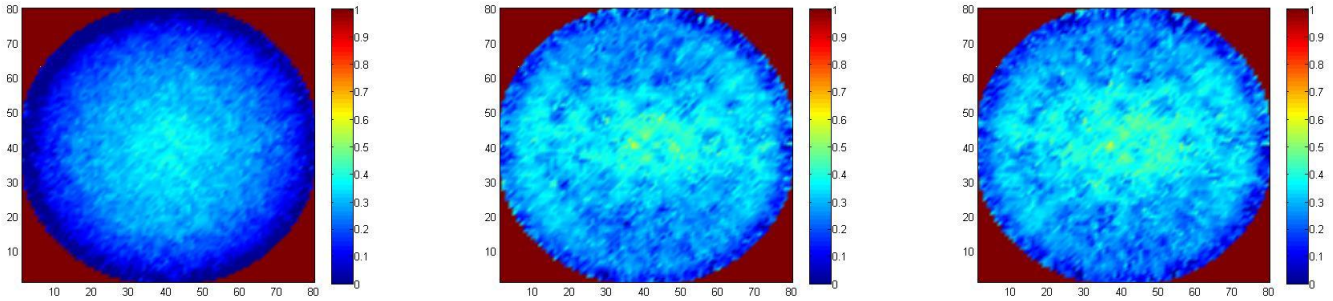

g) 15 cm/s without internals h) 15 cm/s based on free CSA i) 15 cm/s based on total CSA

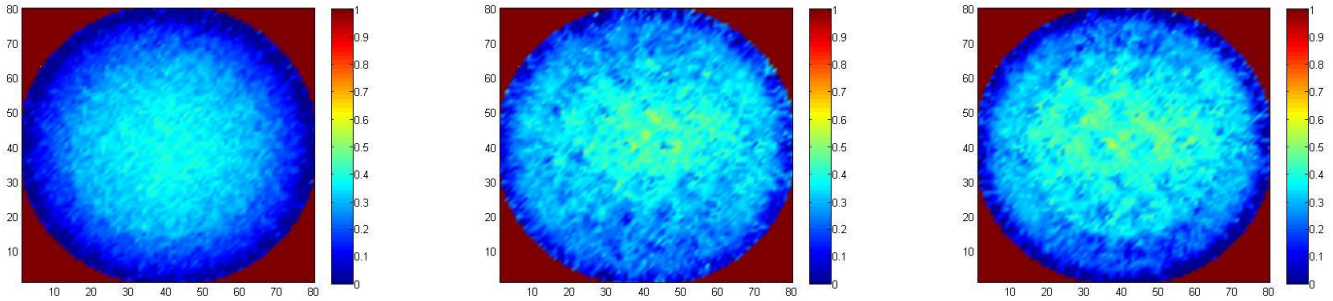

j) 20 cm/s without internals k) 20 cm/s based on free CSA l) 20 cm/s based on total CSA

Figure 4.7. Cross-Sectional Gas Holdup Distributions at Various Gas Velocities Based on Total and Free CSA for Bubble Column with and without Internals (cont.)

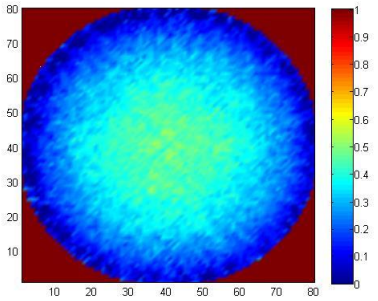

m) 30 cm/s without internals

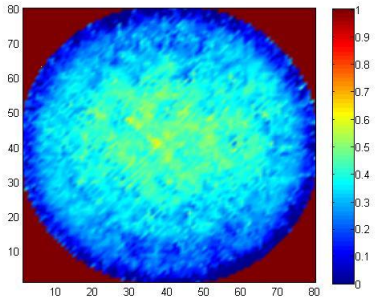

n) 30 cm/s based on free CSA

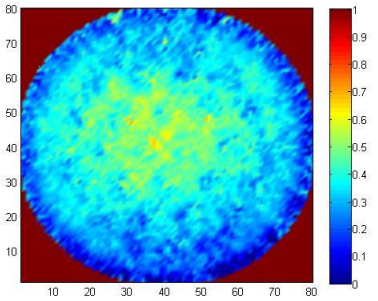

o) 30 cm/s based on total CSA

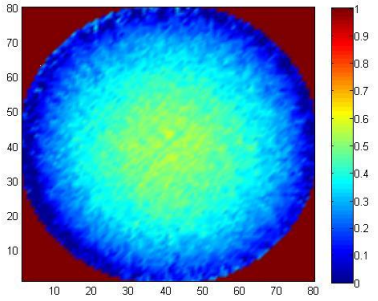

p) 45 cm/s without internals

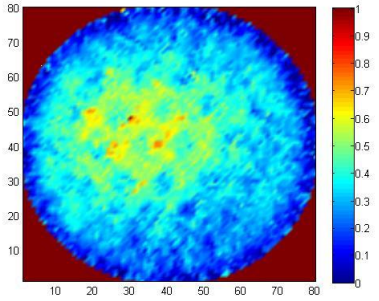

q) 45 cm/s based on free CSA

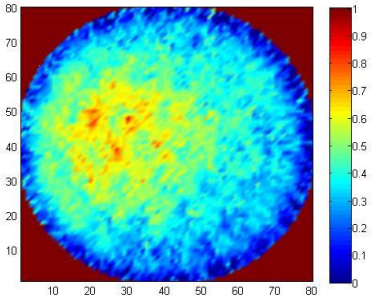

r) 45 cm/s based on total CSA

Figure 4.7. Cross-Sectional Gas Holdup Distributions at Various Gas Velocities Based on Total and Free CSA for Bubble Column with and without Internals (cont.)

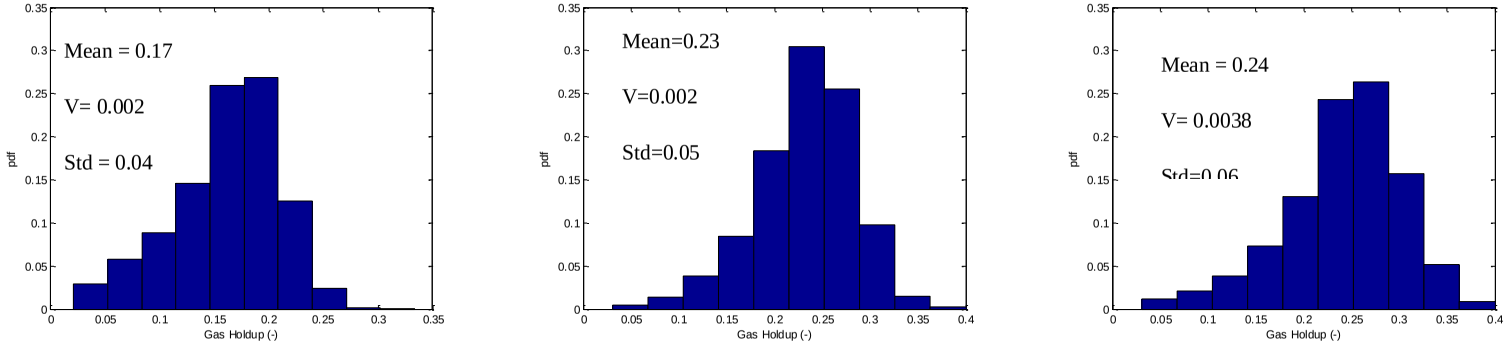

a) 5 cm/s without internals b) 5 cm/s based on free CSA c) 5 cm/s based on total CSA

d) 8cm/s without internals e)8cm/s based on free CSA f) 8 cm/s based on total CSA

Figure 4.8. Probability Density Functions of the Values of Gas Holdup Distribution in the Pixel Cells in Presence of Internals

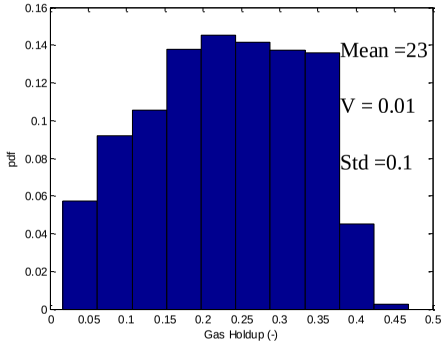

g) 20 cm/s without internals

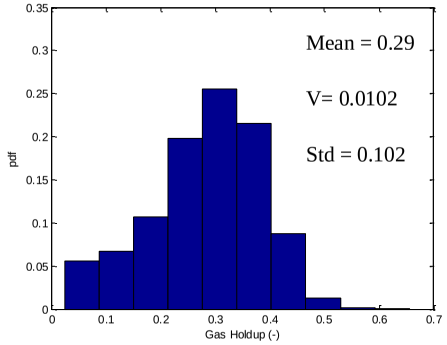

h)20 cm/s based on free CSA

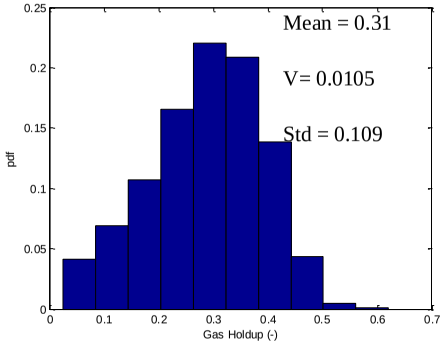

i)20 cm/s based on total CSA

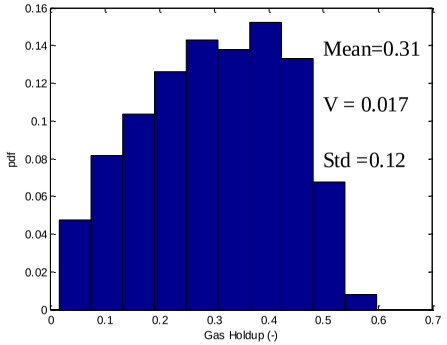

j)45 cm/s without internals

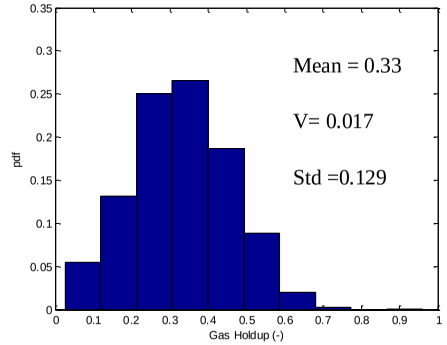

k)45 cm/s based on free CSA

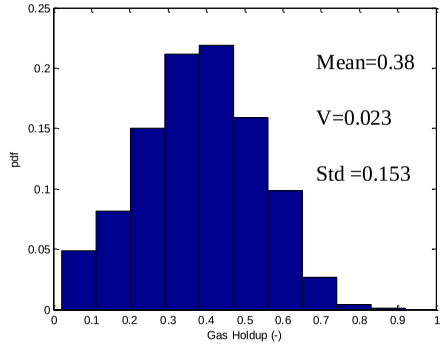

l)45 cm/s based on total CSA

Figure 4.8. Probability Density Functions of the Values of Gas Holdup Distribution in the Pixel Cells in Presence of Internals (cont.)

Table 4.2. Comparison of the Mean Value of Gas Holdup with the Averaged Radial Gas Holdup in the Presence of Internals

Superficial Gas velocity, cm/s		Mean	Variance	$\bar{\varepsilon}_g$
5	Empty	0.17	0.002	0.18
	Free CSA	0.23	0.002	0.23
	Total CSA	0.24	0.0038	0.28
8	Empty	0.21	0.005	0.23
	Free CSA	0.28	0.0058	0.32
	Total CSA	0.31	0.0063	0.34
20	Empty	0.23	0.01	0.28
	Free CSA	0.29	0.0102	0.33
	Total CSA	0.31	0.0124	0.35
45	Empty	0.31	0.017	0.38
	Free CSA	0.33	0.017	0.40
	Total CSA	0.38	0.023	0.46

Figure 4.9 depicts the effect of internals on the radial gas holdup profiles at different gas velocities based on the total and free CSA available for flow. Clearly, the presence of internals not only influences the magnitude value of the gas holdup and its distribution, but also impacts the shape of the gas holdup radial profile. With internals, the shape becomes wavy (zigzag) and less steep (flatter), while without internals, there is a smoother, more parabolic shape. As Figure 4.9 depicts, in the presence of internals, all profiles at different superficial gas velocities, either based on the total or free CSA, have the same trend and shape, which depends upon the configuration of internals (absence or presence of internals at that point). This difference in shape may be attributed to the fact that internals form small cross-sectional areas (space) for the flow of gas and liquid inside the main bubble column. Hence, each set of internals creates a certain flow pattern. The formation of smaller bubbles with internals was attributed to the flatter (less steep) radial profile of the gas holdup. As a result, the flow regime transition would be delayed and

would not occur until reaching a higher gas velocity compared to the case without internals. The sharp decrease in gas holdup near the column walls has to do with the configuration of the internals (refer to Figure 3.3), whose impact will be diminished in those areas. These results provide a very clear picture of the effect of internals on the flow pattern. This is the first study, to our knowledge, that discusses this kind of influence. Such profiles did not appear in previous investigations for the following reasons:

- Limited ability of the measurement techniques to capture and provide images of a sufficient resolution.
- Lack of point measurements taken along the radius or diameter of the column, e.g., a maximum of three or four points were taken to investigate the effect of internals on the radial gas holdup using an optical probe.
- The number of internals covering the small CSA of the column and the internals covering 5% of the column's CSA had no significant effect on the hydrodynamics (Chen et al., 1999; Youssef & Al-Dahhan, 2009; Youssef, 2010); thus, no effect on the radial gas holdup profile with internals covering 5% of the column's CSA was observed.

The gas holdup values near the wall behaved differently than in the core of the column, i.e., some gas holdup values measured at lower velocities were higher than those measured at elevated velocities; this phenomenon began at a reasonable distance from the wall. For instance, at $r/R \approx 0$, the radial gas holdup magnitude value increased by approximately 36.5% with an increase in the gas velocity from 8 cm/s to 45 cm/s based on the total CSA, while the decrease occurred close to the wall by 11% at the same

velocities. This would be attributed to the vigorous liquid circulation associated with higher gas velocities, which moves downward near the walls and energizes the breakup of bubbles. These small bubbles lose their buoyancy force and sweep away to the center, leading to much less gas holdup obtained with greater liquid circulation. Close to the column's wall, the internals configuration strongly affected the shape of the gas holdup profiles, which was observed clearly at low velocities (5 -15 cm/s). However, this effect began to disappear when the gas velocity increased from 20 – 45 cm/s due to the intensity of the liquid recirculation in this flow regime. Furthermore, the radial gas holdup profiles became steeper after 15 cm/s.

Clearly with internals, the change in the magnitude value of the gas holdup is somewhat higher at lower superficial gas velocities than at higher gas velocities. For instance, the increase in the gas holdup magnitude at the column's core was approximately 14%, 16% and 34% at 45cm/s, 20 cm/s and 8 cm/s, respectively. This indicates that the internals have a significant effect on the radial profile of gas holdup at lower superficial gas velocities corresponding to the bubbly and transition flow regimes. The effect of the internals on radial profile of gas holdup at higher superficial gas velocities decreased. When the local gas holdups in the column with internals become more similar to those in the column without internals, the CSA available for the liquid and gas flow in the column with internals will be lower. Hence, to achieve mass balance, the local gas and liquid velocities would increase in the column with internals.

The presence of internals enhanced the gas holdup magnitude values in the core of the column at all velocities based on both the total and free CSA. This enhancement diminished with an increase in the superficial gas velocity based on the free CSA; for

instance, the difference between the magnitude of gas holdup obtained with and without internals decreased from ~12% to 2% with an increase in velocity from 5 cm/s to 30 cm/s based on the free CSA. Clearly, at lower superficial velocities based on the total and free CSA, the gas holdup values increased region-wise along the column, while the radial gas holdup values obtained with and without internals in the region from $r/R \approx 0.09$ to $r/R \approx 0.7$ approach until they are approximately identical with the increase in superficial gas velocity based on the free CSA and corresponding to the heterogeneous flow regime. For instance, at $r/R= 0.5$, the absolute difference value between the profiles obtained with and without internals decreased until reaching approximately zero at 45 cm/s based on the free CSA. The difference in the profiles near the column wall and $r/R > 0.7$ in both the total and free CSA at lower velocity can be attributed to the configuration of the internals, whose impact will be eliminated in those areas. Therefore, it can be observed that the overall and radial profile of gas holdup obtained in empty columns operated in the churn turbulent flow regime can be extrapolated to bubble columns equipped with dense internals by matching the superficial gas velocity based on the free CSA available for flow.

The increase in the magnitude of the radial gas holdup at high velocities based on the total CSA is due to the effect of having the same gas mass flow as in the column without internals that must travel through a smaller CSA in the column with internals.

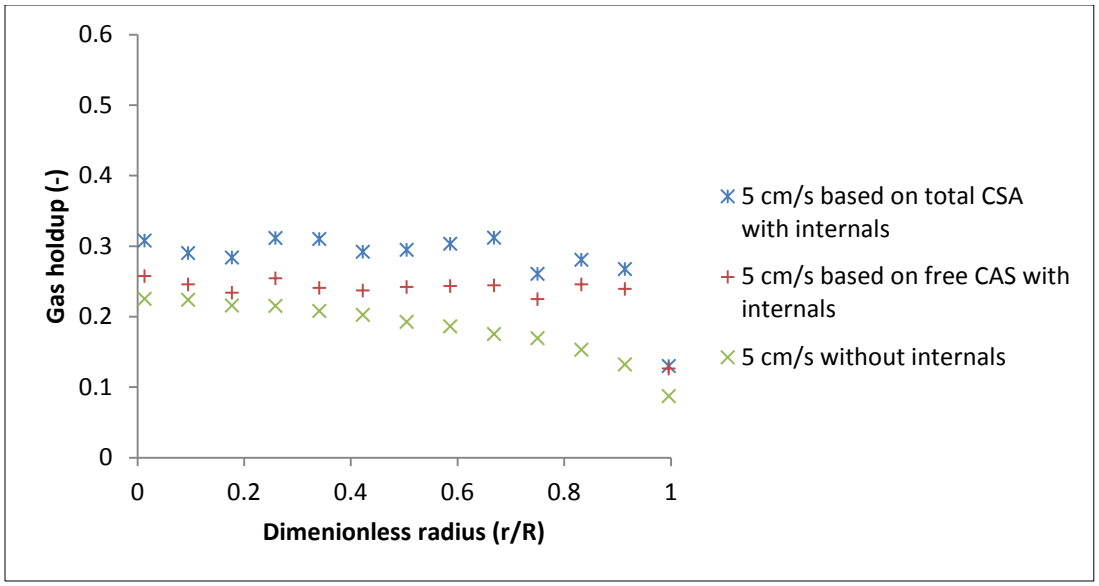

(a) 5 cm/s

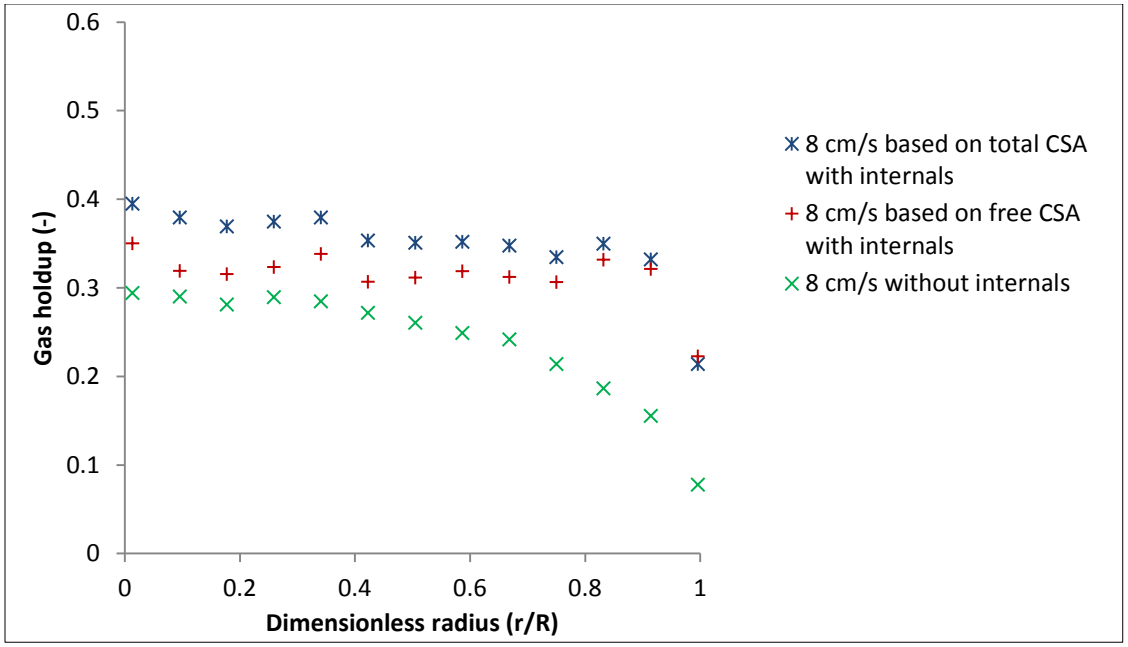

(b) 8 cm/s

Figure 4.9. Gas Holdup Radial Profiles in Bubble Column with and without Internals for Various Gas Velocities Based on Total and Free CSA

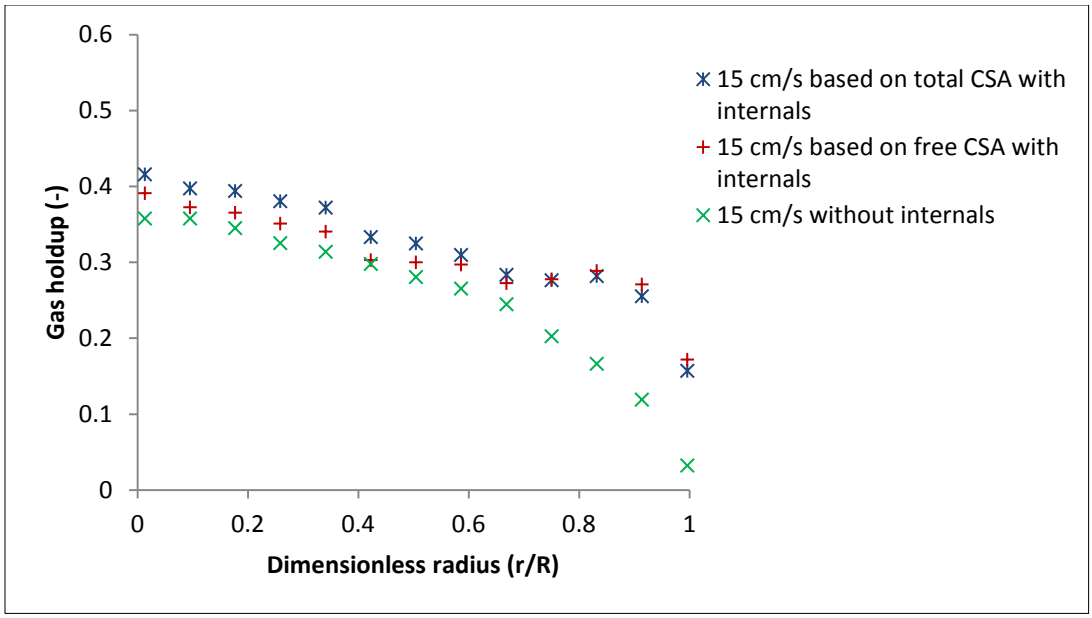

(c) 15 cm/s

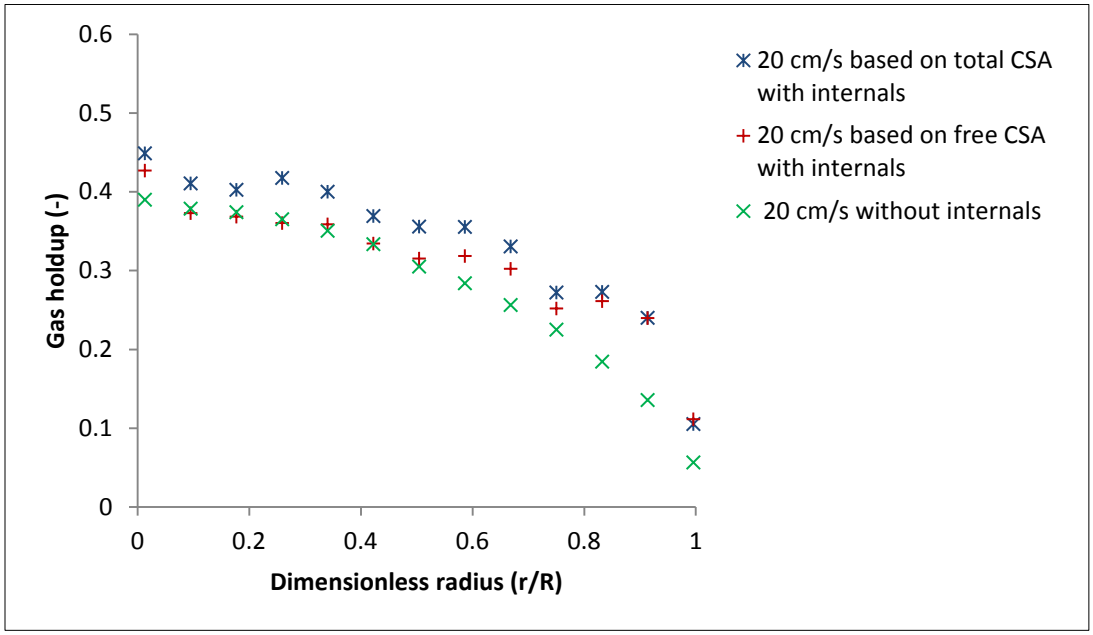

(d) 20 cm/s

Figure 4.9. Gas Holdup Radial Profiles in Bubble Column with and without Internals for Various Gas Velocities Based on Total and Free CSA (cont.)

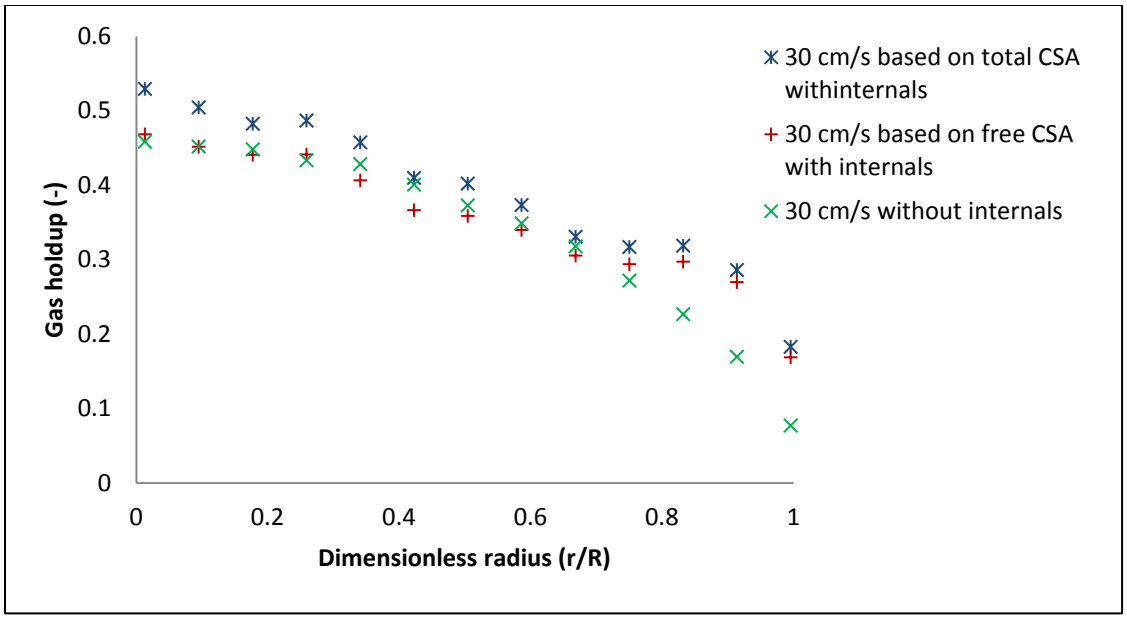

(e) 30 cm/s

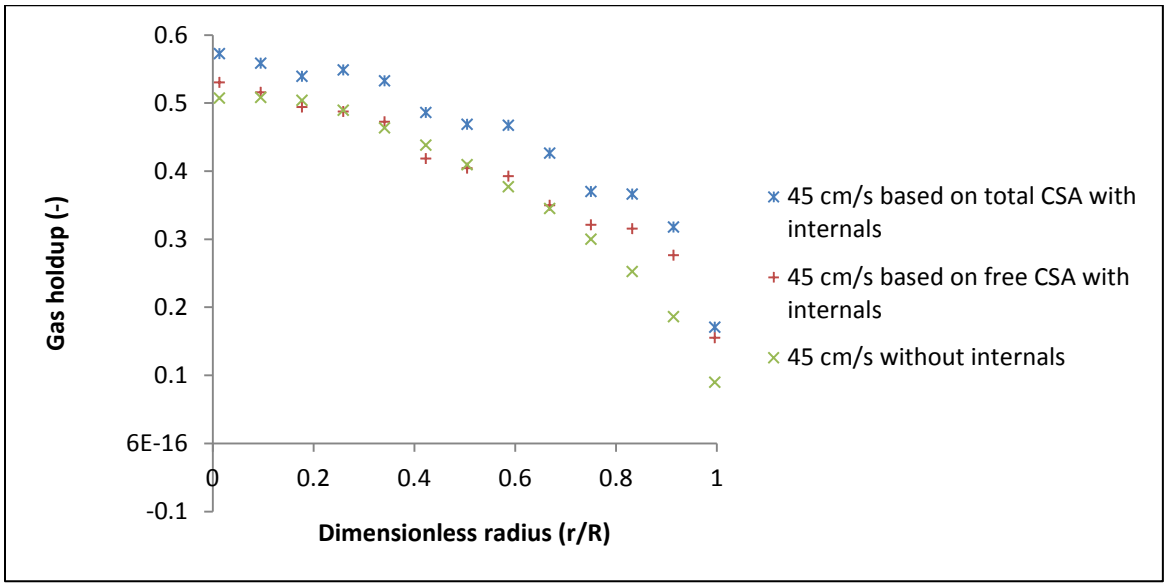

(f) 45 cm/s

Figure 4.9. Gas Holdup Radial Profiles in Bubble Column with and without Internals for Various Gas Velocities Based on Total and Free CSA (cont.)

5. RADIOACTIVE PARTICLE TRACKING STUDY OF LIQUID PHASE HYDRODYNAMICS

In this section, the results of the radioactive particle tracking (RPT) technique are presented. The experimental investigation of the hydrodynamics of a bubble column focused, for the first time, on the effect of the internals (heat exchanging tubes) and superficial gas velocity on the local time-averaged liquid velocity and the time-averaged liquid turbulence parameter (Reynolds stresses, turbulent kinetic energy and eddy diffusivities) profiles at atmospheric pressure and temperate. The experiments were conducted for 12 hours, and during this time, the radiation emitted by the radioactive particle was recorded by the detectors at a frequency of 50 Hz for each sampling instance. Then, the instantaneous position of the particle at each compartment was estimated by weighted regressions because the locations of all of the detectors were known. Then, a sequence of instantaneous position data with time differencing of positions yielded the instantaneous Lagrangian velocities of the particle position. Once these velocities were estimated, the velocities, turbulence parameters (Reynolds stresses and turbulent kinetic energy) and eddy diffusivities were computed after filtering the position data.

A short discussion of the sampling compartments of the studied bubble column and a brief summary of the governing equations for calculating the velocity field, turbulence parameters and turbulent eddy diffusivities are provided in Section 5.1; more detailed discussions can be found elsewhere (Devanathan, 1991; Degaleesan, 1997). Section 5.2 includes a discussion of the filtration for raw position data, and then the results of RPT time-averaged liquid velocity component and liquid turbulence parameter profiles are discussed in Section 5.3.

5.1. COMPUTATION OF VELOCITY AND TURBULENCE PARAMETERS

5.1.1. Sampling Compartments. In order to obtain the time-averaged hydrodynamic parameters as a function of the position, the column was divided into sampling compartments. Degaleesan (1997) discussed several ways to discretize the column; based on her recommendation, the column was divided into sampling compartments as shown in Figure 5.1 and Table 5.1.

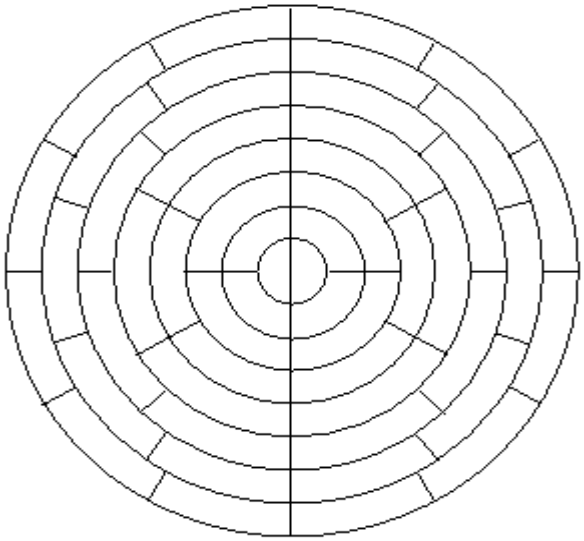

Figure 5.1. Compartment Discretization of the Bubble Column

Table 5.1. Assignment of Compartment for RPT Data Processing

N_r^*	Δr, cm	Δz, cm	N_z^*	N_θ^*
8	0.873	2.54	40	2,4,4,6,6,8,10,12

* N_r, N_z and N_θ represent the number of divisions in the radial, axial and azimuthal directions, respectively.

As shown in Figure 5.1 and Table 5.1, the radial and axial divisions were kept constant, while the azimuthal divisions were varied with the radial position in order to maintain a reasonable, uniform number of occurrences of the particle (statistic) in each compartment. In total, the 5.5" column was divided into 2,340 compartments within the three-dimensional space.

5.1.2. Velocity Field. Instantaneous velocities (axial, radial and azimuthal velocities) were computed from the time differencing of the subsequent particle positions and assigned to the compartment in which the middle point of the two positions fell, as shown in the following equations:

$$u_{z,i-1/2} = \frac{z_i - z_{i-1}}{\Delta t} \tag{21}$$

$$u_{r,i-1/2} = \frac{r_i - r_{i-1}}{\Delta t} \tag{22}$$

$$u_{\theta.i-1/2} = \frac{(\theta_i - \theta_{i-1})}{\Delta t} \frac{(r_i + r_{i+1})}{2} \tag{23}$$

Where $i - 1/2$ is the midpoint of two successive particle positions.

Time-averaged (mean) velocities were calculated by averaging the instantaneous particle velocities for a given compartment (i, j, k).

$$\bar{u}_{p(i,j,k)} = \frac{1}{N_v} \sum_{i=1}^{N_v} u_{p(i,j,k),i} \qquad p = z, r, \theta \tag{24}$$

N_v is the number of velocity occurrences assigned to the midpoint of two successive particle positions for a given compartment (i, j, k).

The fluctuating velocity was computed by subtracting the time-averaged (mean) velocities from the instantaneous velocities.

$$u'_{p(i,j,k)} = u_{p(i,j,k)} - \bar{u}_{p(i,j,k)} \tag{25}$$

The azimuthally averaged velocity was used due to the difficulty of representing three-dimensional velocities as a function of position in the domain.

$$\bar{u}_{(i,k)} = \frac{1}{N_\theta \widetilde{N}_{v(i,k)}} \sum_{j=1}^{N_\theta} \bar{u}_{(i,j,k)} N_{v(i,j,k)} \quad (26)$$

$$\widetilde{N}_{v(i,k)} = \frac{1}{N_\theta} \sum_{j=1}^{N_\theta} N_{(i,j,k)} \quad (27)$$

Where $\bar{u}_{(i,k)}$ is the time-averaged and azimuthally averaged either axial or radial component of the two-dimensional velocity for compartment (i, k); N_θ is the number of divisions in the azimuthal direction, as shown in Figure 5.1 and Table 5.1; and $\widetilde{N}_{v(i,k)}$ is the average number of velocity occurrences for a given two-dimensional compartment (i, k).

5.1.3. Turbulence Stresses and Kinetic Energy. Turbulence parameters are very important in modeling multiphase flows. In bubble columns, the interactions between turbulent eddies in the liquid phase can be characterized by Reynolds stresses. The RPT technique makes it possible to evaluate Reynolds stresses and other parameters. Once the fluctuating velocity was calculated, the turbulence parameters (Reynolds stresses and turbulent kinetic energy) were able to be evaluated. The turbulent stress tensor in cylindrical coordinates can be defined as shown in Equation (28):

$$\tau = \rho_l \begin{pmatrix} \overline{u_r' u_r'} & \overline{u_r' u_\theta'} & \overline{u_r' u_z'} \\ \overline{u_\theta' u_r'} & \overline{u_\theta' u_\theta'} & \overline{u_\theta' u_z'} \\ \overline{u_z' u_r'} & \overline{u_z' u_\theta'} & \overline{u_z' u_z'} \end{pmatrix} \quad (28)$$

The nine unknown components in Equation (28) reduce to six components because of the symmetry of the stress tensor, namely:

Shear stresses: $\rho_l \overline{u_\theta' u_r'}$, $\rho_l \overline{u_\theta' u_z'}$, $\rho_l \overline{u_z' u_r'}$ (29)

where $\overline{\acute{u}_z\acute{u}_r} = \overline{\acute{u}_r\acute{u}_z}$, $\overline{\acute{u}_z\acute{u}_\theta} = \overline{\acute{u}_\theta\acute{u}_z}$ and $\overline{\acute{u}_\theta\acute{u}_r} = \overline{\acute{u}_r\acute{u}_\theta}$

Normal stresses: $\rho_l\overline{u'_r u'_r}$, $\rho_l\overline{u'_\theta u'_\theta}$, $\rho_l\overline{u'_z u'_z}$ (30)

The aim of the present work is to understand the turbulence mechanisms in a bubble column equipped with internals. As the density of liquid is constant, the density and negative sign are not considered here.

The turbulent stress components are calculated as

$$\tau_{pq} = \overline{u'_p u'_q}(i,j,k) = \frac{1}{N_v}\sum_{n=1}^{N_v} u'_{p(i,j,k),n} u'_{q(i,j,k),n} \quad (31)$$

where pq denotes the component of the stress tensor in the cylindrical coordinates system.

The turbulent kinetic energy (TKE) per unit mass is defined as follows:

$$k = \frac{1}{2}\left(\overline{u_r'^2} + \overline{u_\theta'^2} + \overline{u_z'^2}\right) \quad (32)$$

5.1.4. Eddy Diffusivity. Turbulent eddy diffusivities are important parameters for modeling and quantifying liquid mixing and transport in bubble columns. The eddy diffusivity, which is mixing caused by eddies that can vary in size, can be obtained directly from RPT-measured Lagrangian autocorrelation. The procedure for obtaining eddy diffusivities is discussed in detail elsewhere (Degaleesan, 1997), so only a brief outline of the governing equations for calculating the eddy diffusivities is provided in this section.

The particle location displacements Y_r, Y_θ and Y_z caused by the corresponding fluctuation velocity components were evaluated according to the following equations:

$$Y_r(t) = \int_0^t u_r'(t')dt' \quad (33)$$

$$Y_\theta(t) = \int_0^t u_\theta'(t')dt' \tag{34}$$

$$Y_z(t) = \int_0^t (u_z'(t') + \frac{d\overline{u_z}}{dr}|_{Y_r(t')} \cdot Y_r(t')) \cdot dt' \tag{35}$$

The extra term in Equation (35) concerns the axial velocity gradient in the radial direction because the flow is anisotropic with radial non-homogeneity in the bubble column (Degaleesan, 1997). Degaleesan (1997) defined eddy diffusivities as follows:

The normal radial eddy diffusivity is:

$$D_{rr}(t) = \frac{1}{2}\frac{d}{dt}\overline{Y_r^2(t)} = \int_0^t \overline{u_r'(t) \cdot u_r'(t')} \cdot dt' \tag{36}$$

The normal azimuthal eddy diffusivity is:

$$D_{\theta\theta}(t) = \frac{1}{2}\frac{d}{dt}\overline{Y_\theta^2(t)} = \int_0^t \overline{u_\theta'(t) \cdot u_\theta'(t')} \cdot dt' \tag{37}$$

The normal axial eddy diffusivity is:

$$D_{zz}(t) = \frac{1}{2}\frac{d}{dt}\overline{Y_z^2(t)} = \int_0^t \left[\overline{u_z'(t) \cdot u_z'(t')} + \overline{\frac{du_z}{dr}|_{Y_r(t')} \cdot (\int_0^{t'} u_z'(t) \cdot u_r'(t'')dt'')} \right] \cdot dt' \tag{38}$$

Equations (33) through (38), which govern the eddy diffusivities, all are related to the Lagrangian autocorrelation coefficient, which is given by:

$$R_{ij}(\tau) = \overline{\acute{u}_i(t)\acute{u}_j(t+\tau)} \qquad \text{i,j = r, } \theta\text{, z} \tag{39}$$

Where i=j for the autocorrelation coefficient. The other eddy diffusivity components, D_{rz}, $D_{\theta r}$ and $D_{z\theta}$, can be calculated as follows:

$$D_{zr}(t) = \frac{1}{2}\frac{d}{dt}\overline{Y_z(t)Y_r(t)} = \frac{1}{2}\left\{\int_0^t \left\{ \overline{\frac{du_z}{dr}|_{Y_r(\grave{t})}\left(\int_0^{\grave{t}} \acute{u}_r(t)\acute{u}_r(\tau)d\tau\right)} + \overline{\acute{u}_r(t)\acute{u}_z(\acute{t})}\right\} d\acute{t} + \int_0^t \acute{u}_r(\acute{t})\acute{u}_z(t)d\acute{t}\right\} \quad (40)$$

$$D_{r\theta}(t) = \frac{1}{2}\frac{d}{dt}\overline{Y_r(t)Y_\theta(t)} = \int_0^t \overline{\acute{u}_r(t)\acute{u}_\theta(\tau)}d\tau \quad (41)$$

$$D_{z\theta}(t) = \frac{1}{2}\frac{d}{dt}\overline{Y_r(t)Y_\theta(t)} = \frac{1}{2}\left\{\int_0^t \left\{ \overline{\frac{du_z}{dr}|_{Y_r(\grave{t})}\left(\int_0^{\grave{t}} \acute{u}_\theta(t)\acute{u}_r(\tau)d\tau\right)} + \overline{\acute{u}_\theta(t)\acute{u}_z(\acute{t})}\right\} d\acute{t} + \int_0^t \acute{u}_\theta(\acute{t})\acute{u}_z(t)d\acute{t}\right\} \quad (42)$$

The Lagrangian integral time scale, which represents the reaming time for the fluid element in the eddy or the average time required to move from one correlated region to another (Degaleesan, 1997), can be also extracted from the Lagrangian autocorrelation coefficient using the following equation:

$$\tau_{L,i} = \frac{\int_0^\infty \left|\overline{u_i'(t)u_i'(t+t')}\right| dt'}{\overline{u_i'^2}}, \quad i = r, \theta, z \quad (43)$$

This equation is evaluated for each radial compartment from the axially and azimuthally averaged autocorrelation functions. Then, the average radial Lagrangian integral time scale profile is calculated.

5.2. DATA FILTRATION

To obtain reliable estimates of the turbulence parameter, the instantaneous particle position data obtained from RPT experiments must be filtered in order to extract only the coherent part of the signal by eliminating the white noise, as discussed by Degaleesan (1997) and Degaleesan et al. (2002). The discrete wavelet transformation

threshold denoising filtration analysis proposed by Degaleesan (1997) was used in this work. Filtering can be implemented either directly to the radiation intensity count signal obtained by each detector or to the instantaneous particle position signal; the two methods yield the same results (Degaleesan, 1997). To achieve wavelet filtering, the original instantaneous position data should be split into sets of data with lengths of $N=2^L$, L=10 and N=1024. A signal threshold for the wavelet packet coefficient, *st*, is selected to eliminate the incoherent part of the decomposed signal, and its value depends on the extent of noise in the data, x(t), y(t) and z(t). More details about the wavelet filtering analysis and the filtration algorithm have been provided elsewhere (Degaleesan, 1997; Degaleesan et al., 2002). By choosing the estimates of the *st* values, the filtered and unfiltered instantaneous position data were processed to obtain the Lagrangian autocorrelation coefficients for comparing these correlations.

Figure 5.2 compares the radial and the axial Lagrangian autocorrelation coefficient profiles obtained from the unfiltered and filtered instantaneous position data at different *st* values. The filtered data profiles are smoother than those obtained from unfiltered data. This result agrees with the results of Ong's (2003) study in which artificial kinks were observed with unfiltered data profiles. The Lagrangian correlation coefficients were examined until the point at which they were no longer scattered on the Lagrangian correlation coefficients.

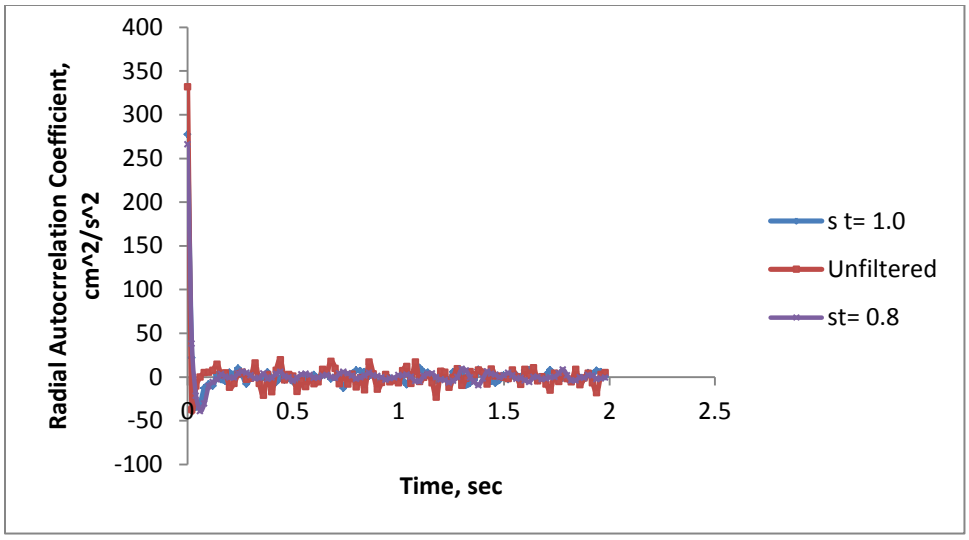

(a) Radial autocorrelation coefficient

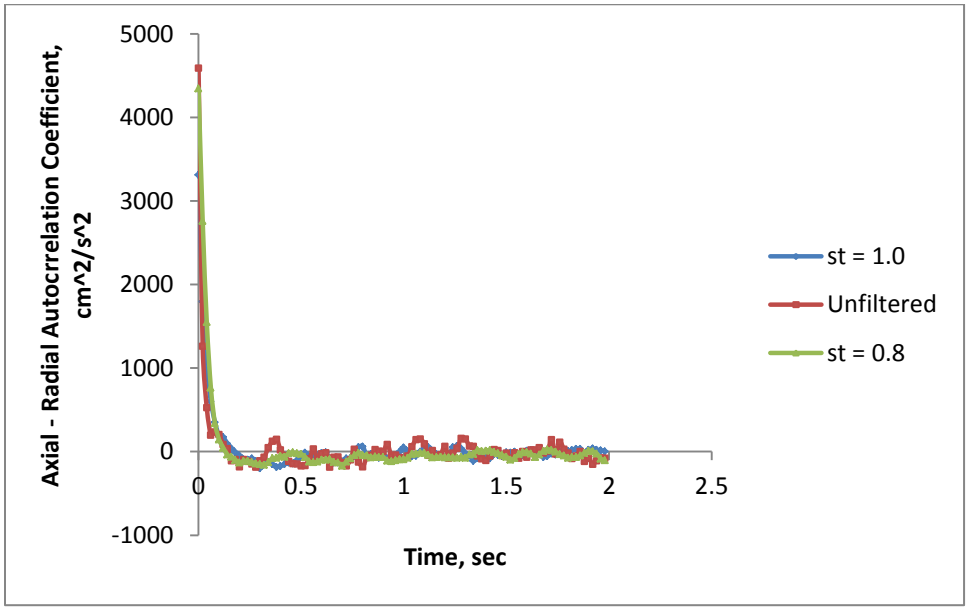

(b) Axial – radial autocorrelation coefficient

Figure 5.2. Lagrangian Correlation Coefficient Using Unfiltered and Filtered Instantaneous Position Data at 45cm/s

An additional step is needed to investigate whether or not filtering affects the liquid velocity components and the turbulence parameters. Figure 5.3 illustrates the comparison of filtered and unfiltered liquid velocity field and turbulence parameters at a superficial gas velocity of 45 cm/s and atmospheric pressure. The plots in Figure 5.3 illustrate that no difference can be observed in the liquid velocity components before and after filtering; however, an absolute difference up to 20% exists in the turbulence parameters. For instance, by comparing the turbulence parameters before and after filtering, the maximum absolute difference was found to be less than 3.5%, 6% and 10% for TKE, τ_{zz} and $\tau_{\theta\theta,}$ respectively.

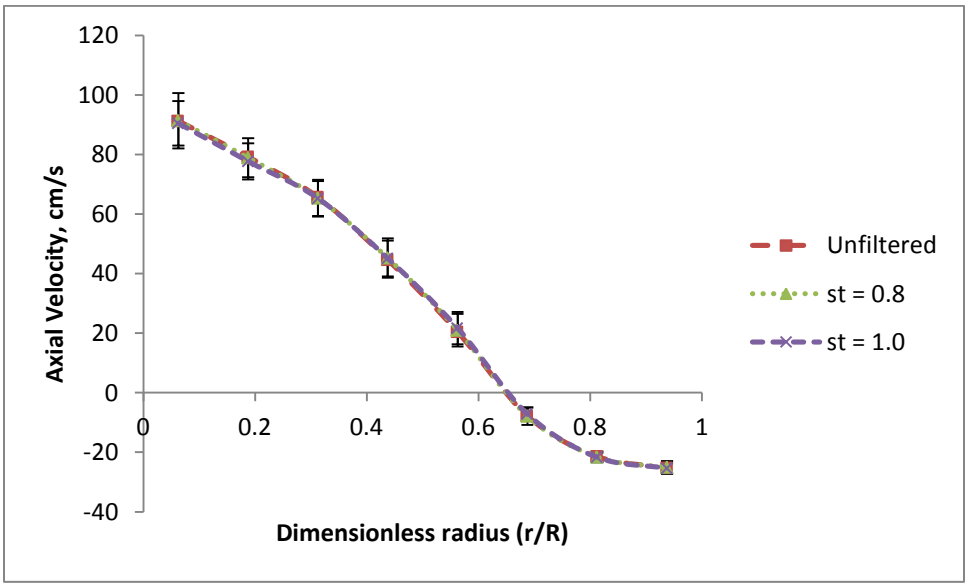

(a) Axial velocity

Figure 5.3. Time-Averaged, Axially Azimuthally Averaged Liquid Velocity and Turbulent Parameters at 45 cm/s

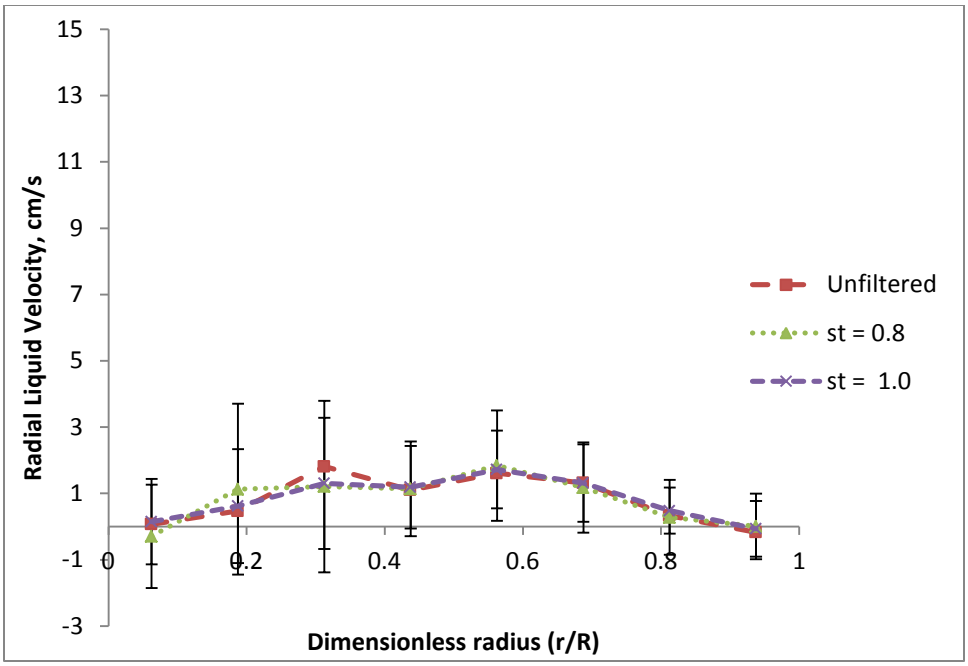

(b) Radial velocity

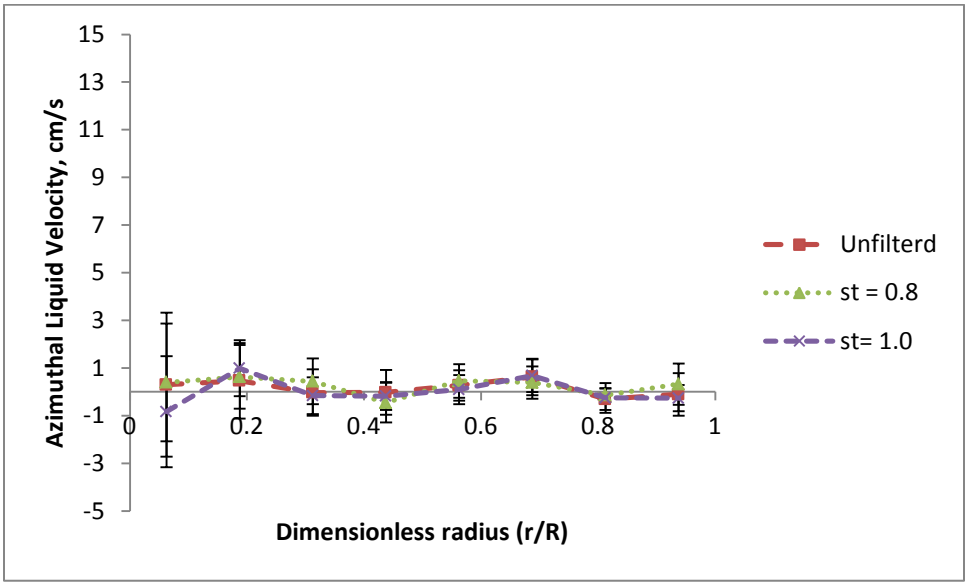

(c) Azimuthal velocity

Figure 5.3. Time-Averaged, Axially Azimuthally Averaged Liquid Velocity and Turbulent Parameters at 45 cm/s (cont.)

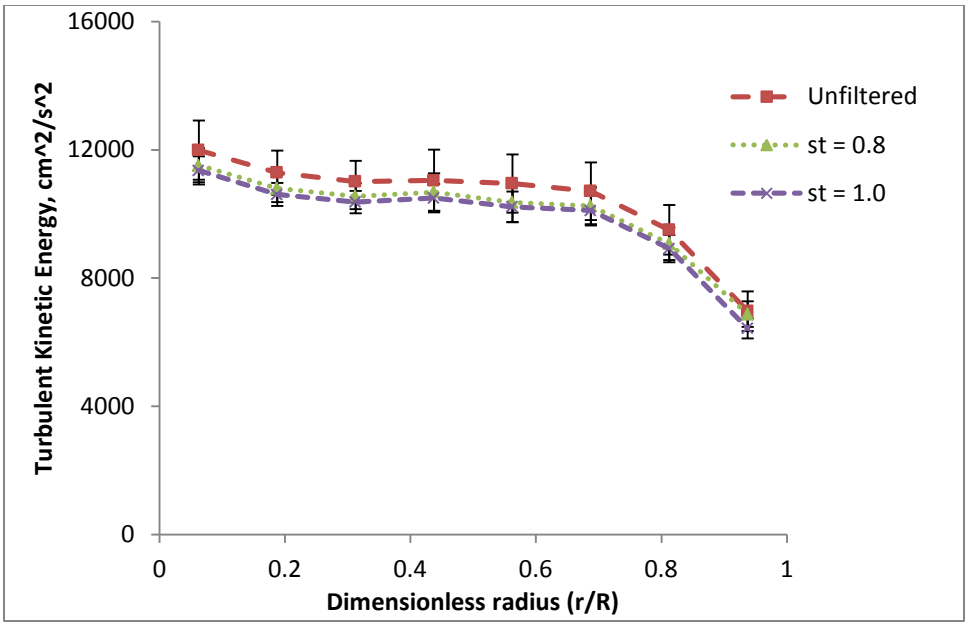

(d) Turbulent kinetic energy

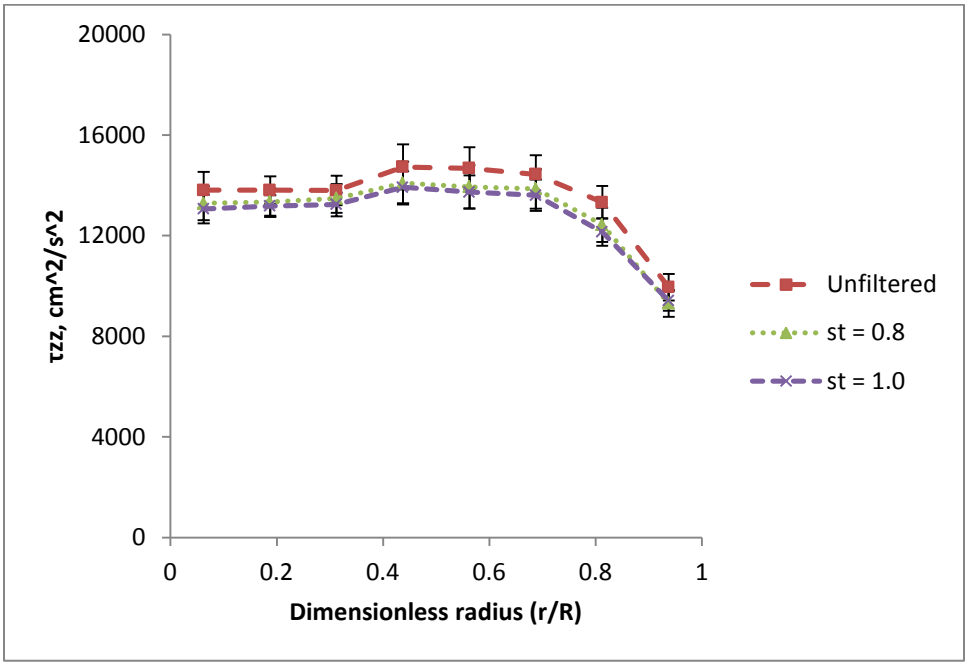

(e) τ_{zz}

Figure 5.3. Time-Averaged, Axially Azimuthally Averaged Liquid Velocity and Turbulent Parameters at 45 cm/s (cont.)

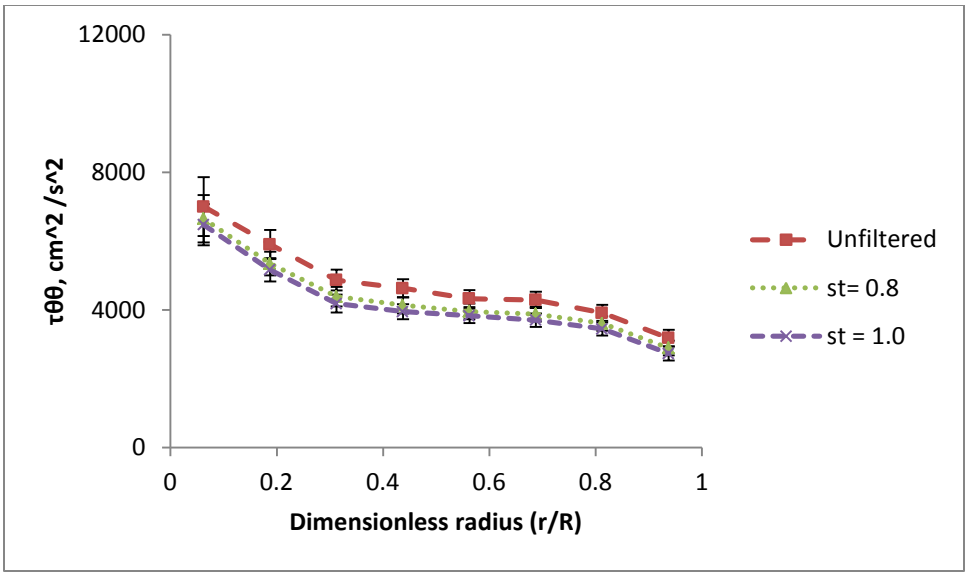

(f) $\tau_{\theta\theta}$

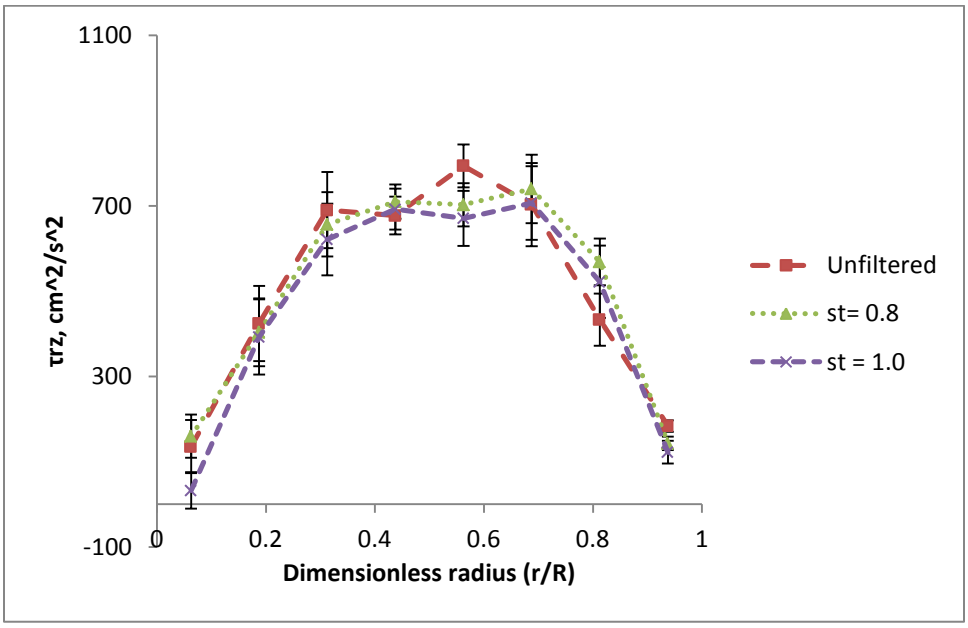

(g) τ_{rz}

Figure 5.3. Time-Averaged, Axially Azimuthally Averaged Liquid Velocity and Turbulent Parameters at 45 cm/s (cont.)

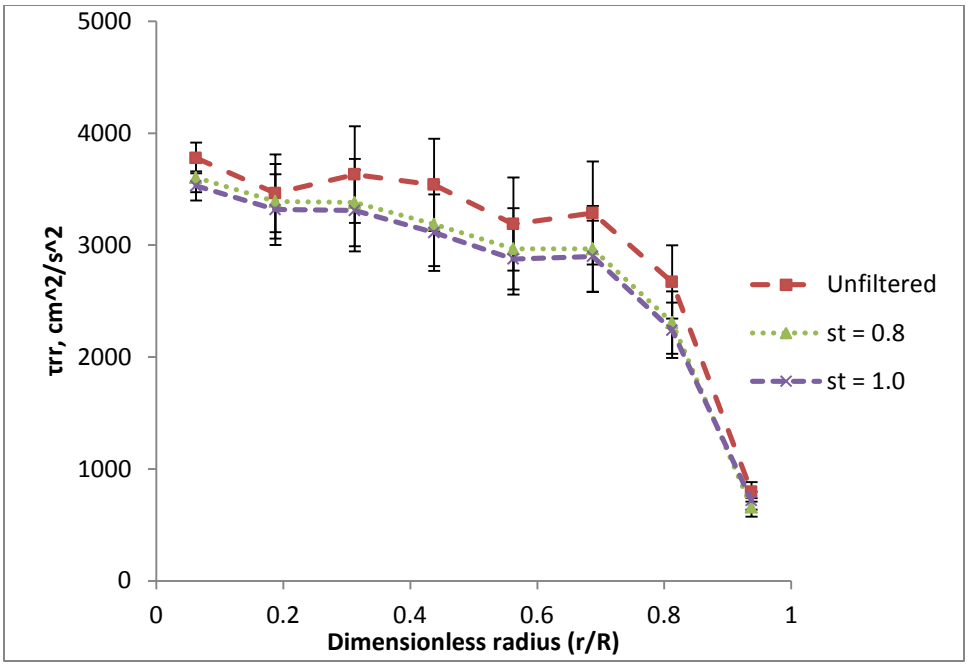

(h) τ_{rr}

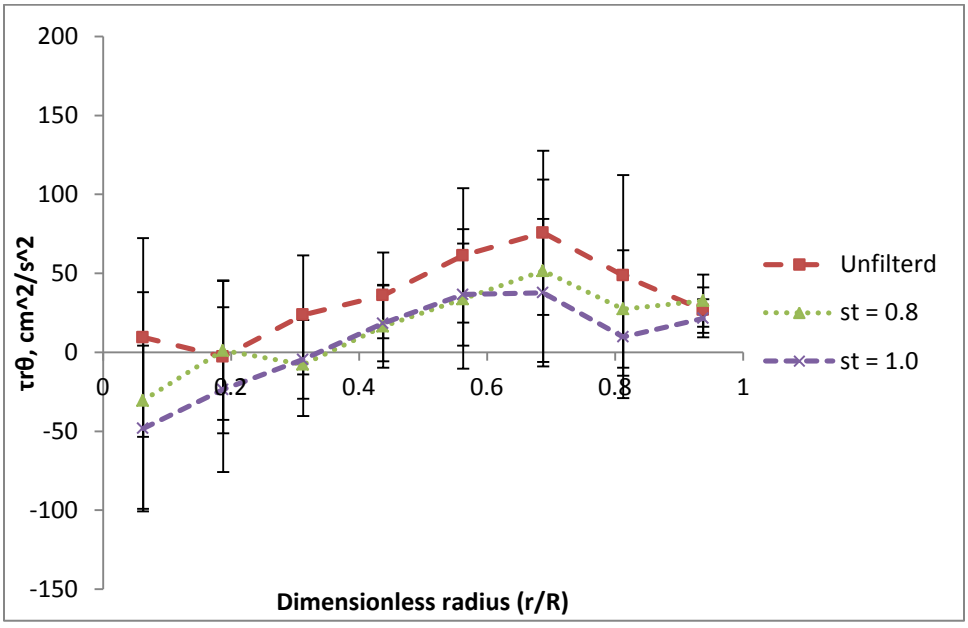

(i) $\tau_{r\theta}$

Figure 5.3. Time-Averaged, Axially Azimuthally Averaged Liquid Velocity and Turbulent Parameters at 45 cm/s (cont.)

Hence, from Figure 5.3, one may conclude that the noise in the data does not affect the liquid velocity components, while the noise or improper filtering of the instantaneous position data causes an over-estimation of turbulence parameters.

5.3. REPRODUCIBILITY OF RPT DATA

As mentioned previously, one of the most important factors to consider before taking any measurements is the reproducibility of the experiments. To check the reproducibility, the RPD data were obtained during another similar run under identical operating conditions (superficial gas velocity of 8 cm/s based on total CSA, with internals). Figure 5.4 shows the time-averaged, axially and azimuthally averaged liquid velocities and turbulence parameters obtained with internals at 8 cm/s based on the total CSA. The profiles shown in Figure 5.4 represent the average of each variable over the fully developed region at r/R, and hence, the error bars represent the standard deviation from that average of each run in the following figures. As shown in Figure 5.4, the reproducibility of RPT is very good for the liquid velocity profiles and the turbulence parameter profiles. Based on the axial liquid velocity profile, the maximum deviation occurred near the center of the column (refer to Figure 5.4 a) and had a value of ±4.6 % from the average. As Figure 5.4 clearly shows, the maximum difference between the runs occurs near the center of the column; for example, the differnce was 4.2%, 5%, 4% and 6.3% for TKE, τ_{zz}, τ_{rr}, and $\tau_{\theta\theta,}$ respectively.

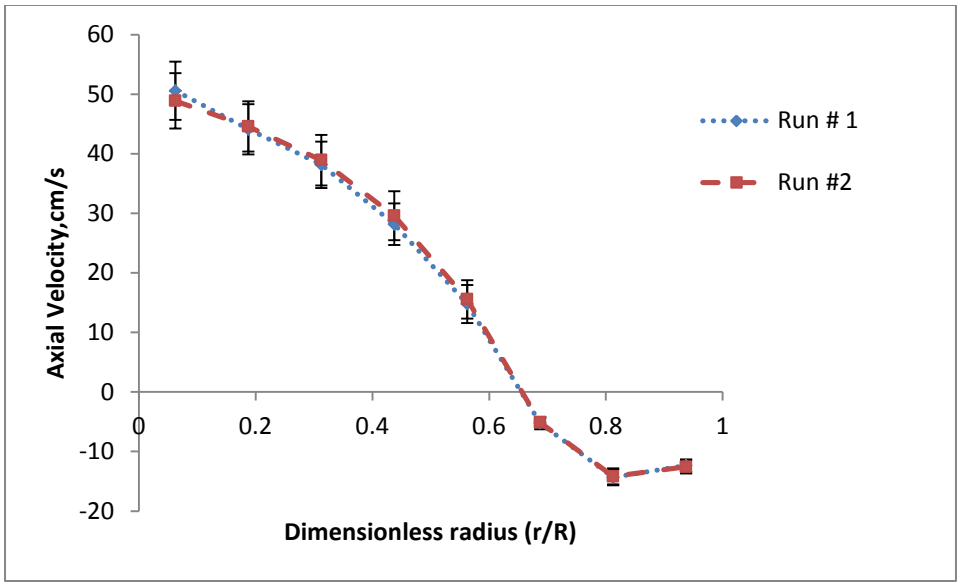

(a) Axial velocity

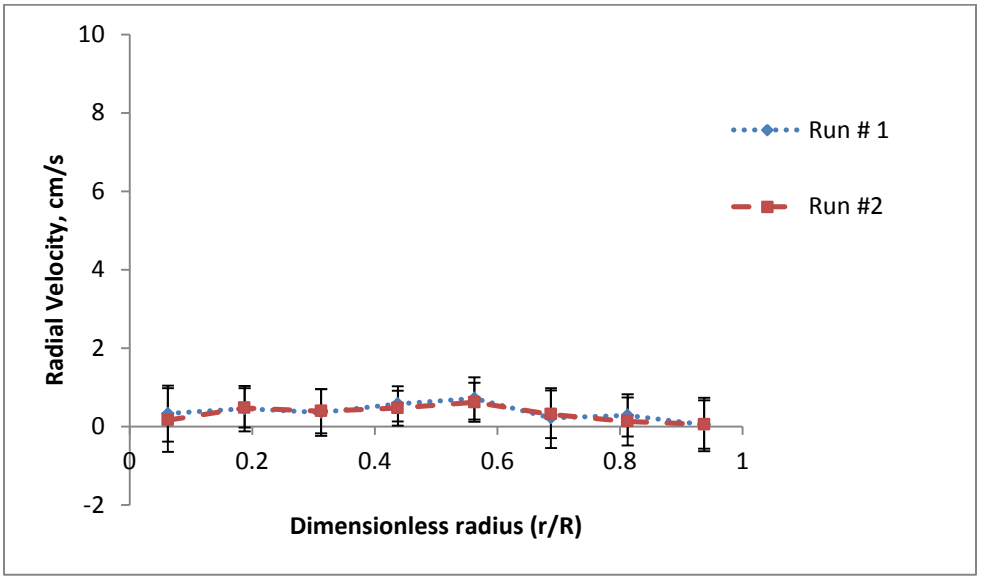

(b) Radial velocity

Figure 5.4. Time-Averaged, Axially and Azimuthally Averaged Liquid Velocity and Turbulence Parameters at 8 cm/s Based on Total CSA (with Internals)

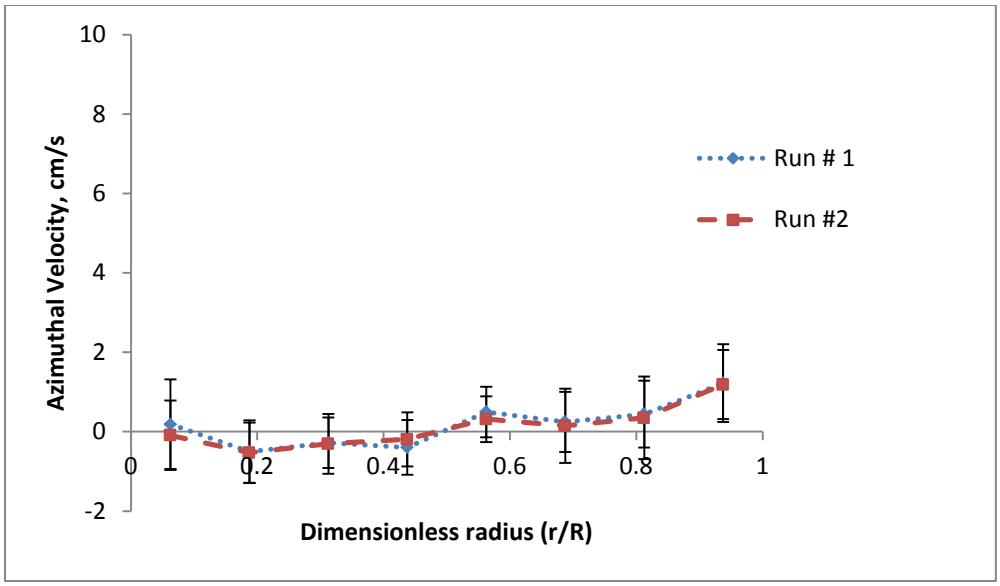

(c) Azimuthal velocity

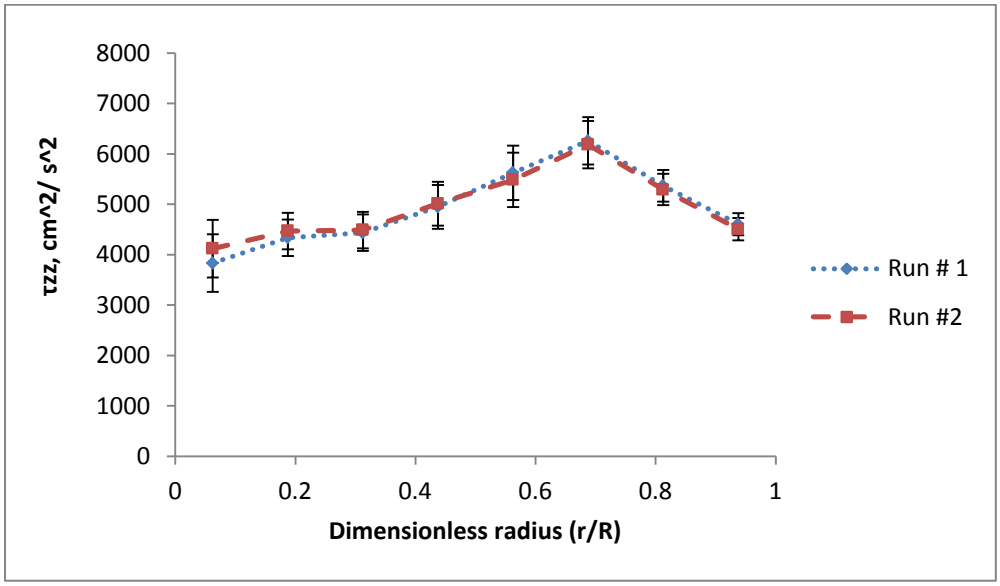

(d) τ_{zz}

Figure 5.4. Time-Averaged, Axially and Azimuthally Averaged Liquid Velocity and Turbulence Parameters at 8 cm/s Based on Total CSA (with Internals) (cont.)

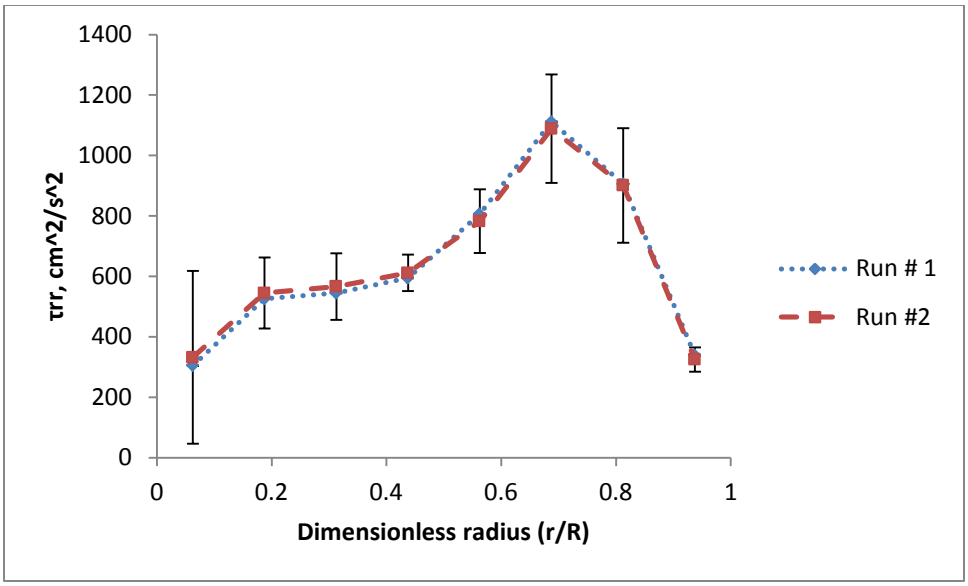

(e) τ_{rr}

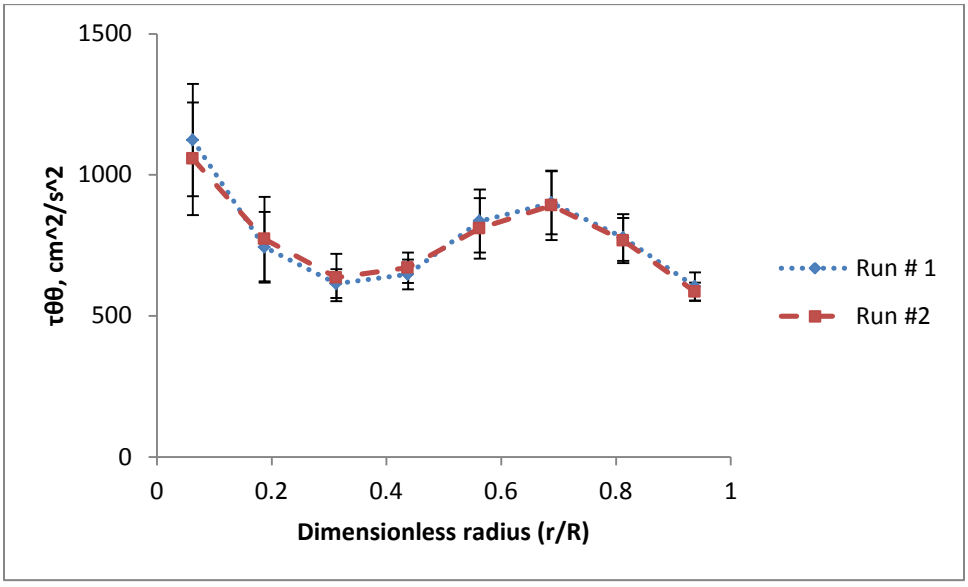

(f) $\tau_{\theta\theta}$

Figure 5.4. Time-Averaged, Axially and Azimuthally Averaged Liquid Velocity and Turbulence Parameters at 8 cm/s Based on Total CSA (with Internals) (cont.)

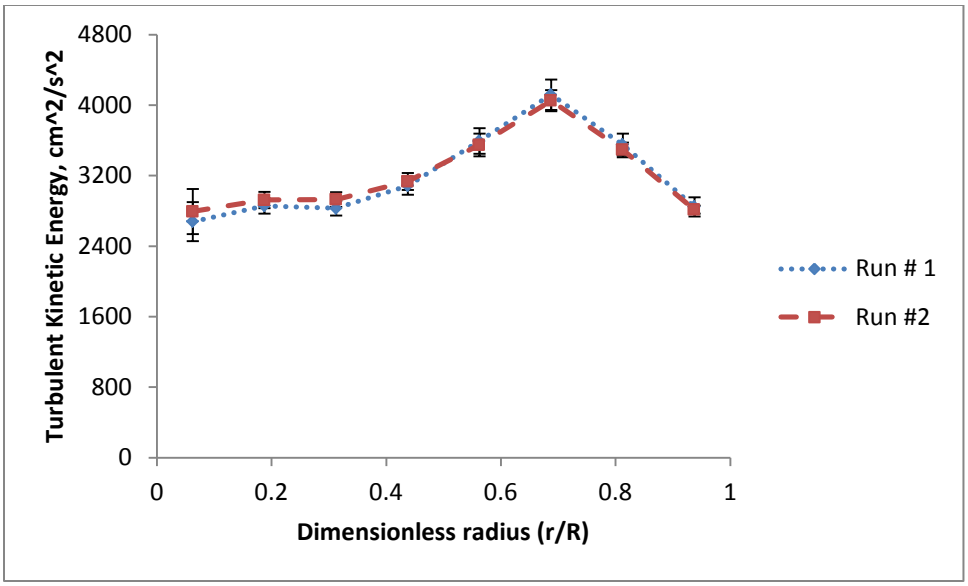

(g) Turbulent kinetic energy

Figure 5.4. Time-Averaged, Axially and Azimuthally Averaged Liquid Velocity and Turbulence Parameters at 8 cm/s Based on Total CSA (with Internals) (cont.)

5.4. EFFECTS OF OPERATING PARAMETERS

The accurate design and scale-up of the bubble column depends upon the quality of the description of the liquid flow behavior (Devanathan, 1991). As noted previously, the gas holdup results in liquid recirculation, so a complete understanding of liquid recirculation is needed to quantify the liquid mixing, which plays an important role in determining the performance in a bubble column. Achieving a fundamental model that can capture the physics of flow needed for the design and scale-up of the bubble column requires reliable data for the local fluid dynamics, such as bubble size, holdup distribution, phase velocities and turbulence parameters. In this section, the investigation of the effect of superficial gas velocity and internals (heat exchanging tubes) on the liquid velocity field, turbulence parameters and eddy diffusivity profiles is discussed. For

turbulence parameters, axial and radial normal stresses, the shear stress, and the axial and radial eddies are presented, as they are frequently used and of the most interest in two-dimensional bubble column modeling. The obtained data can both validate the fundamental modeling parameters and provide a clear picture of the mechanisms that drive the flow.

5.4.1. Effect of Superficial Gas Velocity without Internals. Figure 5.5 depicts the effect of superficial gas velocities on time-averaged liquid velocity field profiles and velocity vector plots in absence of internals. These profiles and plots are averaged axially from z=2D to H_D –D, which represents the fully developed flow region. The bars shown in the figures represent the standard deviation around the mean as mentioned earlier. As the superficial gas velocity increased, so did the liquid centerline and negative axial velocity. For example, with an increase in superficial gas velocity from 20 cm/s to 45 cm/s, the liquid centerline velocity magnitude value increased by approximately 38% on average, while the velocity magnitude increased by approximately 78% on average when the gas velocity increased from 8 cm/s to 45 cm/s. In the central region of the column (r/R= 0 - 0.66), the axial velocity was upward, while the liquid velocity was downward in the wall region of $r/R \geq 0.7$. The inversion point was approximately 0.68 of r/R where the axial velocity was zero. This finding aligns with the results of previous studies conducted by Rados (2003), Ong (2003), Han (2007) and Shaikh (2007) in other systems. As Figure 5.5 shows, the time-averaged radial liquid velocities had insignificant magnitudes and increased with an increase in the superficial gas velocity; the time-averaged azimuthal velocities also had small values. This can be referred to as the axis-symmetry construction and verticality of the bubble column. Therefore, the following discussion

will focus on the axial velocity profiles because they characterize the global recirculation in the bubble column, and the radial and azimuthal velocities were negligible.

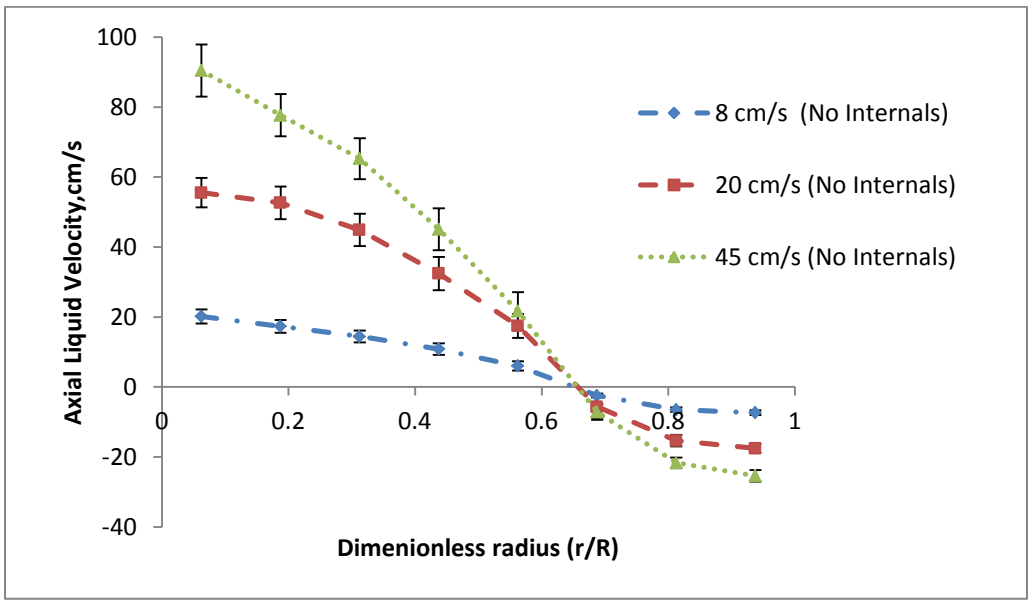

(a) Axial liquid velocity

Figure 5.5. Effect of Superficial Gas Velocity on Velocity Components Profiles at Atmospheric Pressure and Velocity Vector Plots in the r-z Plane in the Absence of Internals

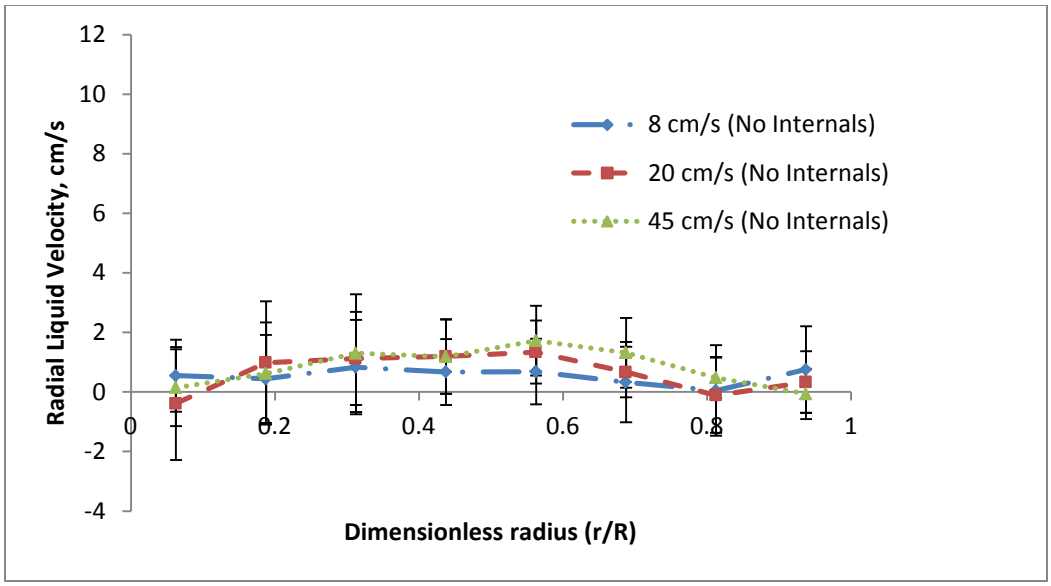

(b) Radial liquid velocity

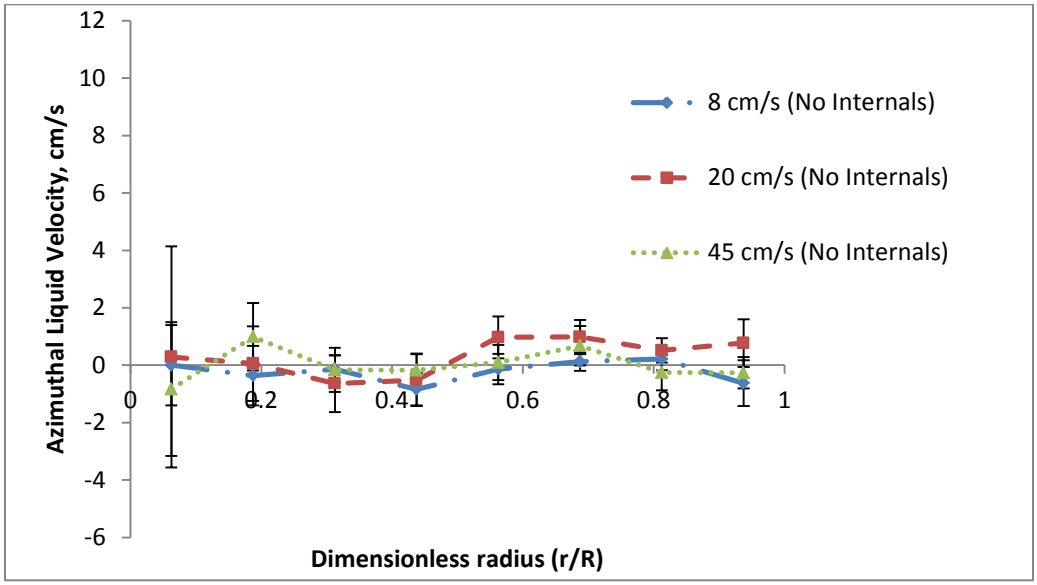

(c) Azimuthal liquid velocity

Figure 5.5. Effect of Superficial Gas Velocity on Velocity Components Profiles at Atmospheric Pressure and Velocity Vector Plots in the r-z Plane in the Absence of Internals (cont.)

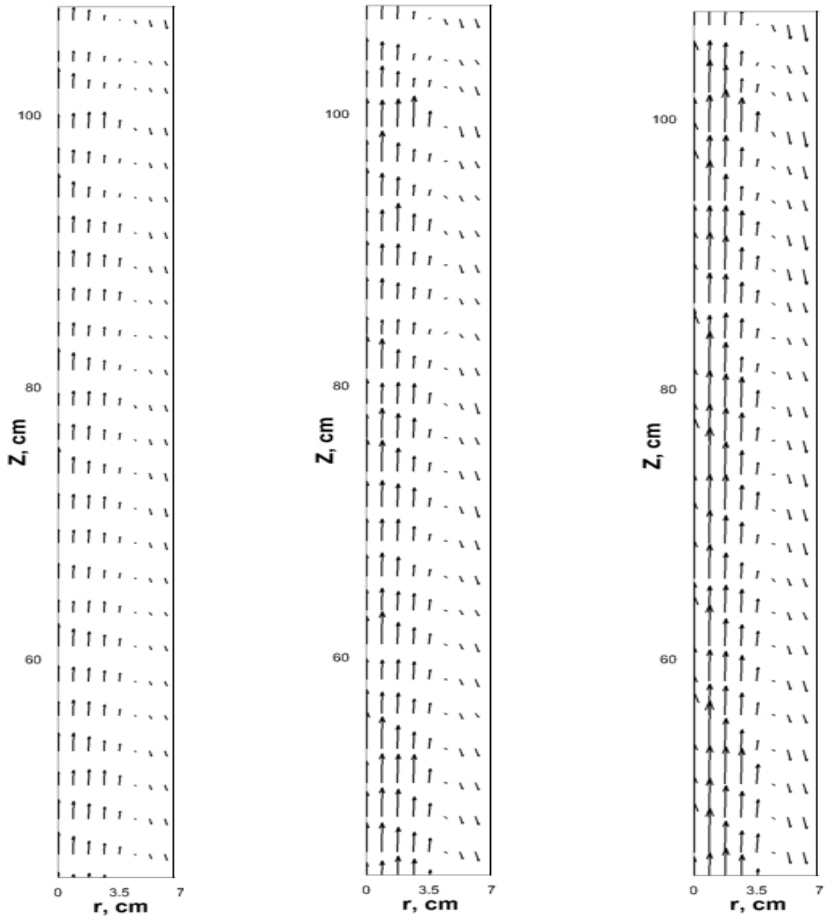

8 mc/s 20 cm/s 45 cm/s

(d) Velocity vector plots in the r-z plane without internals

Figure 5.5. Effect of Superficial Gas Velocity on Velocity Components Profiles at Atmospheric Pressure and Velocity Vector Plots in the r-z Plane in the Absence of Internals (cont.)

Table 5.2 shows the average Lagrangian integral time scale in the radial and axial directions. Clearly, the integral time scale in the axial direction is larger than along the radial direction. Furthermore, with an increase in superficial gas velocity, the axial

Lagrangian integral time scale decreases, which means that the reaming time for the fluid element in the eddy or the average time required to move from one correlated region to another decreases with an increase in the gas velocity, while no clear trend can be observed for the radial integral time scale. This may be because, at high superficial gas velocities, intense turbulence and liquid recirculation occur; hence, the length scale of turbulence is much larger in the axial direction than in the radial direction. In other words, there is no restriction along the axial direction as there is in the radial direction. These findings are consistent with Degaleesan (1997) and Ong (2003).

Table 5.2. Cross-Sectional Average Lagrangian Integral Time Scales

U_g , cm/s	**τ_{rL}, sec**	**τ_{zL}, sec**
8	0.0159	0.0293
20	0.0156	0.023
45	0.0165	0.0212

Figure 5.6 depicts the radial profiles of the axial, radial and azimuthal normal liquid stresses in the absence of internals. The azimuthal liquid Reynolds stress (5.6c) profiles seemed to decay in the radial direction monotonically, while the axial liquid Reynolds stress (5.6a) profiles clearly began to decrease after the inversion point of the flow ($r/R \approx 0.68$). The radial normal stress (5.6b) shows a peak close to the inversion point of the flow, which could be due to the change of the flow dynamic from upward to

downward. Therefore, the flow in this region fluctuated more vigorously leading to the peak. In general, the radial profiles of normal liquid stress increase with an increase in the superficial gas velocity. The magnitude of the normal stresses (τ_{zz}) in the axial direction were larger than those in the radial and tangential directions due to non-isotropy in the bubble column.

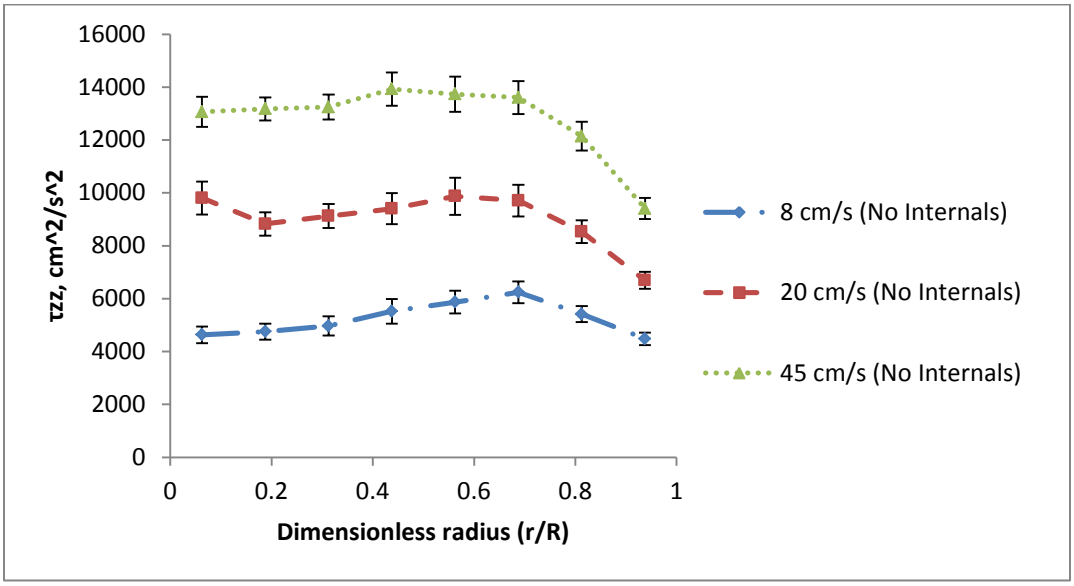

(a) Liquid axial normal stress

Figure 5.6. Effect of Superficial Gas Velocity on Velocity Components Profiles at Atmospheric Pressure and Velocity Vector Plots in the r-z Plane in the Absence of Internals

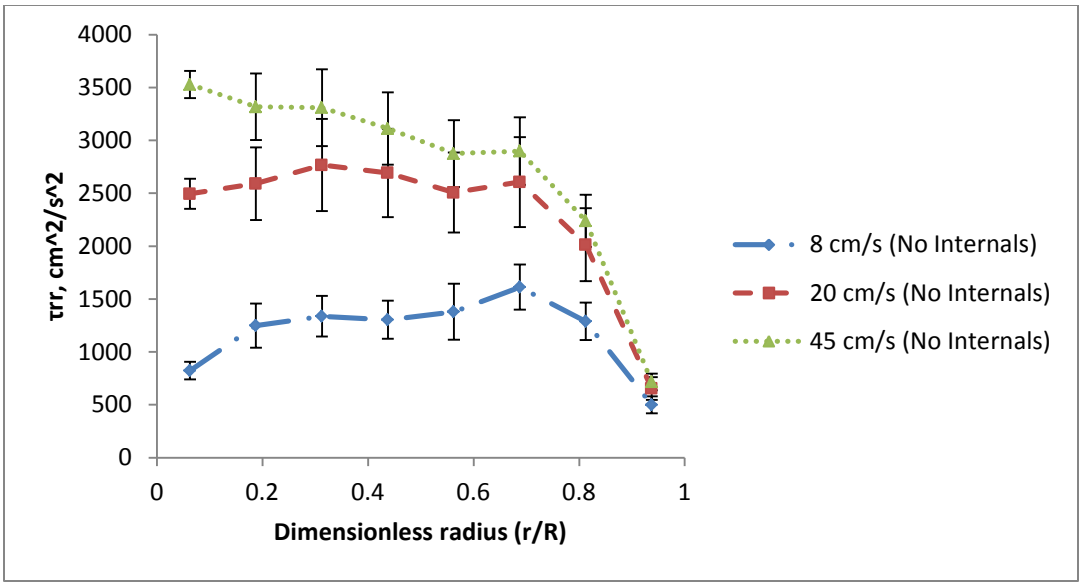

(b) Liquid radial normal stress

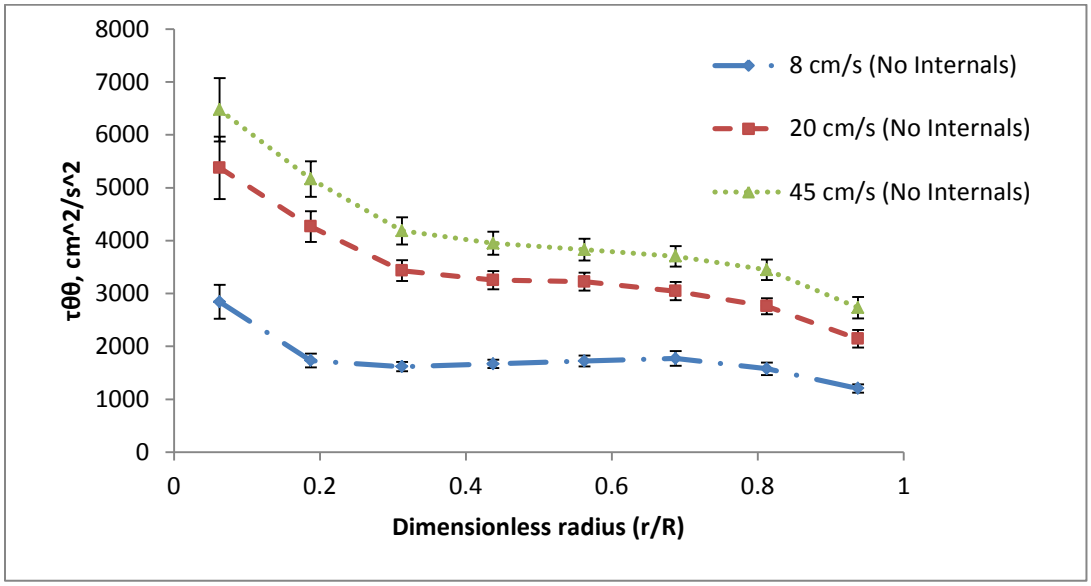

(c) Liquid azimuthal normal stress

Figure 5.6. Effect of Superficial Gas Velocity on the Liquid Normal Stresses in Gas-Liquid System without Internals (cont.)

The Reynolds shear stress profile is proportional to the liquid axial velocity radial gradient. As the superficial gas velocity increased, so did the shear stress, as shown in Figure 5.7. For instance, at r/R ≈ 0.69, the difference of the shear stress magnitude when the gas velocity increased from 8 cm/s to 20 cm/s was 20%; that difference became 40% when the superficial gas velocity increased from 8 cm/s to 45 cm/s. The maximum shear stress profile values occurred close to the inversion point of the flow, while the minimum values occurred at the center and the wall of the column. The magnitudes of the shear stresses (τ_{rz}) were lower than those of the normal stresses. The other component of the shear stresses, $\tau_{r\theta}$ and $\tau_{z\theta,}$ had much lower magnitudes than the shear stresses in the axial and radial directions; these are not used frequently in the modeling of bubble columns.

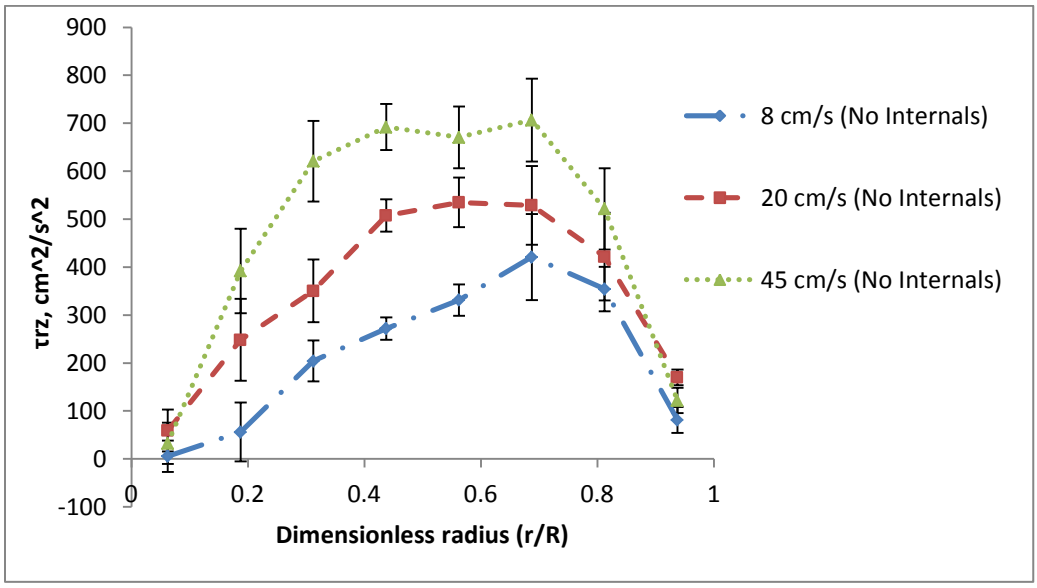

Figure 5.7. Effect of Superficial Gas Velocity on the Liquid Shear Stresses Profiles in Gas-Liquid System without Internals

Figures 5.8 and 5.9 show the time averaged turbulent kinetic energy and eddy diffusivity profiles. The turbulent kinetic energy and eddy diffusivity magnitudes increased because as the superficial gas velocity increased, the system became increasingly more turbulent, which affected the TKE and eddy diffusivity profiles. Figures 5.6 and 5.8 show that the radial turbulent kinetic energy profiles followed the behavior of the axial normal stress, which had a higher magnitude value.

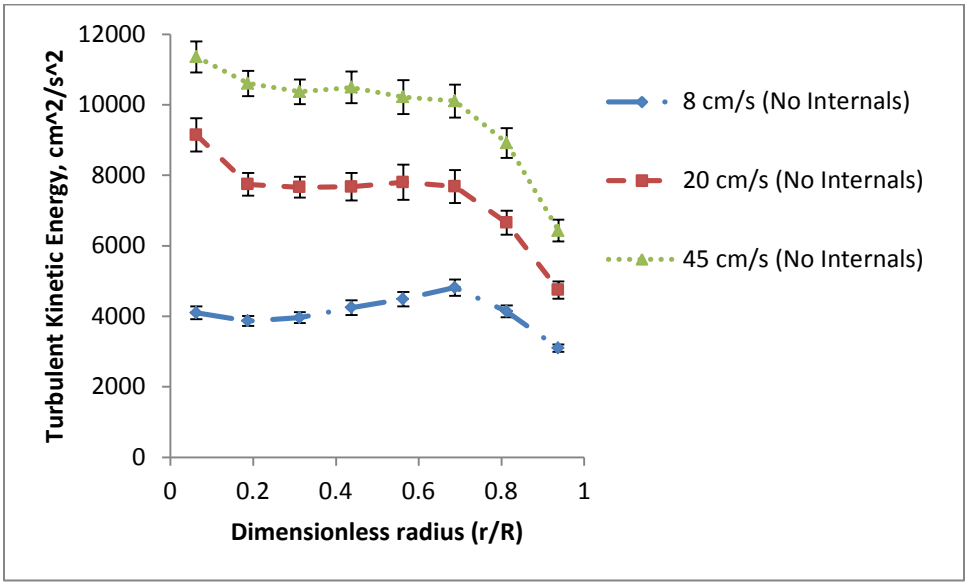

Figure 5.8. Effect of Superficial Gas Velocity on the Liquid Turbulent Kinetic Energy (TKE) Radial Profiles in Gas-Liquid System without Internals

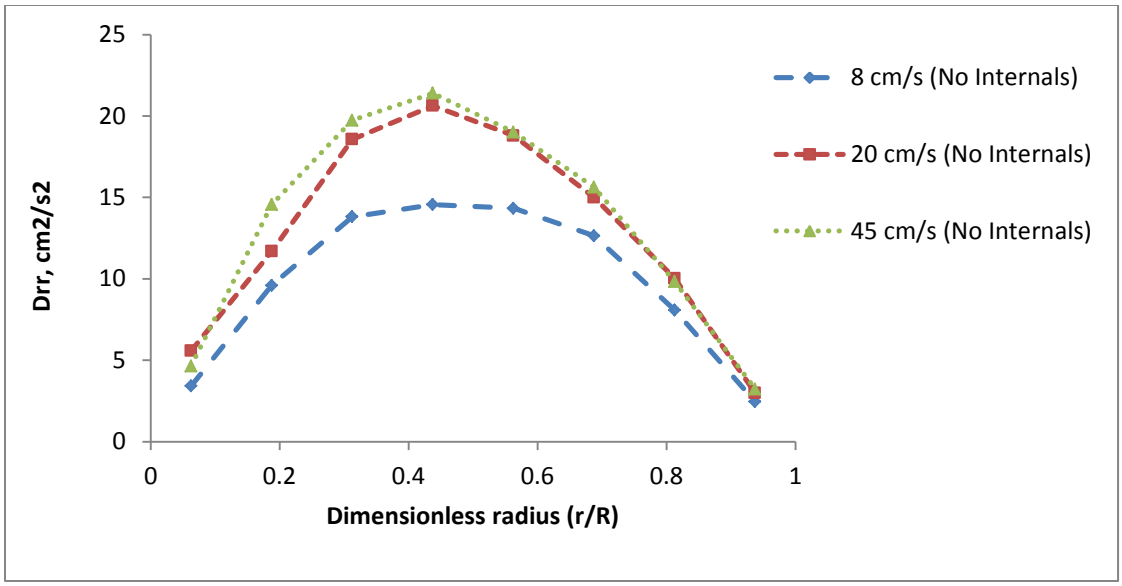

(a) Liquid radial eddy diffusivity

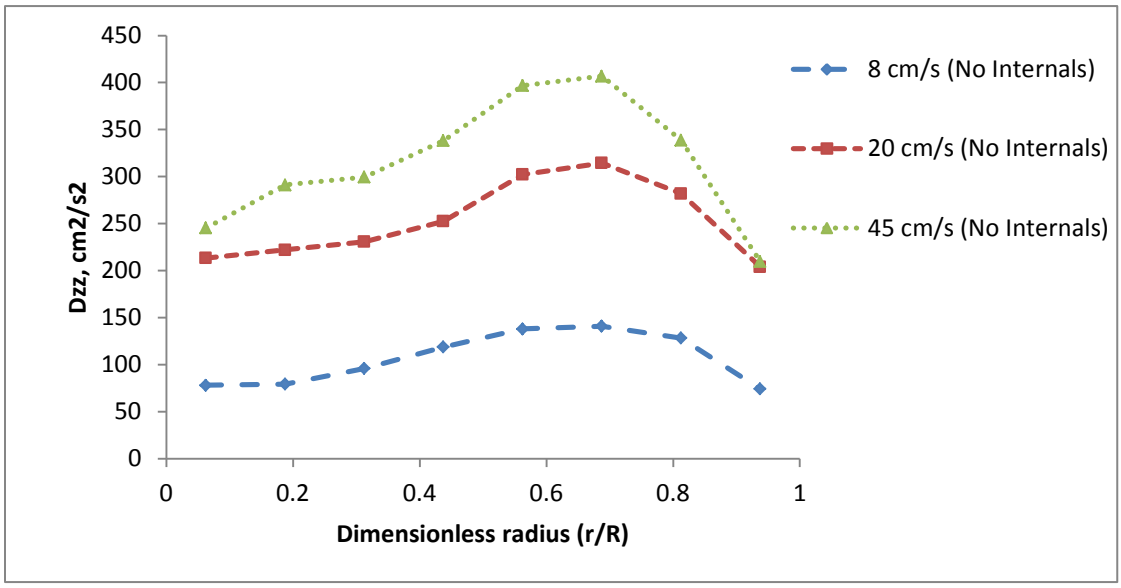

(b) Liquid axial eddy diffusivity

Figure 5.9. Effect of Superficial Gas Velocity on Eddy Diffusivity Radial Profiles in Gas-Liquid System without Internals

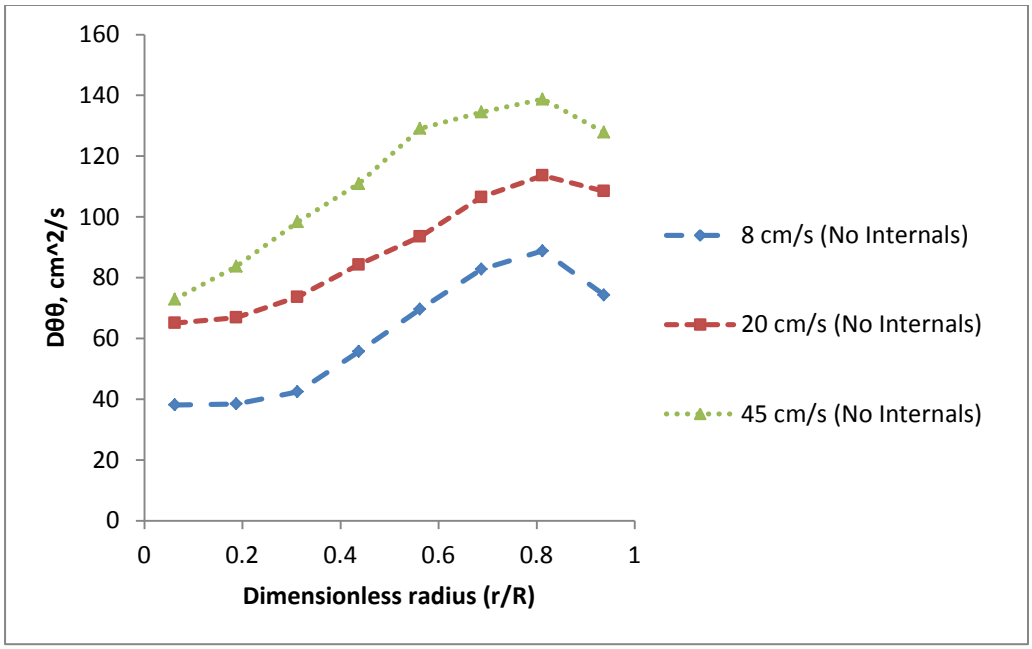

(c) Liquid azimuthal eddy diffusivity

Figure 5.9. Effect of Superficial Gas Velocity on Eddy Diffusivity Radial Profiles in Gas-Liquid System without Internals (cont.)

The radial eddy diffusivity profiles followed the same trend as the shear stress profiles. The liquid axial and azimuthal eddy diffusivity profiles indicate that the maximum axial and azimuthal eddy diffusivities occurred at a point close to the inversion point of the flow($r/R \approx 0.68$), where the axial velocity fluctuation is higher. In addition, the maximum radial eddy diffusivity occurred at $r/R \approx 5$, where the liquid was less confined, while at the center and the wall of the column, they were minimal. Degaleesan (1997) reported that the maximum axial eddy diffusivity occurs close to the inversion point of the liquid circulation where the maximum shear stress occurs.

Clearly, the shear stress magnitude value was very small compared to the normal stress magnitude, indicating that the cross-correlation between the velocity components was not as strong as the autocorrelation in normal stresses. A similar finding has been observed (Chen et al., 1994; Degalessan, 1997; Ong, 2003). Although an increase in the superficial gas velocity caused an increase in the turbulence parameter magnitudes, the change in the magnitude value of these parameters when the gas velocity increased from 8 cm/s to 20 cm/s was somewhat higher than that obtained when the velocity increased from 20 cm/s to 45 cm/s. For instance, at r/R =0.68, the difference of the magnitude values of the TKE, τ_{rr} and D_{rr} when the gas velocity increased from 8 cm/s to 20 cm/s were approximately 37%, 38% and 15.7%, respectively, while their change values were 24%, 10%, and 4%, respectively, when the gas velocity increased from 20 cm/s to 45 cm/s.

All of these results align with the results of previous studies in gas-liquid systems (Degalessan, 1997; Ong, 2003) and gas-liquid–solid systems (Rodas, 2003; Han, 2007; Shaikh, 2007).

5.4.2. Effect of Internals for a Given Velocity. As noted previously, it is particularly important to understand the effect of internals on the hydrodynamics in bubble column reactors because most of the reactions in such reactors are exothermic, requiring heat exchange mechanisms to remove the generated heat in order to maintain the desired temperature and isothermal operating conditions. The effect of the internals (25% covered CSA meeting the requirements for Fischer-Tropsch heat removal) on the time–averaged liquid axial velocity, turbulent parameters and eddy diffusivity profiles

was investigated for the first time at different superficial gas velocities based on either the total or free CSA of the column in order to fairly compare their effect.

5.4.2.1. Effect of internals on liquid axial velocity for a given gas velocity. Figure 5.10 compares the liquid axial velocity with and without internals at various gas velocities based on the total and free CSA of the column. The bars shown in the figures represent the standard deviation around the mean as mentioned earlier. Clearly, the presence of internals at any given superficial gas velocity resulted in an increased magnitude of the liquid centerline and negative axial velocity due to the increase in the intensity of liquid recirculation. The internals caused the bubbles to break up into numerous small bubbles, whose longer residence time caused the gas holdup to increase; thus, the large amount of small bubbles entrained the liquid more effectively than a smaller amount of large bubbles, causing higher liquid axial velocity profiles. Also, even with internals, the inversion point of the liquid recirculation velocity still takes place at $r/R \approx 0.68$, which aligns with the conclusion reached by Hills (1974) and Forret et al. (2003). The change in the magnitude value of the liquid centerline axial velocity was somewhat higher at lower superficial gas velocities than at higher gas velocities. For instance, the increase in the centerline axial velocity magnitude was approximately 30%, 36% and 60% at 45cm/s, 20 cm/s and 8 cm/s, respectively, based on the total CSA. A similar finding with a smaller percentage of difference was found at a gas velocity based on the free CSA, which was approximately 16%, 27% and 44% at 45 cm/s, 20 cm/s and 8 cm/s, respectively. This indicates that internals have a significant effect on the flow patterns at lower superficial gas velocities corresponding to the bubbly and transition flow regimes; this is experimentally supported by the obtained gas holdup profiles (refer

to Figure 4.8) in this work. The effect of internals at higher superficial gas velocities on the liquid axial velocity decreased, as seen by comparing the percentage of change at 20 cm/s and 45 cm/s. As Figure 5.10 depicts, the similarity of the overall gas holdup and the gas holdup radial profile with and without internals when applying gas velocity based on the free CSA does not show similar liquid recirculation. This is because the CSA available for the flow of gas and liquid in bubble columns with internals is smaller than that in columns without internals. The local gas holdup is similar in both columns (with and without internals), hence the CSA available for the liquid to flow in the column with internals is smaller than that in the column without internals. Therefore, to maintain mass balance of the batch operated liquid phase between the central region of up flow and the wall region of down flow, while inversion points remain the same in both columns (with and without internals), the local axial liquid velocity should increase, as confirmed by the obtained data. These results do not contradict the conclusion reached or the scale up methodology proposed and demonstrated by Shaikh (2007) based on obtaining hydrodynamics similarities when radial gas holdup profiles become similar in magnitude and shape. This is because there is no geometrical similarity between empty columns and columns with internals, especially if the internals are dense, as they were in the current study. Therefore, Shaikh's (2007) proposed methodology for the scale-up of bubble columns remains applicable provided that the bubble columns maintain the same internals, configuration and geometrical similarity. This point requires further assessment in terms of the current study. In the presence of internals, the liquid axial velocity profiles became steeper, causing intensive global recirculation between the center region of the column and the wall. This is because the internals reduced the turbulent intensity, causing

an increase in the steepness of the liquid velocity profiles; hence, the liquid velocity fluctuations were restricted where the energy of the gas phase dissipated to the mean velocity. A similar trend was observed in the previous studies (Bernemann, 1989; Chen et al., 1999; Forret et al., 2003; Laraachi et al, 2006). The effect of internals on the liquid axial velocity profiles was as strong as the effect of the superficial gas velocity. For instance, an increase in the superficial gas velocity from 8 to 20 cm/s substantially increased the change in the magnitude of the centerline axial velocity by approximately 63%, while the change in the magnitude of the centerline axial velocity in the presence of internals at 8 cm/s based on the total CSA increased by approximately 60%. When moving toward the inversion point of the liquid recirculation velocity ($r/R \approx 0.68$), the difference of the axial liquid velocity magnitudes based on empty columns decreased until reaching zero; subsequently, it increased until reaching the maximum negative velocity and then decreased again. For example, a change of the magnitude value of 8 cm/s based on the free CSA was 43.6%, 23% and 0% at $r/R = 0$, 0.5 and 0.68 (inversion point), respectively, while close to the wall of the column, it increased by 23.3% at $r/R = 0.8$, then decreased by 19%. The same situation occurred with 8 cm/s based on the total CSA; 20 and 45 cm/s based on both the total and free CSA was found.

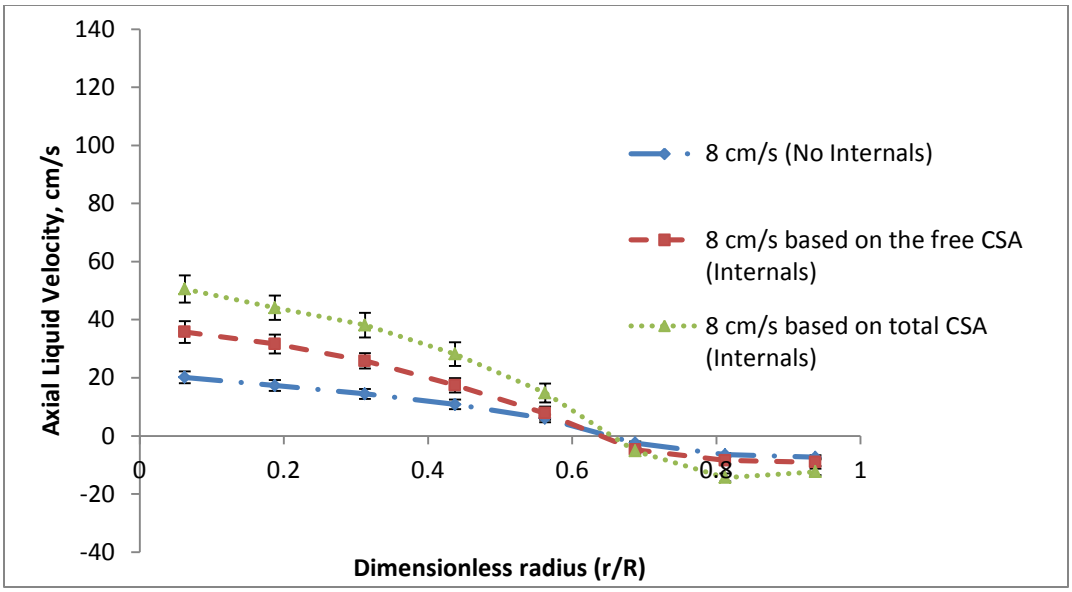

(a) Liquid axial velocity at 8 cm/s

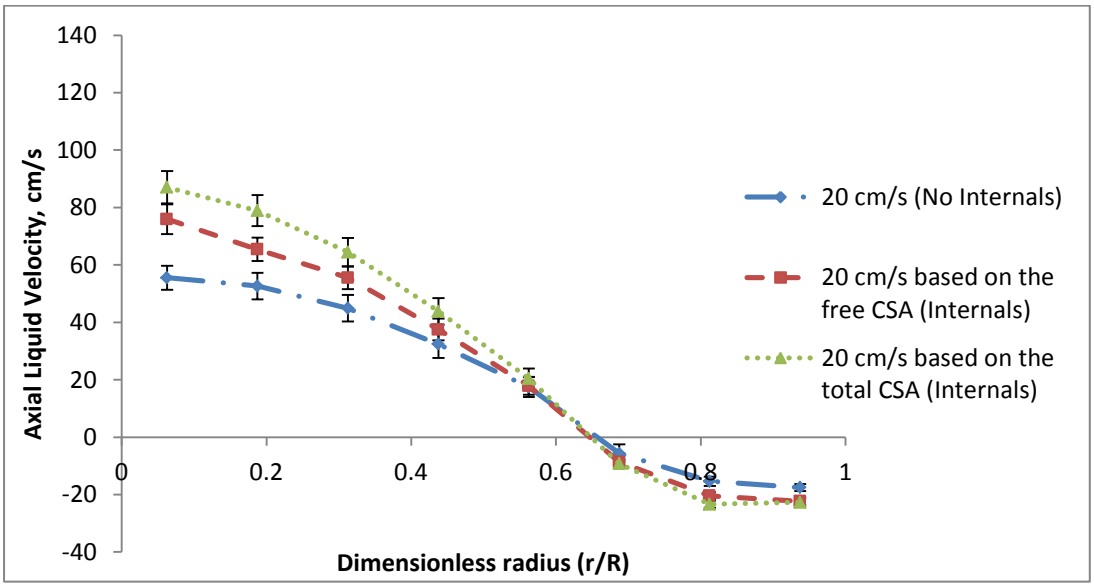

(b) Liquid axial velocity 20 cm/s

Figure 5.10. Comparison of Radial Profile of Liquid Axial Velocity with and without Internals at Gas Velocities Based on the Total and Free CSA in Gas-Liquid System

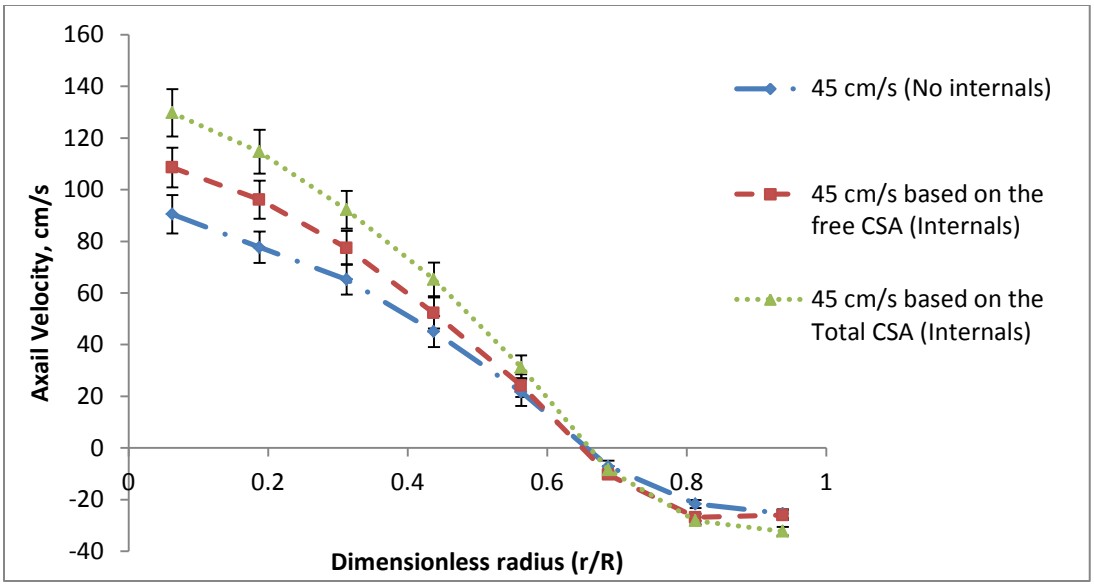

(c) Liquid axial velocity 45 cm/s

Figure 5.10. Comparison of Radial Profile of Liquid Axial Velocity with and without Internals at Gas Velocities Based on the Total and Free CSA in Gas-Liquid System (cont.)

5.4.2.2. Effect of internals on liquid Reynolds stresses for a given gas velocity.

A sharp decrease in the normal liquid stresses was found in the presence of internals compared to their values located between the center of the column and close to the inversion point in the column without internals, as shown in Figure 5.11. For instance, the magnitude value of the normal liquid stress decreased at r/R ≈0 by approximately 44% and 21% for 8 cm/s based on the free and total CSA, respectively. The figures show a peak close to the inversion point of the flow (r/R ≈ 0.68), which is due to the change of the flow dynamic from upward to downward. Therefore, the flow in this region consisted of more vigorous fluctuations leading to the peak. The liquid stress profiles at the gas

velocity based on the total CSA had magnitude values higher than those obtained at the gas velocity based on the free CSA, possibly because of the greater gas velocity (higher gas flow rate). The maximum value of the normal stresses occurred close to the inversion point. In addition, the normal stress values converged after the maximum value, which can be attributed to the configuration of the internals, whose impact will be eliminated in those areas. This trend is supported by the gas holdup profiles (refer to Section 4).

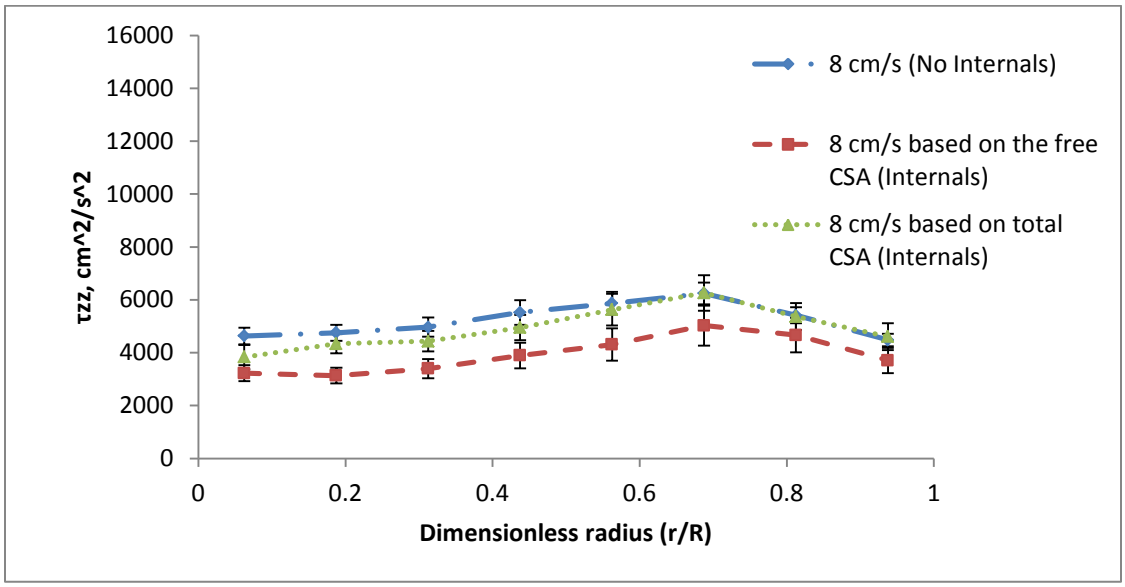

(a) Liquid axial normal stress at 8 cm/s

Figure 5.11. Comparison of Radial Profile of Liquid Axial Normal Stresses with and without Internals at Various Gas Velocities Based on the Total and Free CSA in Gas-Liquid System

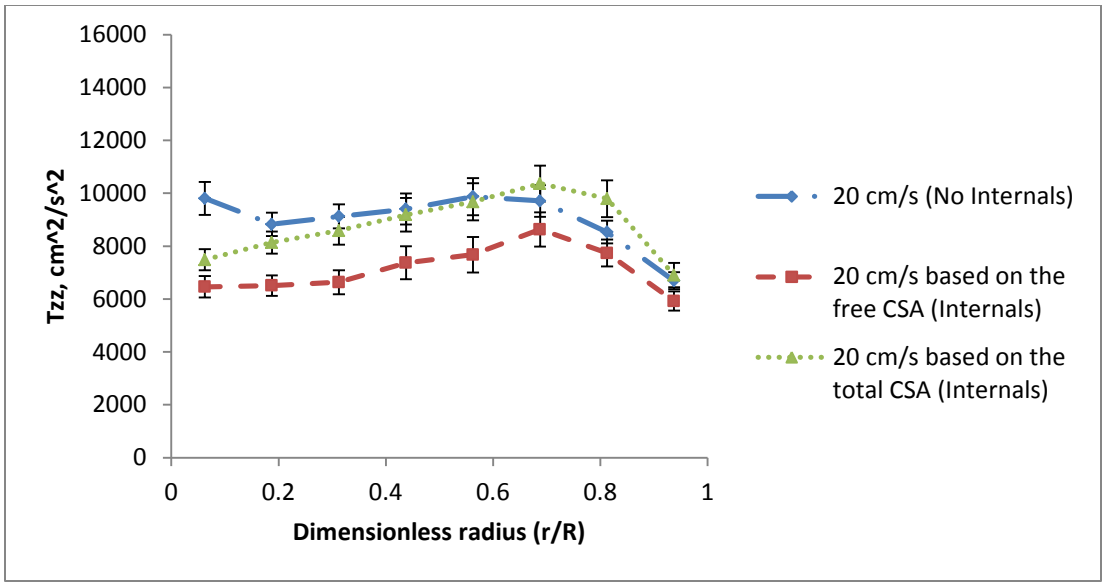

(b) Liquid axial normal stress at 20 cm/s

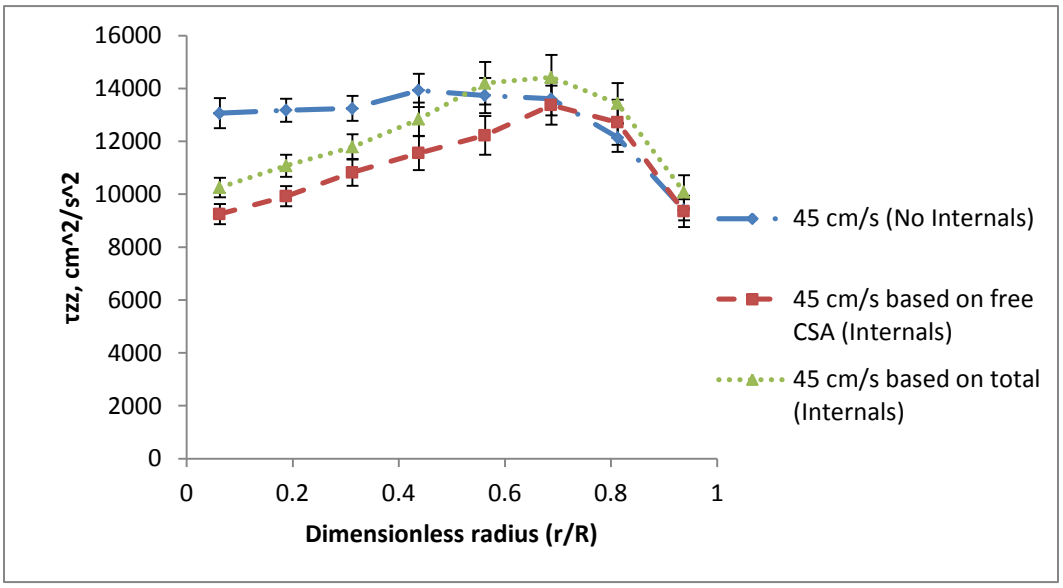

(c) Liquid axial normal stress at 45 cm/s

Figure 5.11. Comparison of Radial Profile of Liquid Axial Normal Stresses with and without Internals at Various Gas Velocities Based on the Total and Free CSA in Gas-Liquid System (cont.)

Figure 5.12 compares the liquid shear stresses at various superficial gas velocities based on the total and free CSA with internals and without internals. A sharp decrease in the liquid shear stress occurred in the presence of internals at the given gas velocity. For instance, at $r/R \approx 0.69$, the magnitude values of the shear stresses in the presence of internals decreased by 96% and 124% at 8 cm/s and 45 cm/s, respectively, based on the total CSA. The maximum value of the shear stress profiles occurred close to the inversion point of the flow ($r/R \approx 0.68$), while the minimum values occurred at the center and the wall of the column. Little difference exists between shear stresses when applying a gas velocity based on either the total or free CSA in the presence of internals, indicating that the effect of the minimal gas velocity on the shear stress is not as strong as that of the internals. Although the shear stress values decreased sharply in the region between the center and the wall, the more pronounced decrease occurred in the region between the center and close to the inversion point due to the configuration of the internals, whose impact was more pronounced in this area but nonexistent near the wall, as shown in Figure 5.12.

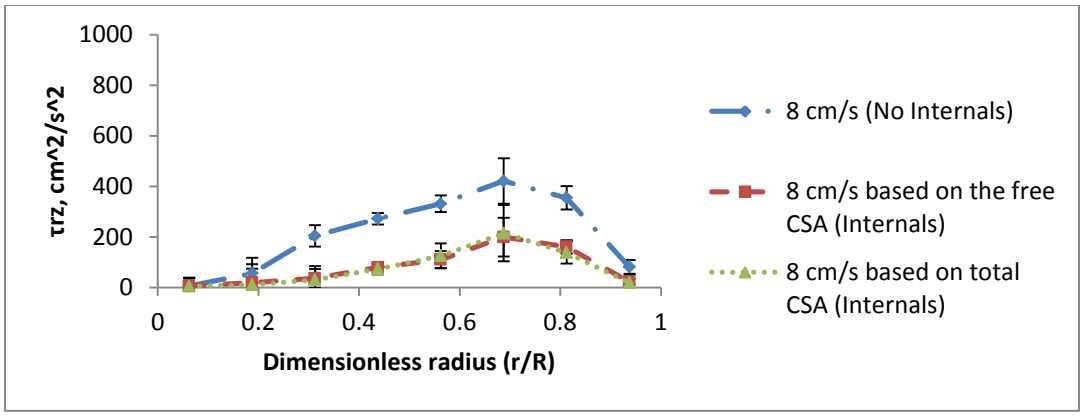

(a) Liquid shear stress at 8cm/s

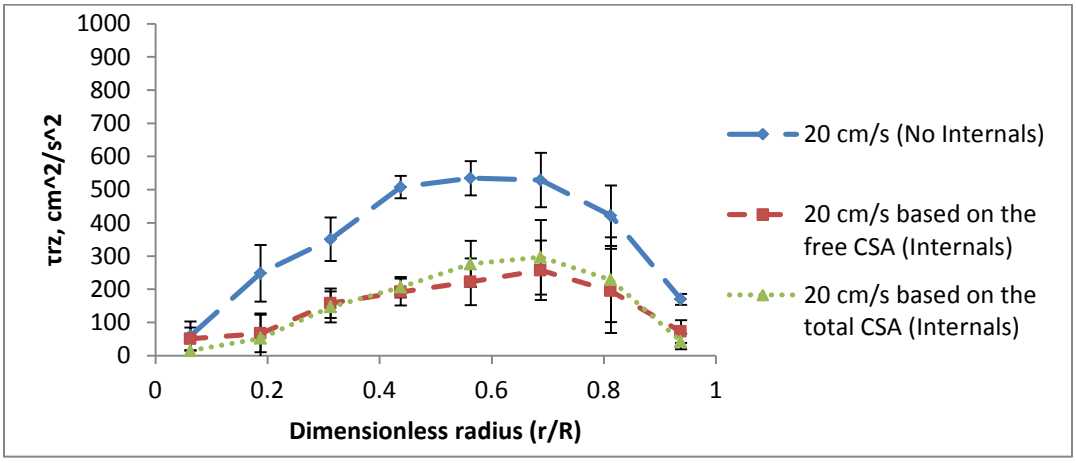

(b) Liquid shear stress at 20 cm/s

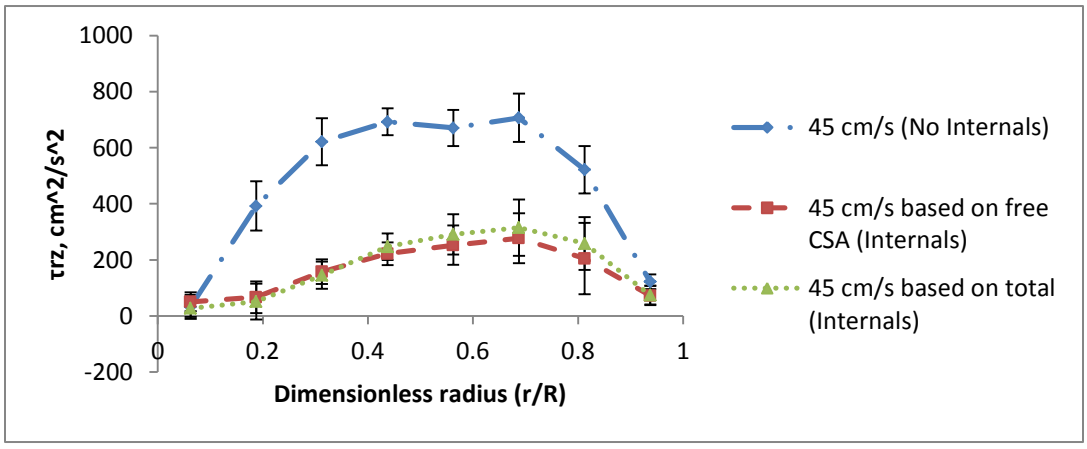

(c) Liquid shear stress at 45 cm/s

Figure 5.12. Comparison of Radial Profile of Liquid Shear Stresses with and without Internals at Gas Velocities Based on the Total and Free CSA in Gas-Liquid System

5.4.2.3. Effect of internals on liquid kinetic turbulent energy for a given gas velocity. Figure 5.13 shows the effect of internals on the time-averaged turbulent kinetic energy (TKE) radial profiles at 8 cm/s, 20 cm/s and 45 cm/s based on the total and free CSA. A sharp decrease in the liquid TKE was found in the presence of internals compared to their values located between the center of the column and close to the inversion point in the column without internals, as shown in Figure 5.13. For instance, at r/R ≈ 0.0, the magnitude values of the average turbulent kinetic energy in the presence of internals decreased by 91% and 53% at 8 cm/s based on the free and total CSA, respectively. The radial turbulent kinetic energy profiles still followed the axial normal stress trend. The turbulent kinetic energy values converged after the inversion point and close to the wall of the column, where the effect of the internals diminished.

This result aligns with the results obtained by Larachi et al. (2006) that a sharp decrease in the liquid kinetic turbulent energy in the bubble column occurred in the presence of the heat exchange tubes.

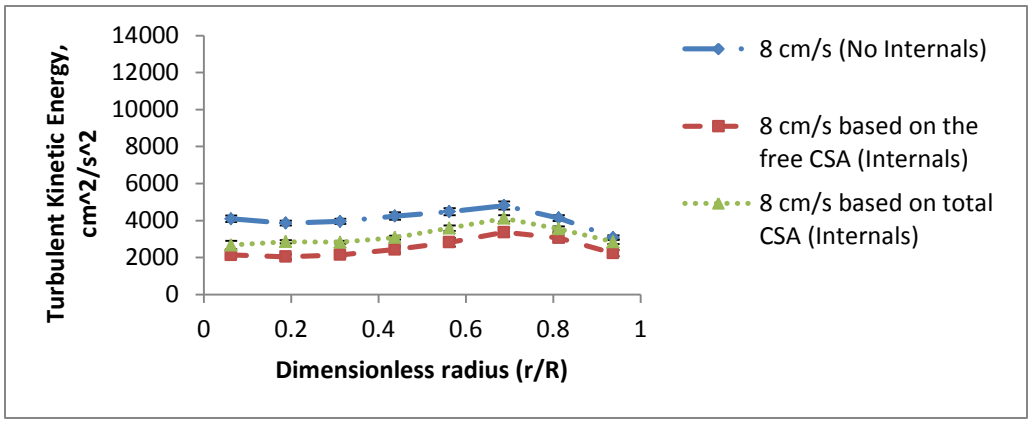

(a) Liquid Turbulent Kinetic Energy at 8 cm/s

Figure 5.13. Comparison of Radial Profile of Liquid Turbulent Kinetic Energy with and without Internals at Gas Velocities Based on the Total and Free CSA in Gas-Liquid System

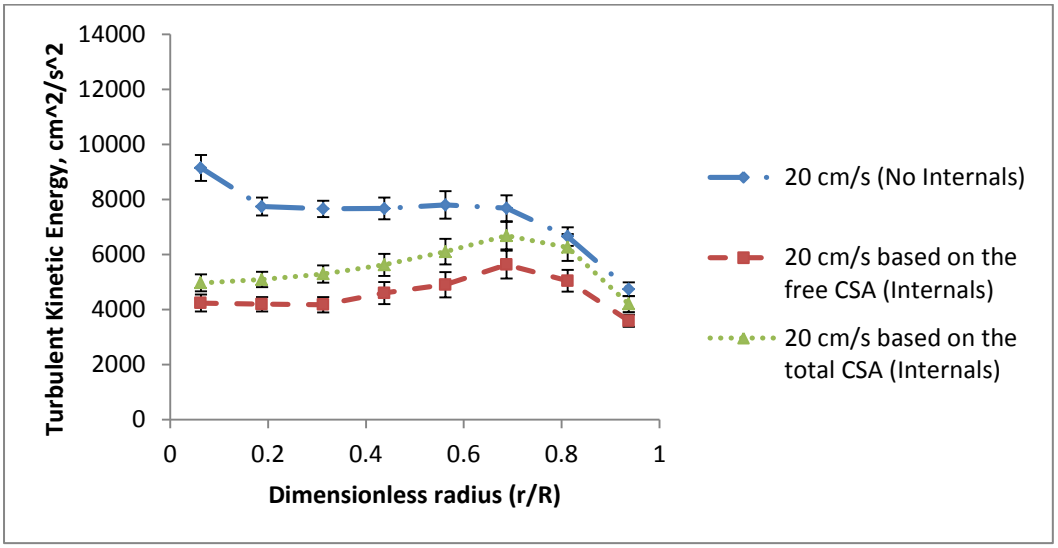

(b) Liquid Turbulent Kinetic Energy at 20 cm/s

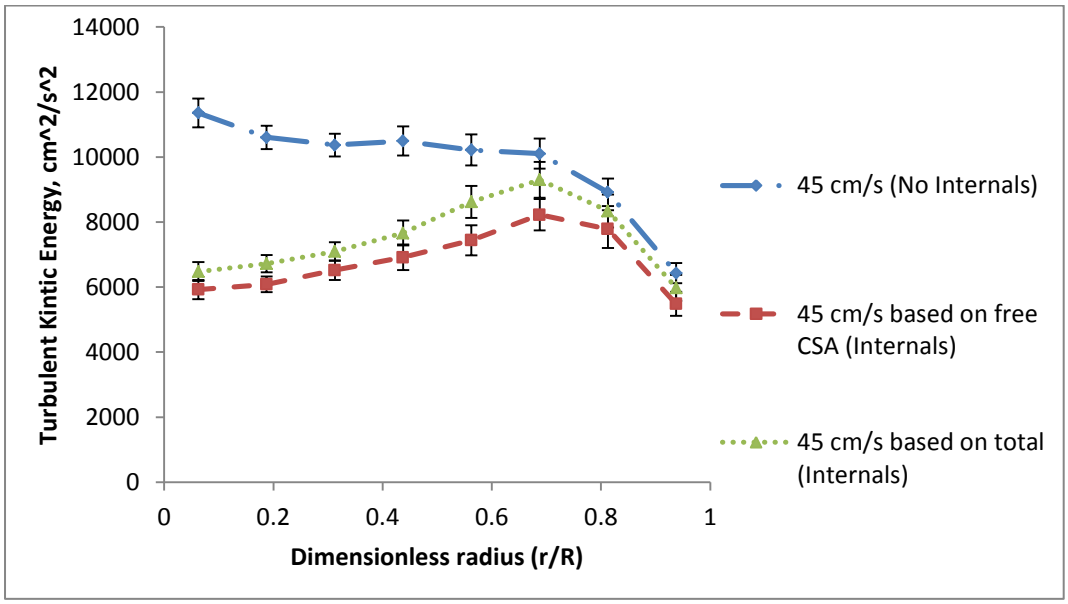

(c) Liquid Turbulent Kinetic Energy at 45 cm/s

Figure 5.13. Comparison of Radial Profile of Liquid Turbulent Kinetic Energy with and without Internals at Gas Velocities Based on the Total and Free CSA in Gas-Liquid System (cont.)

5.4.2.4. Effect of internals on liquid eddy diffusivity for a given gas velocity. As shown previously regarding the turbulence parameters, at a given superficial gas velocity, the internals decreased the radial and axial eddy diffusivities, as illustrated in Figure 5.14. In the presence of internals, the maximum values for the axial eddy diffusivity still occurred around the inversion point, where the axial velocity fluctuation was higher, indicating better mixing. Degalessen (1997) reported that the maximum axial eddy diffusivity occurs close to the inversion point of the liquid recirculation velocity, where the maximum shear stress occurs. The sharp decrease in the magnitude value of the axial eddy diffusivity occurred at $r/R \approx 0$; for example, the difference in the magnitude of the axial eddy diffusivity at that point in the presence of internals was 74% and 68% at 45 cm/s based on the free and total CSA, respectively. In the case of the radial eddy diffusivity, even with internals, the maximum values still occurred at $r/R \approx 0.5$, where a sharp decrease occurred for the magnitude value of radial diffusivity. For instance, in the presence of internals, the difference of the radial eddy diffusivity at $r/R \approx 0.5$ was 142%, 114%, and 103% at 8 cm/s, 20 cm/s and 45 cm/s, respectively, based on the free CSA. When applying the gas velocity based on the total CSA in the presence of internals, the axial eddy diffusivity had a somewhat large magnitude value because it was affected by the higher flow rate caused by the presence of internals, which resulted in less area available for the flow compared to the case with the free CSA. However, little or no difference existed in the radial eddy diffusivity between the cases of total and free CSA because the velocity in the radial direction was very small compared to the velocity in the axial direction; furthermore, the internals restricted the bubble-induced eddies in the radial direction to a greater extent. The decrease in the turbulent diffusivities in the

presence of internals can be attributed to the fact that the internals reduced the turbulence; this finding aligns with the work of Chen et al. (1999), Forret et al. (2003) and Larachi et al. (2006). Chen et al. (1999) also found that the liquid turbulent diffusivities and turbulent stresses are lower in the presence of internals and that the internals lead to decreases in the fluctuating velocity. In addition, these findings are supported by Forret et al. (2003) and Hamed (2012) for the gas turbulent diffusivities. This finding can be explained fundamentally in that the vertical internals restrict and break the bubbles, which decreases the bubble-induced turbulence and breaks the large turbulent wakes, causing the large turbulent eddies to dampen. Thus, it can be concluded that the presence of internals leads to a decrease in the turbulence and turbulence-related parameters due to the previously mentioned effects. Based on that the presence of internals leads to stabilization of the flow by smaller bubble sizes and as a result, lowering of the turbulence parameters.

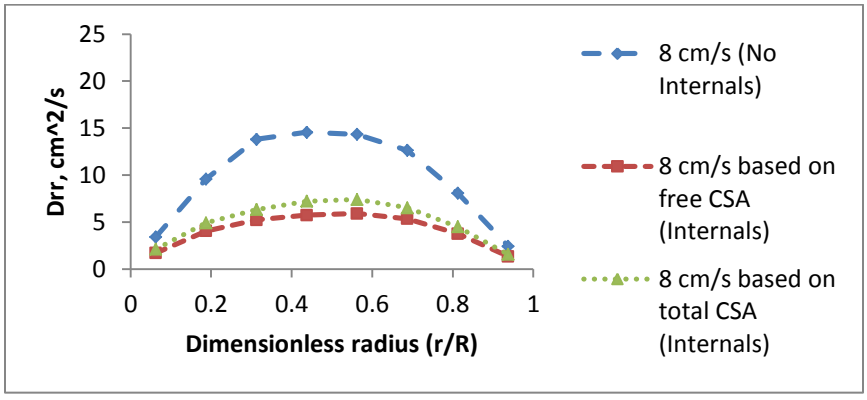

(a) Liquid radial eddy diffusivity at 8 cm/s

Figure 5.14. Comparison of Radial Profile of Liquid Radial and Axial Eddy Diffusivities with and without Internals at Gas Velocities Based on the Total and Free CSA in Gas-Liquid System

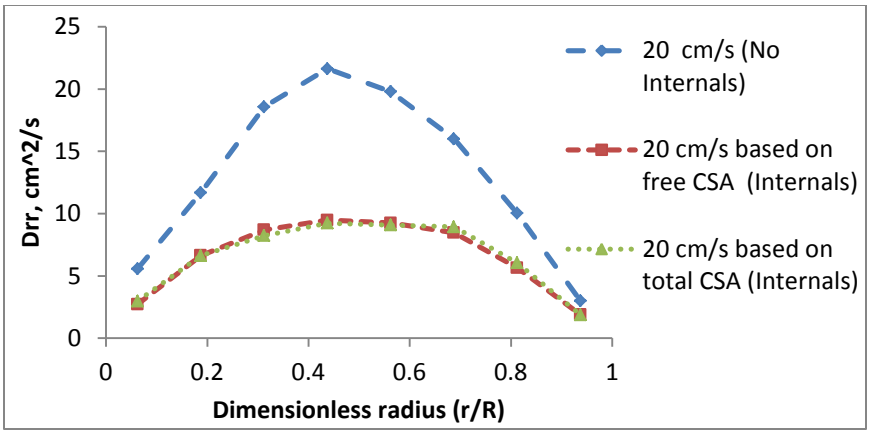

(b) Liquid radial eddy diffusivity at 20 cm/s

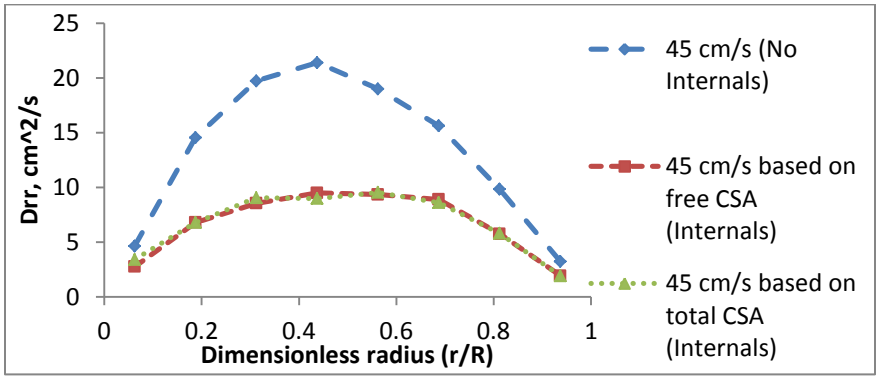

(c) Liquid radial eddy diffusivity 45 cm/s

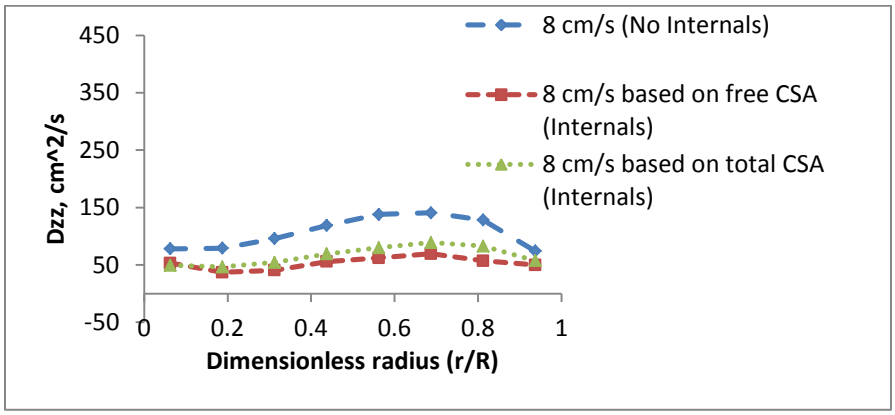

(d) Liquid axial eddy diffusivity at 8 cm/s

Figure 5.14. Comparison of Radial Profile of Liquid Radial and Axial Eddy Diffusivities with and without Internals at Gas Velocities Based on the Total and Free CSA in Gas-Liquid System (cont.)

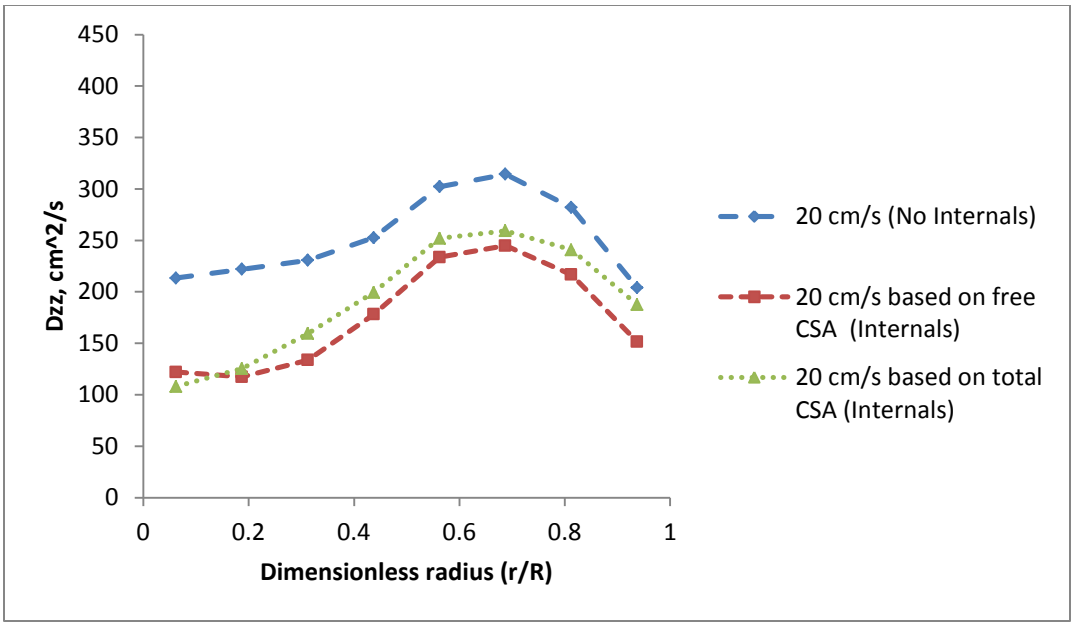

(e) Liquid axial eddy diffusivity at 20 cm/s

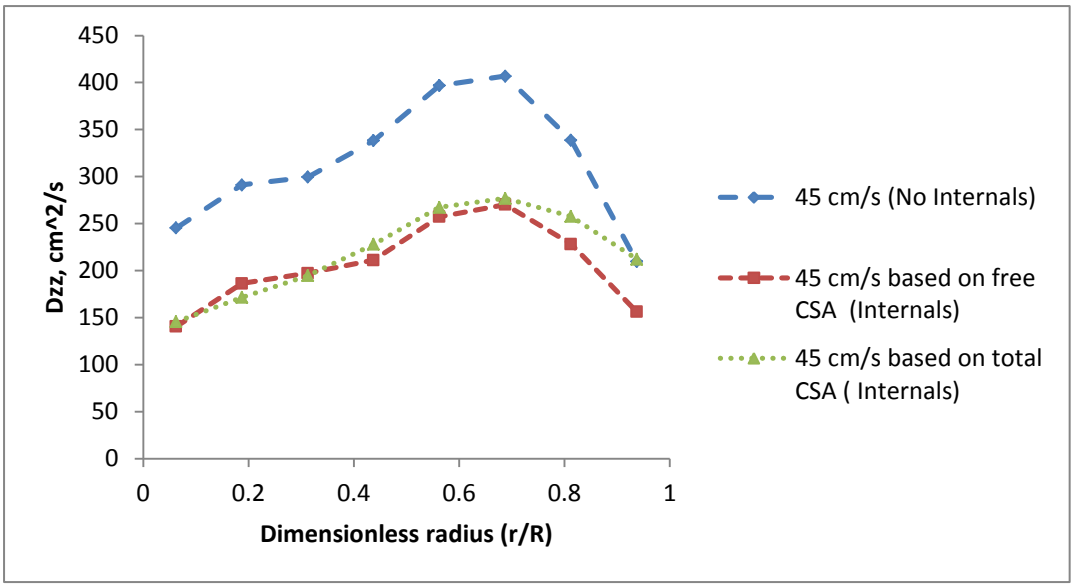

(f) Liquid axial eddy diffusivity at 45 cm/s

Figure 5.14. Comparison of Radial Profile of Liquid Radial and Axial Eddy Diffusivities with and without Internals at Gas Velocities Based on the Total and Free CSA in Gas-Liquid System (cont.)

5.4.3. Effect of Internals and Superficial Gas Velocity

5.4.3.1. Effect of internals and superficial gas velocity based on free cross-sectional area (CSA). Figure 5.15 shows the effect of the superficial gas velocities based on the free CSA on the time-averaged liquid velocity profiles and velocity vector plots in the presence of internals. As the superficial gas velocity based on the free CSA increased, so did the liquid centerline and negative axial velocity. For example, increasing the superficial gas velocity from 8 cm/s to 20 cm/s and from 20 cm/s to 45 cm/s increased the liquid centerline velocity magnitude value by approximately 53% and 30% on average, respectively, while the negative axial velocity magnitude increased by approximately 58% and 24% on average when the gas velocity increased from 8 cm/s to 20 cm/s and from 20 cm/s to 45 cm/s, respectively. Even with internals, the inversion point of flow still occurred at r/R ≈ 0.68, where the axial velocity was zero. The presence of internals enhanced the intensity of liquid recirculation due to the decrease in the fluctuating velocity.

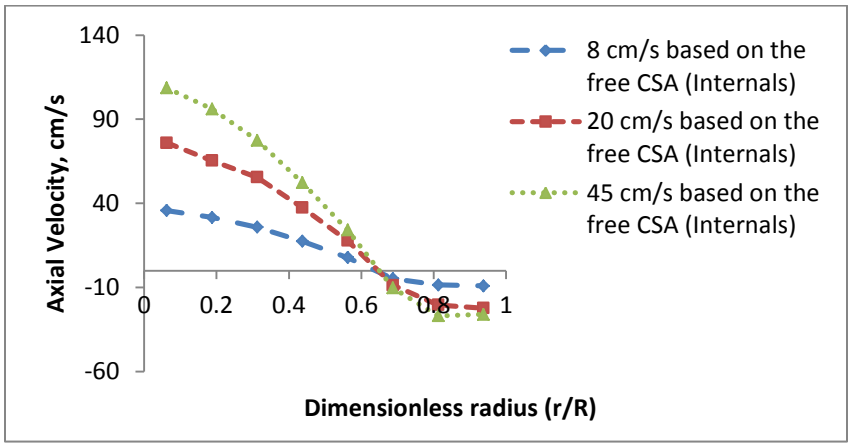

(a) Liquid Axial Velocity

Figure 5.15. Liquid Axial Velocities and Velocity Vectors Plots at Different Superficial Gas Velocities Based on Free CSA

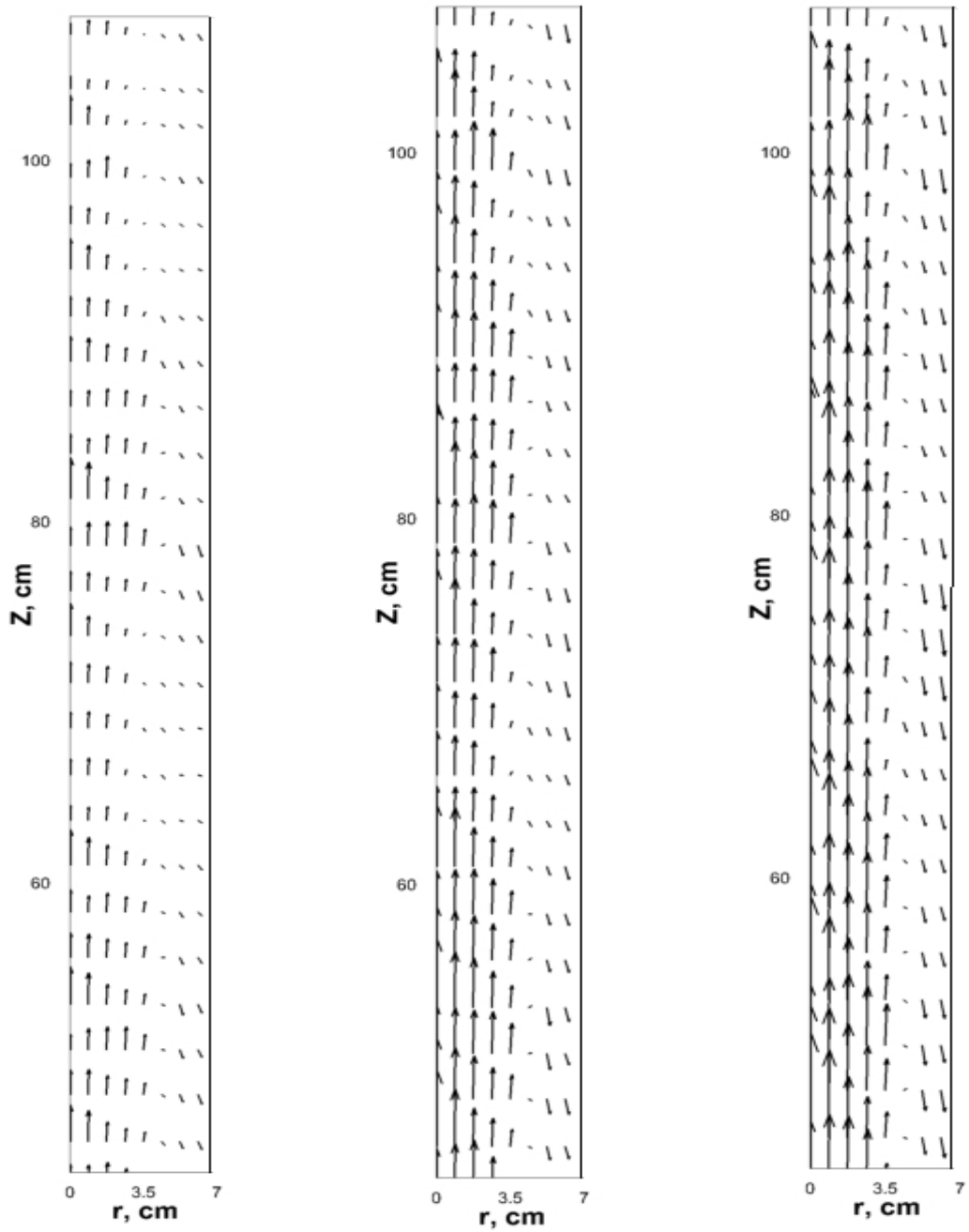

8 cm/s based on free CSA 20 cm/s based on free CSA 45 m/s based on free CSA

(b) Velocity vector plots in the r-z plane

Figure 5.15. Liquid Axial Velocities and Velocity Vectors Plots at Different Superficial Gas Velocities Based on Free CSA (cont.)

Figure 5.16 shows the effect of the superficial gas velocity based on the free CSA on the radial profiles of the time-averaged Reynolds stresses, namely, the axial normal stress and the shear stress in the axial and radial directions. As the superficial gas velocity based on the free CSA increased, so did the liquid axial normal stresses in the presence of internals. For example, as the superficial gas velocity increased from 8 cm/s to 20 cm/s and from 20 cm/s to 45 cm/s at r/R ≈ 0, the magnitude of the liquid normal stresses increased by approximately 50% and 30% on average, respectively. These values are very close to the percentage of the difference obtained with the centerline axial velocity under the same conditions. The maximum values for both the normal and shear stresses occurred around the inversion point of the flow. Approximate identical values for shear stresses were observed in the center of the region (r/R ≈ 0 – 0.3) and close to the wall of the column (r/R ≥ 0.8), where the flow was confined, as shown in Figure 5.16.

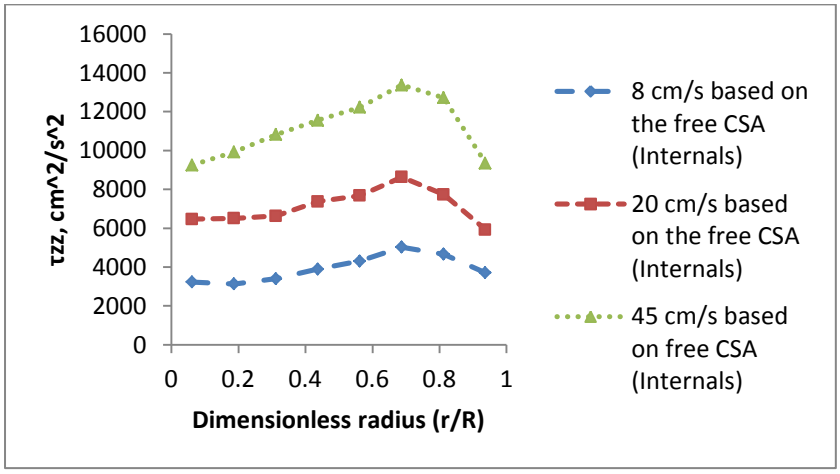

(a) Liquid Axial Normal Stress

Figure 5.16. Comparison of Radial Profile of Liquid Reynolds Stresses with Internals at Different Gas Velocities Based on the Free CSA in Gas-Liquid System

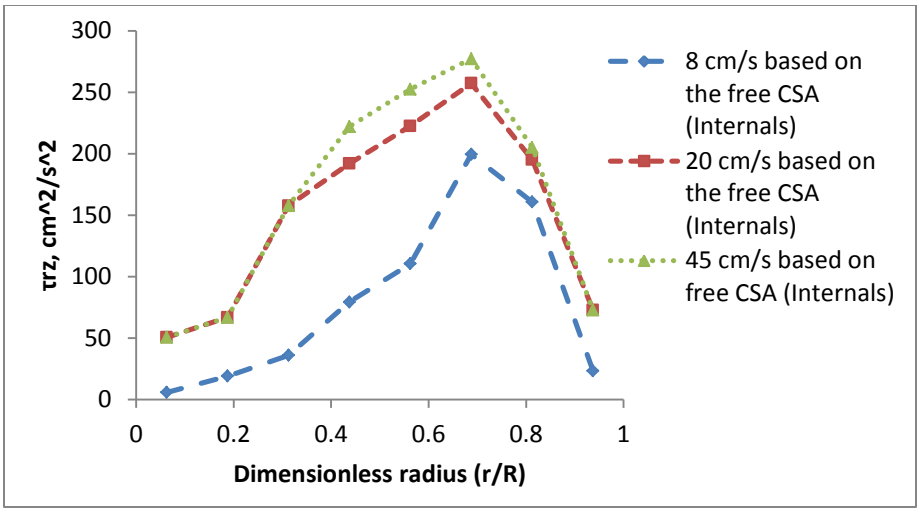

(b) Liquid Shear Stress

Figure 5.16. Comparison of Radial Profile of Liquid Reynolds Stresses with Internals at Different Gas Velocities Based on the Free CSA in Gas-Liquid System (cont.)

With an increase in the superficial gas velocity based on the free CSA, the magnitude of the turbulent kinetic energy and axial eddy diffusivity increased in the presence of internals. The same trend occurred with the radial eddy diffusivity at a lower velocity, as shown in Figure 5.17. When the superficial gas velocity increased from 8 cm/s to 20 cm/s and from 20 cm/s to 45 cm/s at r/R ≈ 0, the turbulent kinetic energy magnitude value increased by approximately 50% and 29% on average, respectively. These values are very close to the percentage of the difference obtained with the centerline axial velocity under the same conditions, which is not surprising because the turbulent kinetic energy follows the axial normal stress, which has the same difference. The higher magnitude values of the TKE and axial normal eddy diffusivity were in the region close to the inversion point (r/R ≈0.68) of the axial velocity, where more

interaction occurred. Under a fully developed turbulent regime (higher gas velocities), the radial eddy diffusivities were approximately identical due to the additional restriction of eddies presented by the internals, as well as the negligible velocity in that direction.

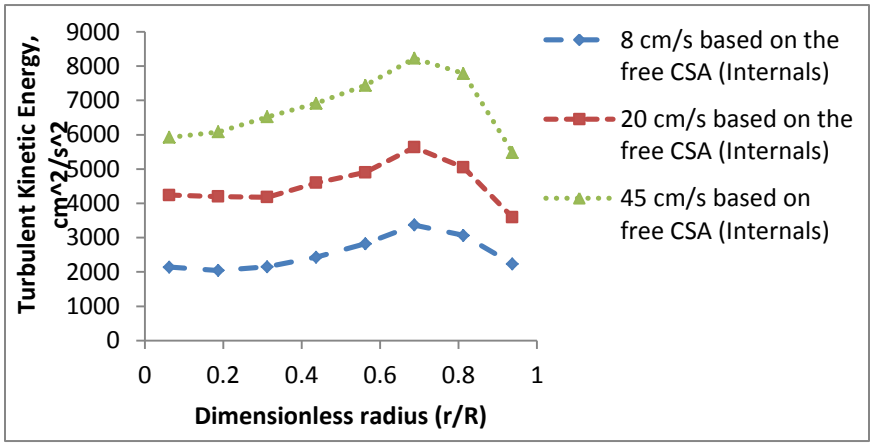

(a) Liquid Turbulent Kinetic Energy

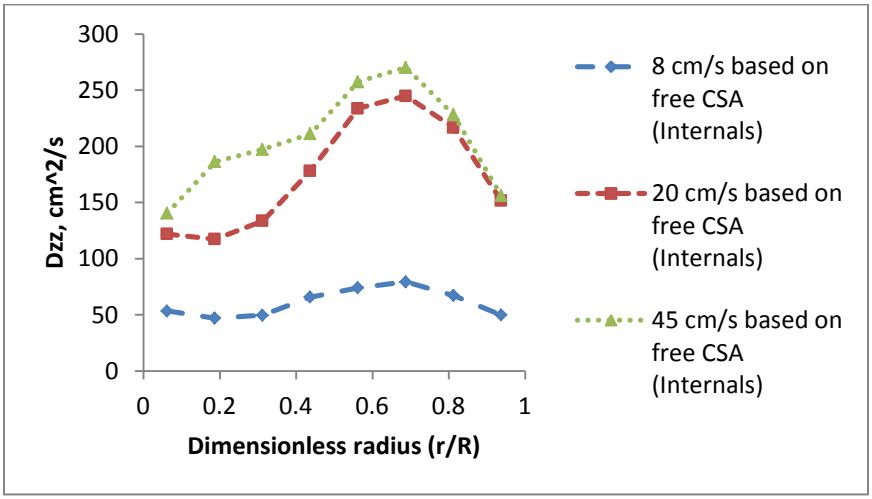

(b) Liquid Axial Eddy Diffusivity

Figure 5.17. Comparison of Radial Profile of Liquid Turbulent Kinetic Energy and Axial and Radial Eddy Diffusivities with Internals at Different Gas Velocities Based on the Free CSA in Gas-Liquid System

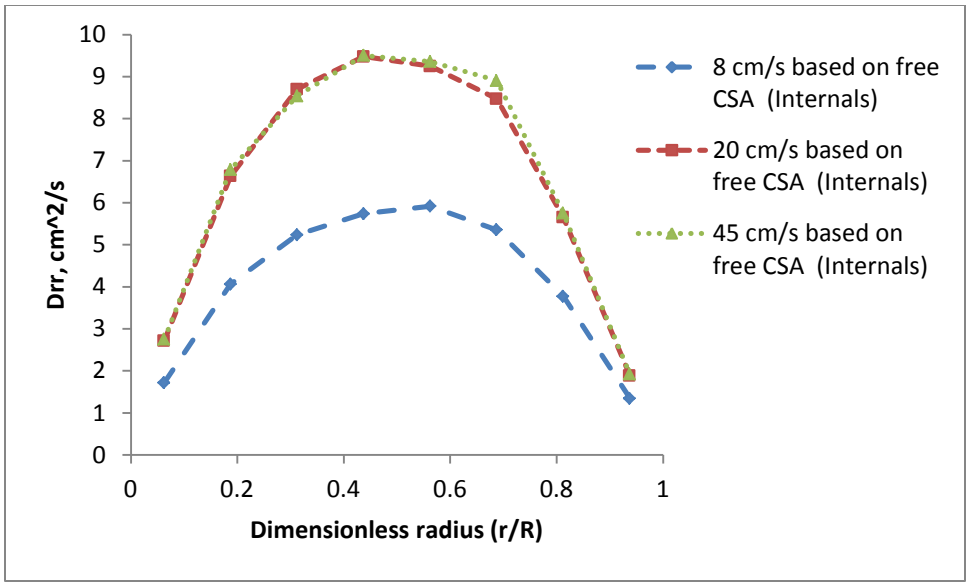

(c) Liquid radial Eddy Diffusivity

Figure 5.17. Comparison of Radial Profile of Liquid Turbulent Kinetic Energy and Axial and Radial Eddy Diffusivities with Internals at Different Gas Velocities Based on the Free CSA in Gas-Liquid System (cont.)

5.4.3.2. Effect of internals and superficial gas velocity based on total cross-sectional area (CSA). Figures 5.18 and 5.19 show the effect of the superficial gas velocities based on the total CSA in the presence of internals on the time averaged of axial velocity and turbulent parameters. The same pronounced effect of increasing the superficial gas velocity on the liquid axial velocity and the turbulence and turbulence-related parameters was observed in the presence of internals. As the superficial gas velocity increased, so did the magnitude of the liquid centerline and the negative axial velocity (Figure 5.18). For instance, with an increase in the superficial gas velocity from 8 cm/s to 20 cm/s and from 20 cm/s to 45 cm/s, the liquid centerline velocity magnitude

value increased by approximately 42% and 31% on average, respectively, while the negative axial velocity magnitude increased by approximately 38% and 17% on average when the gas velocity increased from 8 cm/s to 20 cm/s and from 20 cm/s to 45 cm/s, respectively. Even with a velocity based on the total CSA, the inversion point of the flow still occurred at r/R ≈ 0.68. This finding is consistent with the previous study using an air-water system with and without internals.

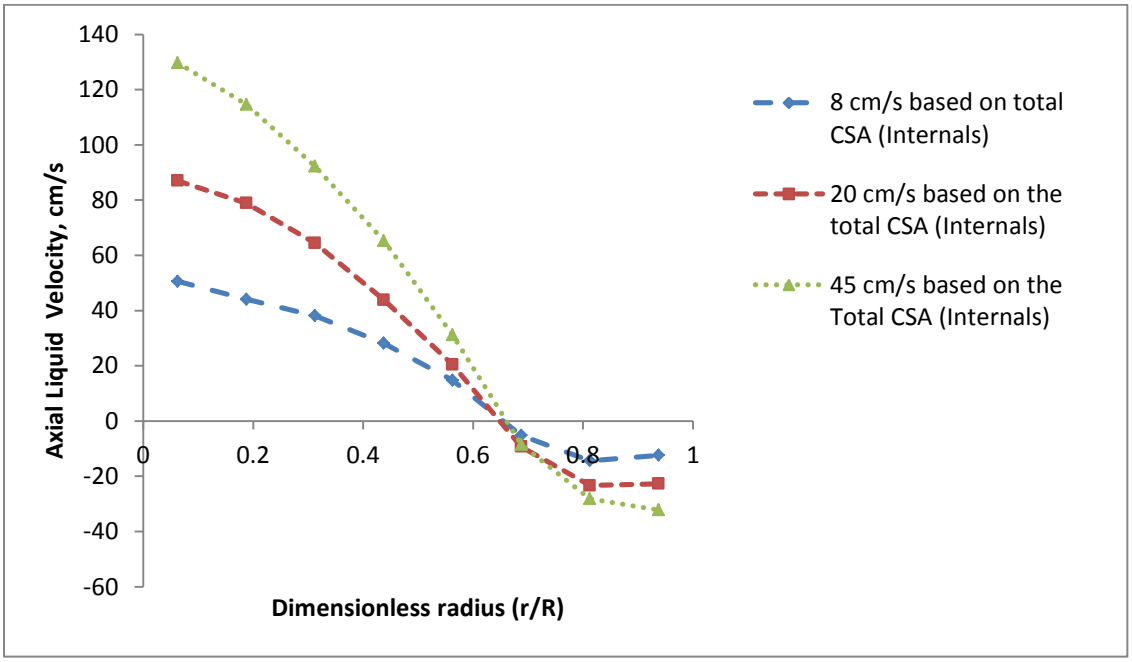

(a) Liquid axial velocity

Figure 5.18. Velocity Vector Plots and Liquid Axial Velocity at Different Superficial Gas Velocities Based on Total CSA

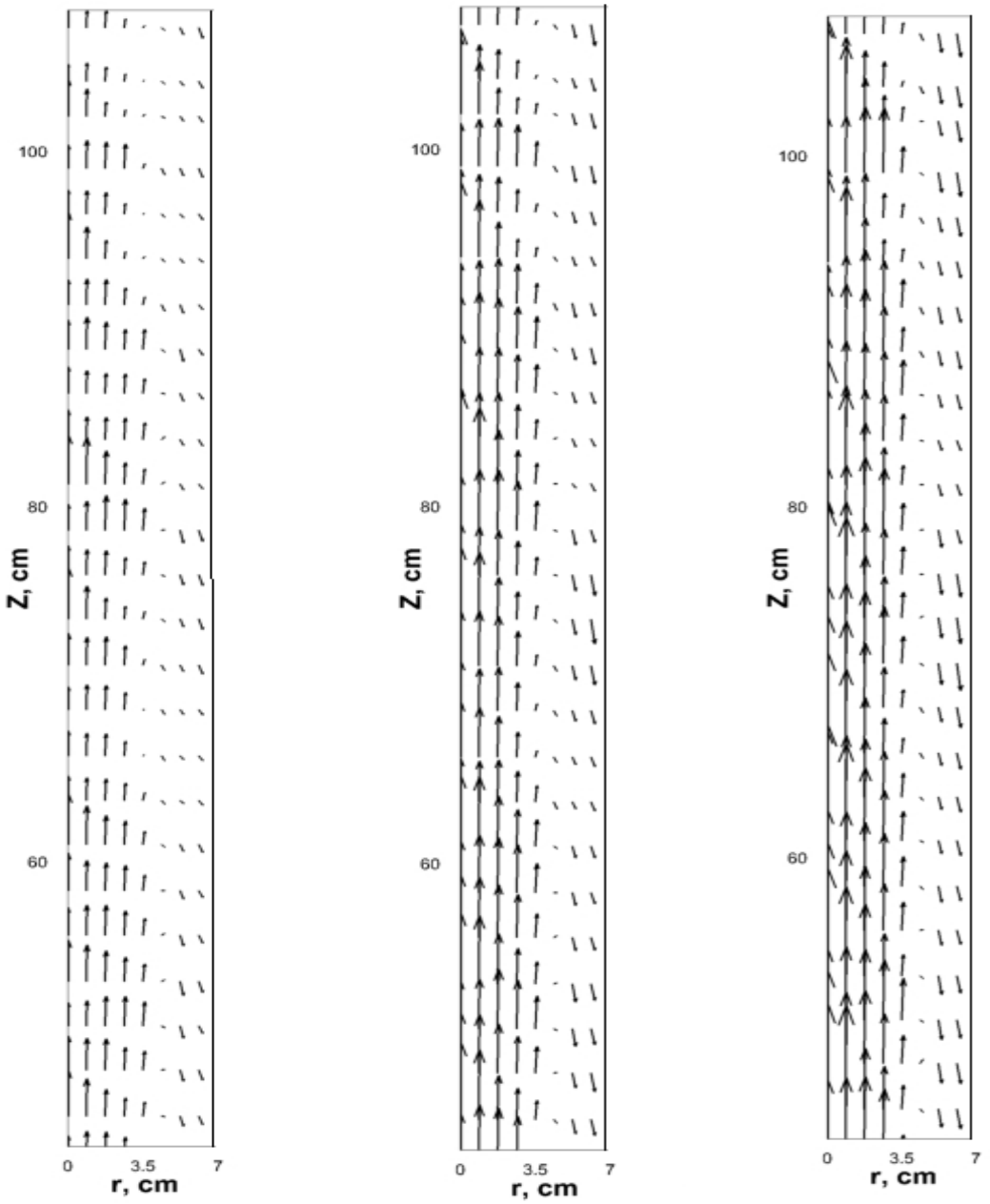

8 cm/s based on total CSA 20 cm/s based on total CSA 45 cm/s based on total CSA

(b) Velocity vector plots in the r-z plane

Figure 5.18. Velocity Vector Plots and Liquid Axial Velocity at Different Superficial Gas Velocities Based on Total CSA (cont.)

The turbulence parameters, including the liquid normal and shear stresses, turbulent kinetic energy and eddy diffusivity profiles, increased as the superficial gas velocities based on total CSA increased (Figure 5.19) because the turbulence increased at higher superficial gas velocities, which caused an increase in the fluctuating velocities. For example, at r/R ≈ 0 an increase in superficial gas velocity from 8 cm/s to 45 cm/s based on total CSA substantially increased the axial normal stress, TKE and axial eddy diffusivity by 61%, 59% and 66%, respectively. The higher magnitude values of the turbulent kinetic energy, axial normal stress, and axial normal eddy diffusivity occurred in the region close to the inversion point (r/R ≈0.68) of the axial velocity, where more interaction occurred, while the maximum value of the radial eddy diffusivity occurred at r/R ≈ 0.5, where the liquid flow was less confined than the flow at the wall and the column's center (axial symmetric).

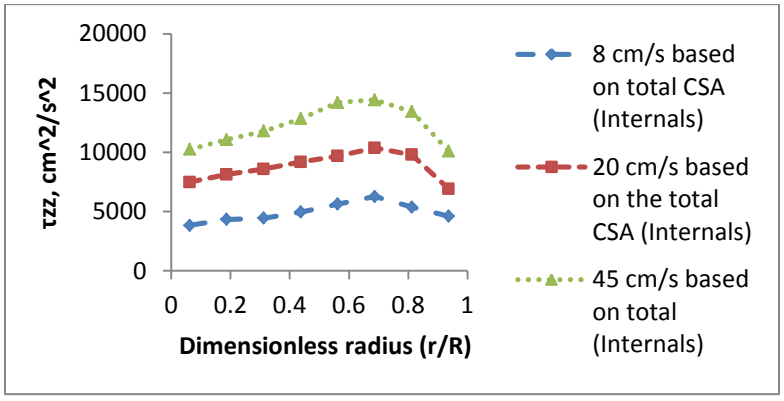

(a) Liquid axial normal stresses

Figure 5.19. Comparison of Radial Profile of Liquid Radial and Axial Turbulence and Turbulent-related Parameters with Internals at Different Gas Velocities Based on the Total CSA in Gas-Liquid System

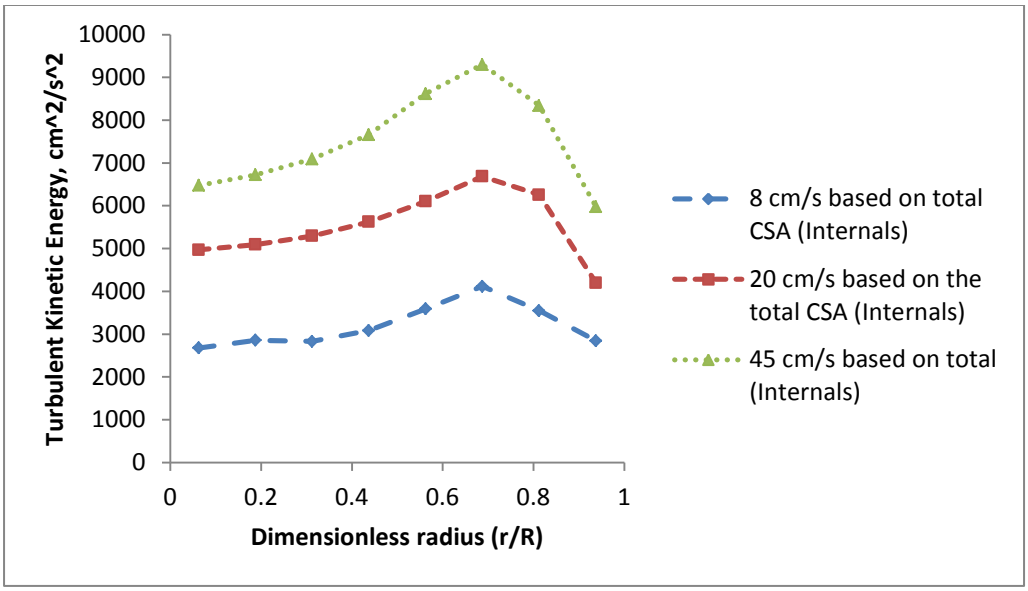

(b) Liquid turbulent kinetic energy

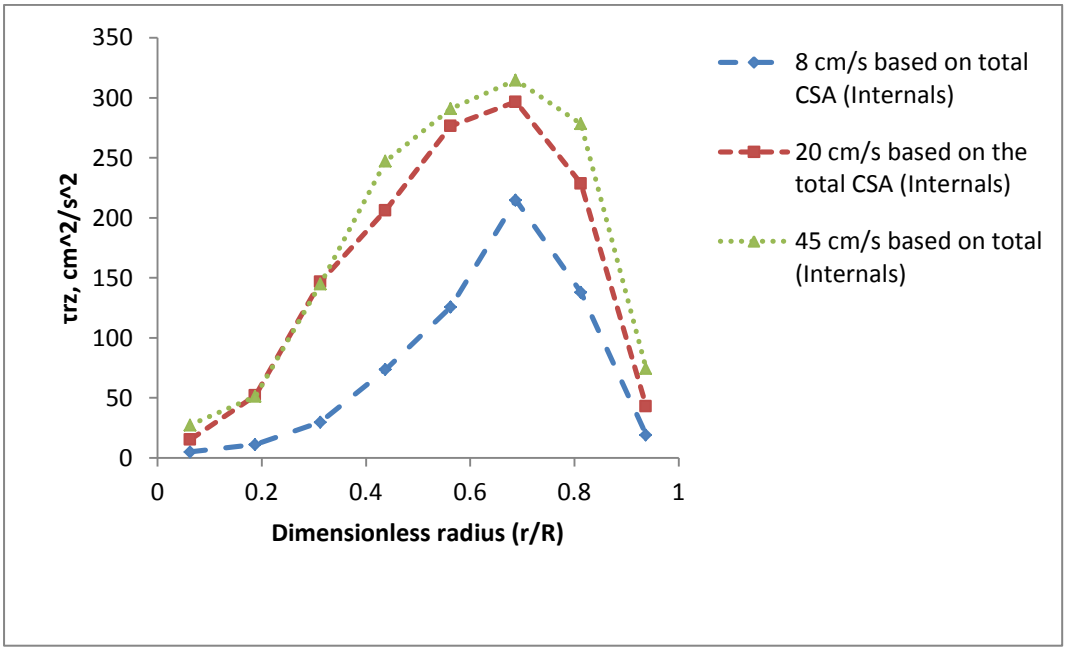

(c) Liquid shear stress

Figure 5.19. Comparison of Radial Profile of Liquid Radial and Axial Turbulence and Turbulent-related Parameters with Internals at Different Gas Velocities Based on the Total CSA in Gas-Liquid System (cont.)

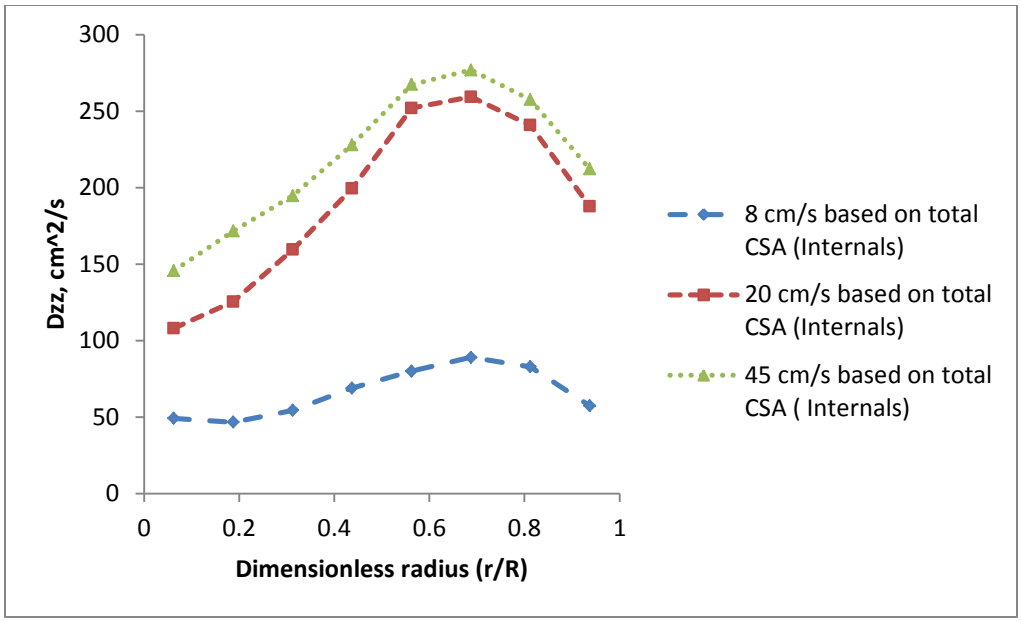

(d) Liquid axial eddy diffusivity

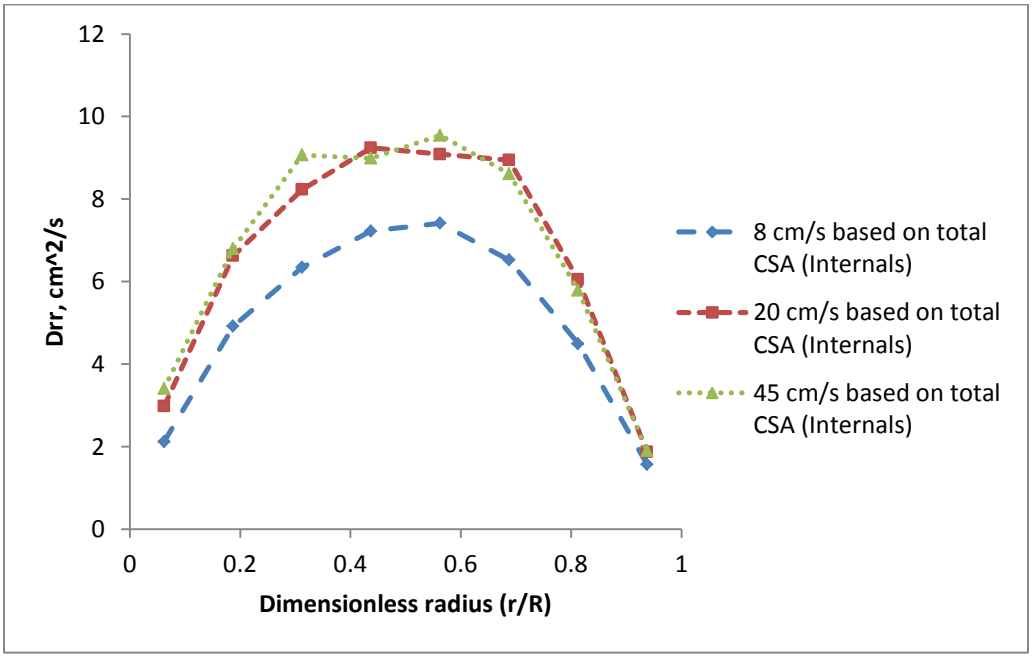

(e) Liquid radial eddy diffusivity

Figure 5.19. Comparison of Radial Profile of Liquid Radial and Axial Turbulence and Turbulent-related Parameters with Internals at Different Gas Velocities Based on the Total CSA in Gas-Liquid System (cont.)

The increase in the superficial gas velocity in the presence of internals resulted in an increase in the shear stress in the bubble column (Figure 5.19), which increased the rate of bubble breakup, leading to the formation of smaller bubbles. As noted in the previous sections, the maximum shear stress profiles occurred close to the inversion point of the flow ($r/R \approx 0.68$) with an increase in the gas velocity in the presence of internals. Degalessen (1997) reported that the maximum axial eddy diffusivity occurs close to the inversion point of the liquid recirculation velocity ($r/R \approx 0.7$), where the maximum shear stresses occur. Figure 5.19 shows that in fully developed turbulent regimes (higher superficial gas velocities), the radial eddy diffusivities are close (the difference between the profiles is less than 12%) because of the additional restrictions of eddies presented by internals and the negligible velocity in the radial direction.

6. CONCLUSIONS AND RECOMMENDATIONS

This work discussed the hydrodynamics in bubble columns in the presence of internals that meet the requirements of Fischer-Tropsch heat removal, using the non-invasive techniques of Computed Tomography (CT) and Radioactive Particle Tracking (RPT).

A set of experimental investagations was conducted to achieve the objectives of this work. Reliable data were obtained for the radial gas holdup distribution, liquid velocity field and turblence parameter profiles; these data provide answers to some questions but raise additional ones. The results for each objective were discussed in Sections 4 and 5, but the key findings are briefly summarized as follows:

- The overall gas holdup acted as a function of the superficial gas velocity both with and without internals; whether considering the total or just the free cross-sectional area, the overall gas holdup increased with an increase in the superficial gas velocity. No significant effect on the overall gas holdup was observed with or without internals in the case of superficial gas velocity based on the free CSA for any given gas velocity because of the similarity of the areas available for the flow.
- The effect of the superficial gas velocity on the time-averaged gas holdup radial profile at different superficial gas velocities was investigated. All CT scans were acquired at one fixed axial position (5.8 d_c) in the fully developed region. With an increase in the superficial gas velocity, the magnitude value of the gas holdup increased along the radial position, except at the region close to the column wall. At lower superficial gas velocities corresponding to the homogenous (bubbly)

flow regimes, the magnitude value of the gas holdup in the region close to the wall was found to be larger than that obtained at some higher velocities.

- With an increase in the superficial gas velocity, the gas holdup radial profile became steeper and more parabolic (Hills, 1974; Kumar, 1994; Joshi et al., 1998; Rados, 2003; Ong, 2003).
- Internals progressively enhanced the time-averaged gas holdup for all superficial gas velocities corresponding to bubbly and transition flow regimes and based on the total CSA in a churn-turbulent regime compared with those obtained for the same range of velocities in the column without internals. This effect could be attributed to the fact that the internals enhanced the break-up of bubbles into smaller bubbles with lower rise velocities and a longer residence time, which increased the gas holdup. The increase in the magnitude value of the radial gas holdup at high velocities based on the total CSA could be due to the effect of increasing the gas velocity (gas flow rate) rather than the effect of the internals because the internals had an insignificant effect on radial gas holdup profiles with increases in gas velocities based on the free CSA. This concerns the similarity of the area available for the flow.
- The gas holdup obtained in the empty column operated in the churn-turbulent flow regime can be extrapolated to bubble columns equipped with dense internals by matching the superficial gas velocity based on the free CSA available for flow.
- The presence of internals impacted the shape of the gas holdup radial profile, causing it to take on a wave-like shape (zigzag) compared to the smoother, more parabolic shape for those without internals. This effect may be attributed to the

fact that the internals formed small columns (channeling) inside the main bubble column. Hence, each set of internals created a certain pattern of flow.

- The change in the magnitude value of the gas holdup with internals was somewhat higher at lower superficial gas velocities than at higher gas velocities.
- As the superficial gas velocity increased, so did the liquid centerline and negative axial velocity. The time-averaged radial liquid velocities had insignificant magnitudes, which increased with an increase in the superficial gas velocity; the time-averaged azimuthal velocities also had small values.
- In general, the radial profiles of normal liquid stress increased with an increase in the superficial gas velocity. The normal stresses in the axial direction were larger than in the radial and tangential directions due to non-isotropy in the bubble column.
- The Reynolds shear stress profile was proportional to the liquid axial velocity radial gradient. An increase in the superficial gas velocity led to an increase in the shear stress. The maximum shear and stress profile values occurred close to the inversion point of the flow ($r/R \approx 0.68$), while the minimum values occurred in the center and at the wall of the column. As the gas velocity increased, so did the turbulent kinetic energy and eddy diffusivity profiles; this can be attributed to the fact that as the superficial gas velocity increased, the system became increasingly more turbulent, which affected the TKE and eddy diffusivity profiles. The radial turbulent kinetic energy profiles followed the behavior of the axial normal stress.
- The presence of internals, at any given superficial gas velocity, resulted in an increased magnitude of the liquid centerline and negative axial velocity. On the

other hand, a sharp decrease in the normal and shear liquid stresses, eddy diffusivity and liquid turbulent kinetic energy profiles at any given gas velocity was found in the presence of internals.

- The same pronounced effect of increasing the superficial gas velocity on the liquid axial velocity and turbulence and turbulence-related parameters was observed in the presence of internals. With an increase in the superficial gas velocity, the magnitude of the liquid centerline and negative axial velocity also increased. The turbulence parameters, including the liquid normal and shear stress, turbulent kinetic energy and eddy diffusivity profiles, increased as the superficial gas velocity increased because of the increase in the turbulence at higher superficial gas velocities, which caused an increase in the fluctuating velocities.

The key findings obtained in the work are summarized in Table 6.1.

Table 6.1. Overall Effects of Key Variables Studied

Varying parameter	Effect		Supporting data
U_g ↑ (In the presence and absence of internals)		Overall ε_g ↑ $\varepsilon_g(0)$ ↑ u_l (0 and close to wall) ↑ TKE ↑ liquid shear stress ↑ liquid normal stresses ↑ D_{zz} ↑ Drr ↑	Figure 4.1 Figures 4.6 and 4.9 Figurs 5.5 and 5.10 Figures 5.8 and 5.13 Figures 5.7 and 5.12 Figures 5.6 and 5.11 Figures 5.9 and 5.14 Figures 5.9 and 5.14
Presence of internals (For given U_g)	Based on total CSA	Overall ε_g ↑ $\varepsilon_g(0)$ ↑ u_l (0 and close to wall) ↑ TKE ↓ liquid shear stress ↓ liquid normal stresses D_{zz} ↓ Drr ↓	Figure 4.1 Figure 4.9 Figures 5.10 and 5.18 Figures 5.13 and 5.19 Figures 5.12 and 5.19 Figures 5.11 and 5.19 Figures 5.14 and 5.19 Figures 5.14 and 5.19

Table 6.1. Overall Effects of Key Variables Studied (cont.)

Varying parameter	Effect		Supporting data
Presence of internals (For given U_g)	Based on free CSA	Overall ε_g (Insignificant effect) $\varepsilon_g(0)$ ↑ (Insignificant effect at higher gas velocity) u_l (0 and close to wall) ↑ TKE ↓ liquid shear stress ↓ liquid normal stresses ↓ D_{zz} ↓ Drr ↓	Figure 4.1 Figure 4.9 Figures 5.10 and 5.15 Figures 5.13 and 5.17 Figures 5.12 and 5.16 Figures 5.11 and 5.16 Figures 5.14 and 5.17 Figures 5.14 nad 5.17

RECOMMENDATIONS FOR FUTURE WORK

Although this study provided essential knowledge and answers key questions regarding the effect of internals on the hydrodynamics in bubble columns, it raised additional questions. To answer some of the questions that arose, some recommendations for future work follow:

- The current work was restricted to a two-phase system (gas-liquid), while the FT process uses a three-phase system (gas-liquid-solid) operated at high pressure. Therefore, further tests should be conducted to mimic FT conditions, particularly the presence of solids, and to assess the effects of these different conditions.

- This work was limited to one 6” diameter column, and the column diameter is one of the most important design variables for bubble column reactors. Therefore, further studies should be conducted with a large diameter column, which is particularly important because CT and RPT are designed for large diameters up to 18”.
- In this work, the effect of one configuration of internals with only one diameter size was investigated. The effect of diameter size, configurations and shapes of internals, such as U-shaped internals, should be considered in further studies.
- Future work should assess the scale-up of a bubble column equipped with internals based on the methodology of matching the radial profile of gas holdup proposed by Shaikh (2007).
- It would be interesting to assess key dimensionless groups that can be used to correlate the obtained hydrodynamics parameters.
- In this work, a 2.38 mm tracer particle was used to reduce the drag force and perfectly follow the liquid motion. A smaller tracer particle is recommended for future work.
- Most studies reported in the literature focus on flow regime identification in bubble column reactors without internals. It would therefore be interesting to identify the flow regime in the presence of internals.
- To fully understand the hydrodynamics in bubble/slurry bubble columns, future studies must also investigate the bubble size distribution, heat transfer coefficient, etc.

- In future studies, a computational fluid dynamics model (CFD) should be used to validate the experimental data obtained from CT and RPT. The similarity between information obtained from CT, RPT, and CFD not only provides a detailed understanding of the hydrodynamic characteristics but also positions CFD as an alternative method for obtaining essential information regarding the performance of bubble column reactors with a much lower cost than CT and RPT measurements.

APPENDIX A

EFFECT OF TYPES OF INTERNALS ON THE RADIAL GAS HOLDUP PROFILES AT VARIOUS GAS VELOCITIES

Two different types of internals, stainless steel and Plexiglas rods, with similar diameters and configurations were used because Plexiglas attenuation is low. Additionally, we initially were not sure whether the CT could identify the tubes, so stainless steel internals were manufactured and examined at selected conditions. Figures A.1 – A.2 show the effect of these internals on the time-averaged cross-sectional gas distribution, PDF, of the gas holdup distribution values and gas holdup profiles at a superficial gas velocity of 8 cm/s based on the free CSA. In the presence of internals, either Plexiglas or steel, the variation in the corresponding means, variance and standard deviations was somewhat larger than that obtained in an empty column. The image and statistical results show that the variation with steel internals is roughly larger than that obtained in the column equipped with Plexiglas internals.

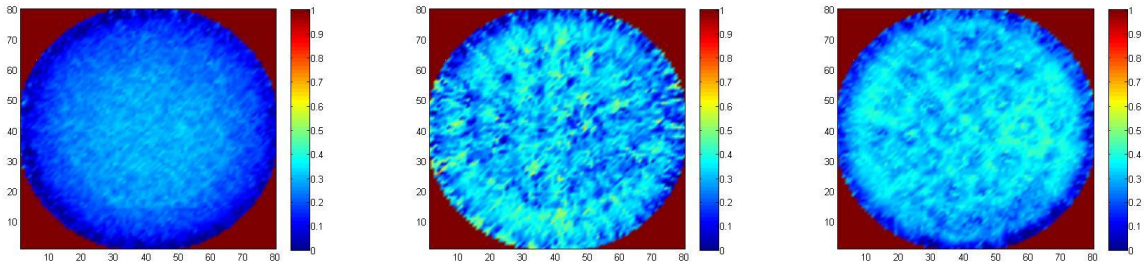

Figure A.1. Effect of Internals' Material on Time-Averaged, Cross-Sectional Gas Distribution at Superficial Gas Velocity of 8 cm/s Based on Free CSA

Plexiglas internals contributed to a higher percentage value of gas holdup than stainless steel internals along the radial position, except at the region close to the column wall because of the lack of internals near the wall (Figure A.3). For instance, at r/R≈ 0, the difference obtained with internals, which is based on the gas holdup magnitude in the empty column, was 9.5% and 19% for steel and Plexiglas internals, respectively, but only

6.6% for steel and 6% for Plexiglas near the wall. This result can be attributed to the flexibility of the Plexiglas internals, which allows bubbles to break up and change their size as they rise (Balamurugan et al., 2010); this result should be examined using a four-point optical probe. Moreover, in both cases, the radial gas holdup profile took on a wavy shape due to the dense internals. To some extent, the steepness of the profiles in the presence of internals is less than that obtained in columns without internals at low superficial gas velocity.

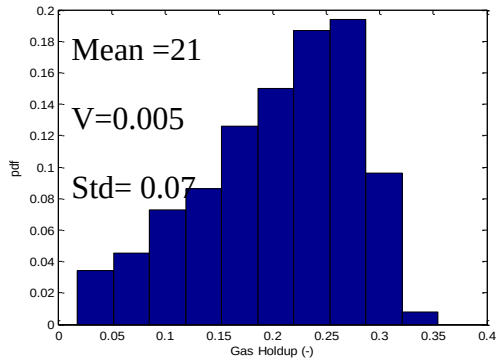

a) 8 cm/s (No internals)

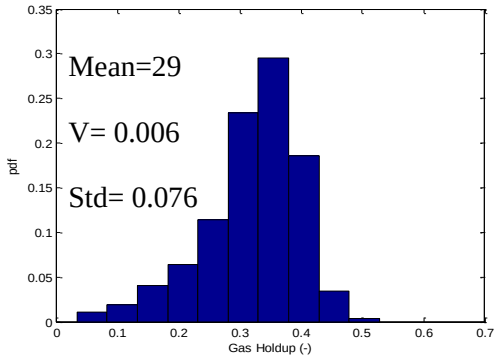

b) 8 cm/s based on free CSA (Plexiglas)

Figure A.2. Comparison of Probability Density Functions of the Values of Gas Holdup Distribution in the Pixel Cells in the Presence and Absence of Internals at 8 cm/s Based on Free CSA

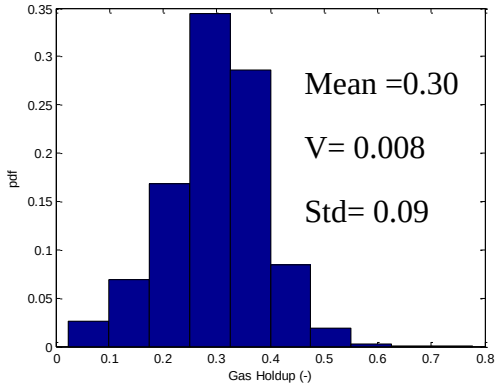

c) 8 cm/s based on free CSA (steel)

Figure A.2. Comparison of Probability Density Functions of the Values of Gas Holdup Distribution in the Pixel Cells in the Presence and Absence of Internals at 8 cm/s Based on Free CSA (cont.)

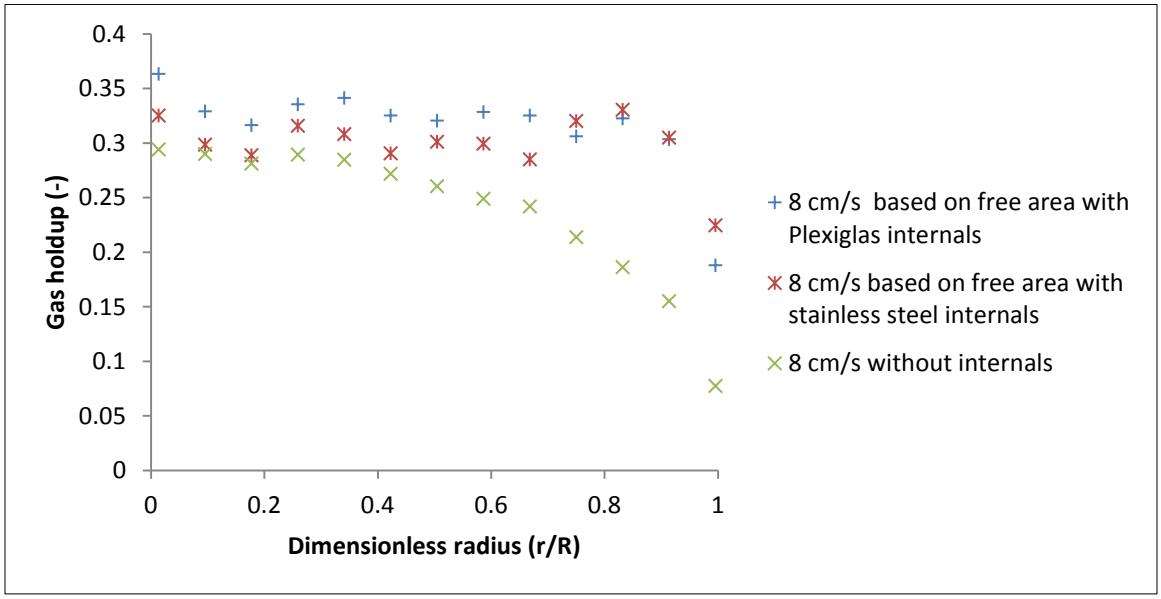

Figure A.3. Comparison of the Effect of Internals' Material on Radial Gas Holdup Profiles at Superficial Gas Velocity of 8 cm/s Based on Free CSA

Figure A.4 depicts the effect of the type of internal on the radial gas holdup profiles at a gas velocity of 45cm/s based on the total and free CSA. Figure A.4. clearly shows that the magnitude values of gas holdup in both Plexiglas and steel internals considering gas velocity based on either the total or free CSA are very close at $r/R \geq 6$, where less attenuation occurs, but very different in the central region of the column, where high attenuation occurs. This difference could be due to error caused by high attenuation (low signal to noise ratio) associated with stainless steel. Therefore, the effect of stainless steel rods still needs to be further assessed in the future.

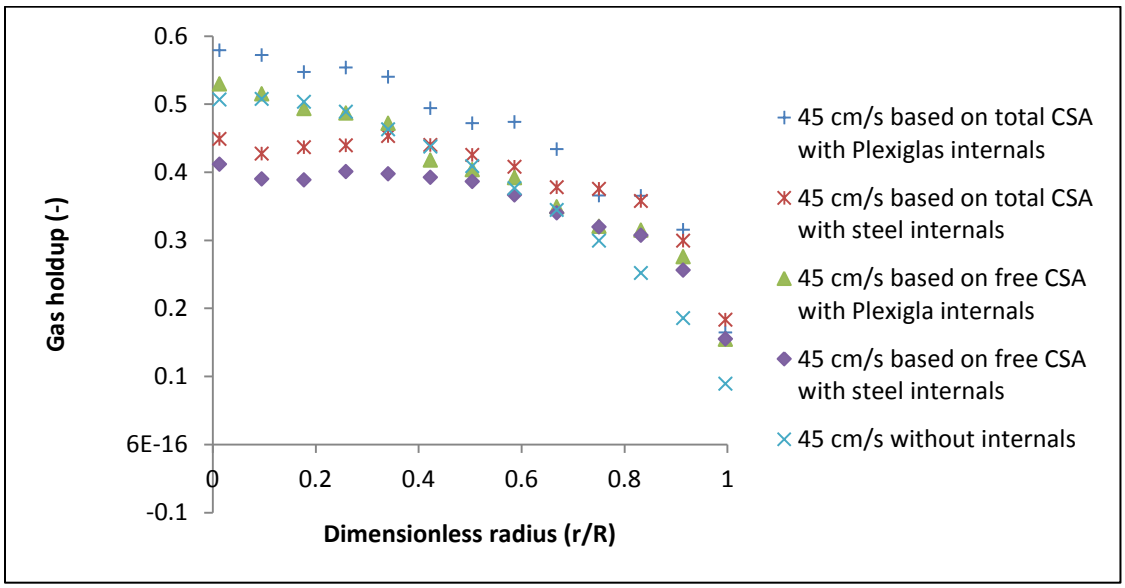

Figure A.4. Comparison of the Effect of Internals' Material on Radial Gas Holdup Profile at Superficial Gas Velocity of 45 cm/s Based on Both Total and Free CSA

Figure A.5 shows a comparison between the effects of the internals' material type on the radial gas holdup profile at different superficial gas velocities based on the free CSA.

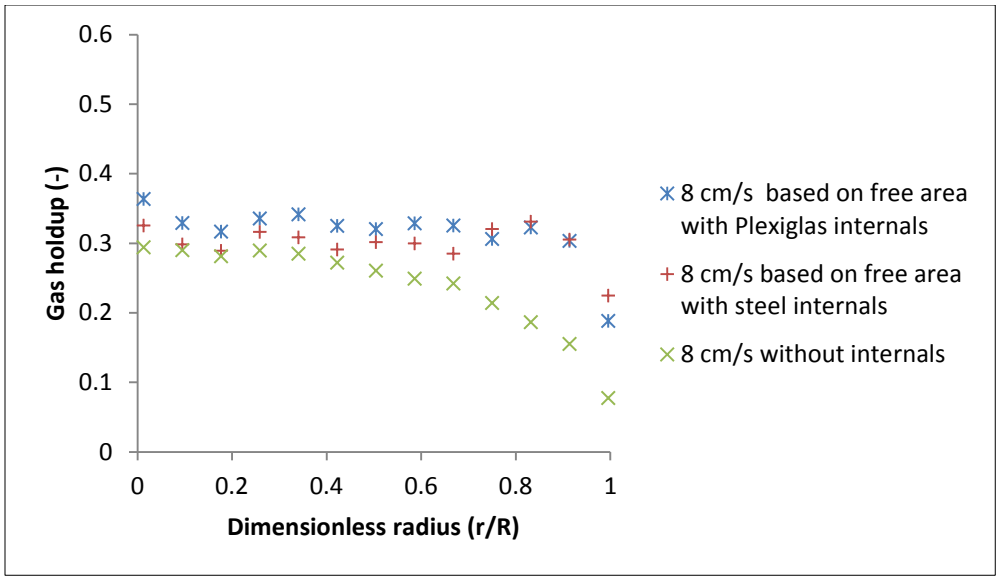

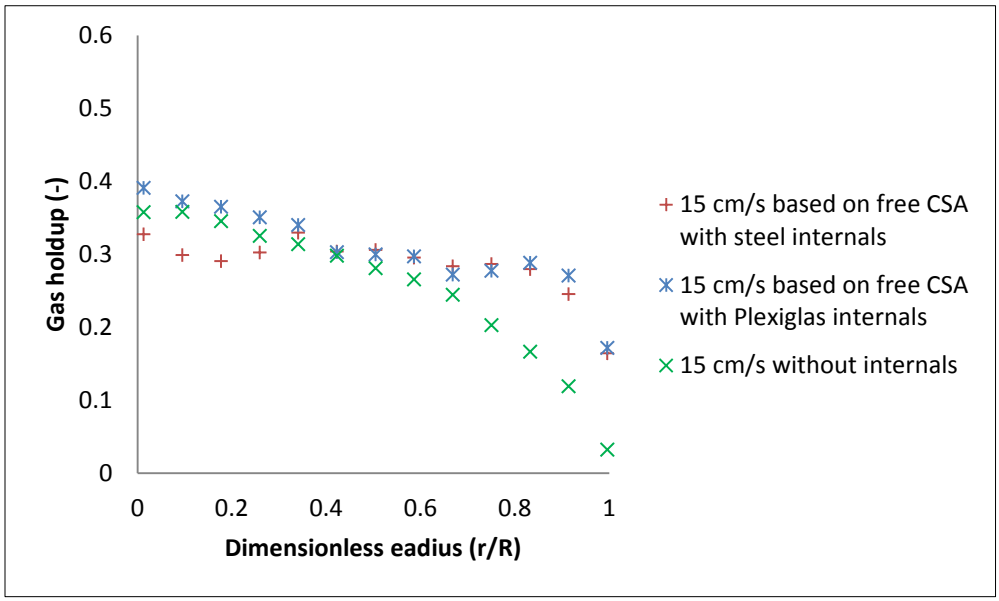

Figure A.5. Comparison between the Effects of Internal Material on Radial Gas Holdup Profile at Different Superficial Gas Velocities Based on Free CSA

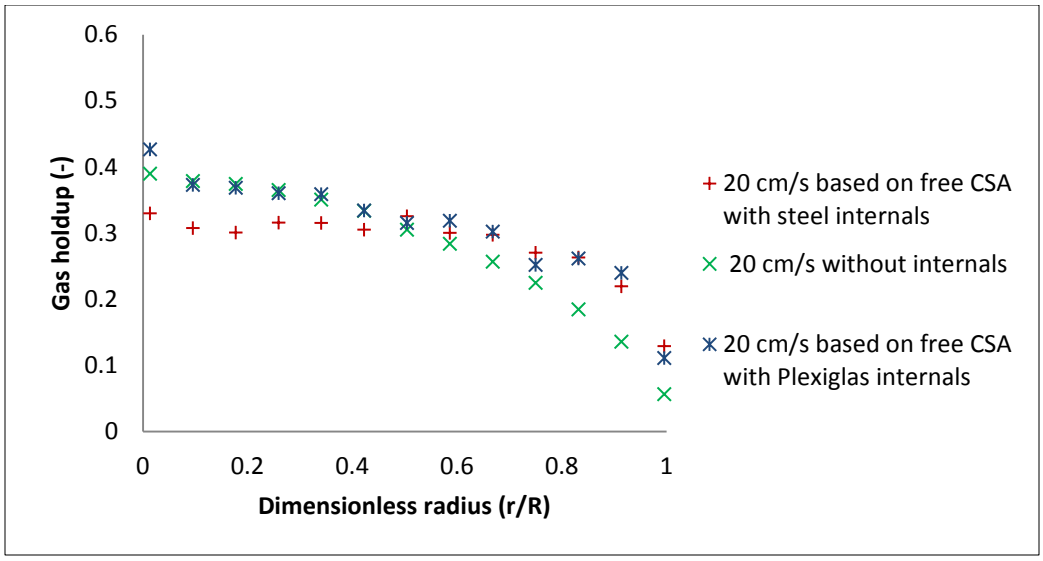

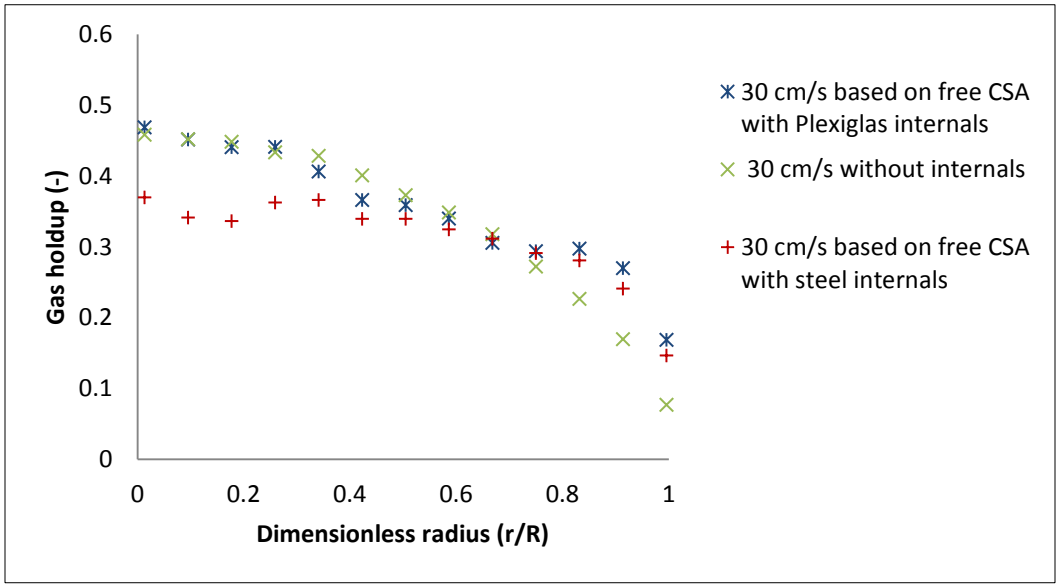

Figure A.5. Comparison between the Effects of Internal Material on Radial Gas Holdup Profile at Different Superficial Gas Velocities Based on Free CSA (cont.)

APPENDIX B

FOUR-POINT OPTICAL PROBE

The four-point optical probe was first developed by Frijlink (1987) and then further refined by Xue (2004) and Xue et al. (2008). The probe is only briefly described here because the exact details have been provided in those previously published studies.

The four-point optical probe is a very good technique that provides important information about the bubble characteristics (local gas holdup, specific interfacial area, bubble velocity, bubble chord length, etc.) in a given system.

The configuration of the four-point probe is shown in Figure B1. It consists of four tips; three tips form a triangle, and the fourth tip, which is longer than the other three, is located in the center of the triangle.

(a) Microphotograph showing side view of the four-point probe

(b) Microphotograph showing bottom view of the four-point probe

Figure B1. Configuration of the Four-Point Optical Probe (Xue, 2004)

A laser beam is sent from a Light Emitting Diode (LED) through the optical fibers; when the optical fibers are immersed in the dynamic system and hit a bubble, the

light is reflected back into the fiber. The light signals are collected via data acquisition and converted into voltage signals. The voltage is high when the bubbles hit the probe and low when the probe is in the liquid phase. By using the modified algorithm developed by Xue et al. (2003) and Xue (2004), the signal processing gives the local gas holdup, bubble chord length, gas-liquid interfacial area, bubble velocity and bubble frequency values. More details on the optical probe can be found elsewhere (Xue, 2004).

BIBLIOGRAPHY

Abdulmohsin, RS, Abid, BA, Al-Dahhan, MH. Heat transfer study in a pilot-plant scale bubble column. Chemical Engineering Research and Design, Vol 89, pp. 78-84, 2011.

Akita, K, Yoshida, F. Gas holdup and volumetric mass transfer coefficient in bubble columns: Effects of liquid properties. Industrial & Engineering Chemistry Process Design and Development, Vol 12(1), pp. 76-80, 1973.

Balamurugan, V, Subbarao, D, Shantanu Roy. Enhancement in gas holdup in bubble columns through use of vibrating internals. The Canadian Journal of Chemical Engineering, Vol 88, pp. 1010-1020, 2010.

Behkish, A, Men, Z, Morsi, BI. Hydrodynamics of CO and H_2 in a slurry bubble column reactor with paraffin oil. Proceedings - Annual International Pittsburgh Coal Conference, 17th, pp. 2268-2287, 2000.

Bhusarapu, SB. Solids flow mapping in gas-solids risers. D.Sc. Thesis. Department of Chemical Engineering, Washington University, St. Louis, 2005.

Bouaifi, M, Hebrard, G, Bastoul, D, and Roustan, M. A comparative study of gas hold-up, bubble size, interfacial area and mass transfer coefficients in stirred gas-liquid reactors and bubble columns. Chemical Engineering and Processing, Vol 40, pp. 97-111, 2001.

Boutet C, Larachi F, Dromard N, Delsart O, Beliard PE, Schweich D. CFD simulations of hydrodynamic/thermal coupling phenomena in a bubble column with internals. AIChE Journal, Vol 56(9), pp. 2397-2411, 2010.

Chen, RC, Reese, J, Fan, L-S. Flow structure in a three-dimensional bubble column and three-phase fluidized bed. AIChE Journal, Vol 40(7), p. 1093, 1994.

Chen, J, Gupta, P, Degaleesan, S, Al-Dahhan, MH, Dudukovic', MP, Toseland, BA. Gas holdup distribution in large diameter bubble columns measured by computed tomography. Flow Measurement and Instrumentation, Vol 9, pp. 91-101, 1998.

Chen, W, Hasegawa, T, Tsutsumi, A, Otawara, K, Shigaki, Y. Generalized dynamic modeling of local heat transfer in bubble columns, Chem. Eng. Journal, Vol 96, pp. 37-44, 2003.

Chen, J, Li, F, Degaleesan, S, Gupta, P, Al-Dahhan, MH, Dudukovic, MP, Toseland, BA. Fluid dynamic parameters in bubble columns with internals. Chemical Engineering Science, Vol 54(13-14), pp. 2187-2197, 1999.

Csiszár I. Why least squares and maximum entropy? An axiomatic approach to inference for linear inverse problems. Annals of Statistics, Vol 19, pp. 2033-2066, 1991.

De, SK, Ghosh, S, Parichha, RK, De, P. Gas hold-up in two phase system with internals. Indian Chem. Engr. Section A, Vol 41(2), pp. T54-T58, 1999.

Deckwer, WD. Bubble column reactors, John Wiley & Sons, 1992.

Deckwer, WD, Schumpe, A. Improved tools for bubble column reactor design and scale-up. Chemical Engineering Science, Vol 48, pp. 889-911, 1993.

Degaleesan, S. Turbulence and liquid mixing in bubble columns, Ph.D. Thesis, Washington University, Saint Louis, Missouri, USA, 1997.

Degaleesan, S, Dudukovic', MP, Pan, Y. Application of wavelet filtering to the radioactive particle tracking technique. Flow Measurement and Instrumentation, Vol 13(1-2), pp. 31-43, 2002.

Degaleesan, S, Dudukovic, MP, Pan, Y. Experimental study of gas induced liquid-flow structures in bubble columns, AIChE J., Vol 47, pp. 1913–1931, 2001.

Devanathan, N, Moslemian, D, Dudukovic', MP. Flow mapping in bubble columns using CARPT. 1990. Where did you find this paper? Journal title is missing.

Devanathan, N. Investigation of liquid hydrodynamics in bubble columns via a computer automated radioactive particle tracking (CARPT), Ph.D. Thesis, Washington University, Saint Louis, Missouri, USA, 1991.

Duduković, MP, Larachi, F, Mills, PL. Multiphase catalytic reactors: A perspective on current knowledge and future trends. Catalysis Reviews, Vol 44, pp. 123-246, 2002.

Ekambara, K, Dhotre, MT, Joshi, JB. CFD simulations of bubble column reactors: 1D, 2D and 3D approach. Chemical Engineering Science, Vol 60, pp. 6733–6746, 2005.

Fair, JR, Lambright, AJ, Anderson, JW. Heat transfer and gas holdup in a sparged contactor. I & EC Process Design and Development, Vol 1, pp. 33-36, 1962.

Fan, L-S. Gas-liquid-solid fluidization engineering. Butterworth Series in Chemical Engineering, Boston, MA, 1989.

Forret, A, Schweitzer, JM, Gauthier, T, Krishna, R, Schweich, D. Liquid dispersion in large diameter bubble columns with and without internals. The Canadian Journal of Chemical Engineering, Vol 81, pp. 360–366, 2003.

Frijlink, JJ. Physical aspects of gassed suspension reactors, Ph.D. Thesis, Delft University of Technology, The Netherlands, 1987.

Hamed, M. Hydrodynamic, mixing, and mass transfer bubble columns with internals. Ph.D. Thesis, Washington University in St. Louis, Saint Louis, Mo, USA, 2012.

Han, L. Hydrodynamics, back-mixing, and mass transfer in a slurry bubble column reactor for Fischer-Tropsch alternative fuels. D.Sc. Thesis, Washington University in St. Louis, Saint Louis, Mo, USA, 2007.

Hills, JH. Radial non-uniformity of velocity and voidage in a bubble column. Transactions of the Institution of Chemical Engineers, Vol 52, pp. 1–9, 1974.

Hyndman CL, Larachi F, Guy C. Understanding gas-phase hydrodynamics in bubble columns: A convective model based on kinetic theory. Chem Eng Sci, Vol 52, pp. 63–77, 1997.

Idogawa, K, Ikeda, K, Fukuda, T, Morooka, S. Behavior of bubbles of the air-water system in a column under high pressure. International Chemical Engineering, Vol 26(3), pp. 468-474, 1986.

Jhawar, AK. Effects of internal on local heat transfer and column hydrodynamics in bubble columns. Thesis, PhD, University of Western Ontario, London, Ontario, 2011.

Jiang, P, Lin, TJ, Luo, X, Fan, LS. Flow visualization of high-pressure (21MPa) bubble column: Bubble characteristics. Trans IChemE, Vol 73, Part A, pp. 269-274, 1995.

Joshi, J, Sharma, M. A circulation cell model for bubble columns. Trans. Inst. Chem. Eng., Vol 57, pp. 244-251, 1979.

Joshi, JB, Veera, UP, Prasad, CV, Phanikumar, DV, Deshphande, NS, Thakre, SS, Thorat, BN. Gas holdup structure in bubble column reactors. PINSA-A, Proc. Indian Natl. Sci. Acad., Part A, Vol 64(14), p. 441, 1998.

Joshi, R, Majumder, SK. CFD simulation of hydrodynamics of bubbly flow in bubble column. Journal of Engineering and Applied Sciences, Vol 6(1), pp. 47-57, 2011.

Kantarci, N, Borak, F, Ulgen, K. Bubble column reactors. Process Biochemistry, Vol 40, pp. 2263-2283, 2005.

Kondukov, NB, Kornilaev, AN, Skachko, IM, Akhromenkov, AA, Kurglov, AS. An investigation of the parameters of moving particles in a fluidized bed by a radioisotope method. Int. Chem. Eng., Vol 4, pp. 43-47, 1964.

Krishna, R, Wilkinson, PM, Van Dierendonck, LL. A model for gas holdup in bubble columns incorporating the influence of gas density on flow regime transitions. Chemical Engineering Science, Vol 46(10), p. 2491, 1991.

Krishna, R, de Swart, JWA, Hennephof, DE, Ellenberger, J, Hoefsloot, HC. Influence of increased gas density on hydrodynamics of bubble column reactors. AIChE J, Vol 40(1), pp. 112-119, 1994.

Krishna, R, Ellenberger, J. Gas hold-up in bubble column reactors operating in the churn-turbulent flow regime. American Institute of Chemical Engineers Journal, Vol 42, pp. 2627-2634, 1996.

Krishna, R, de Swart, JWA, Ellenberger, J, Martina, GB, Maretto, C. Gas holdup in slurry bubble columns: Effect of column diameter and slurry concentrations. AIChE J, Vol 43, p. 311, 1997.

Krishna, R. A Scale-up strategy for a commercial scale bubble column slurry reactor for Fischer-Tropsch synthesis. Oil & Gas Science and Technology, Vol 55(4), pp. 359-393, 2000.

Krishna, R, Sie, ST. Design and scale-up of the Fischer-Tropsch bubble column slurry reactor. Fuel Processing Technology, Vol 64(1-3), pp. 73-105, 2000.

Krishna, R, van Baten, JM, Urseanu, MI, Ellenberger, J. Design and scale-up of the bubble column slurry reactor for Fischer-Tropsch synthesis, Chem. Eng. Sci., Vol 56, p. 537, 2001.

Krishna, R, van Baten, JM. A strategy for scaling up the Fischer-Tropsch bubble column slurry reactor. Topics in Catalysis, Vol 26(1-4), pp. 21-28, 2003.

Kumar, SB, Devanathan, N, Moslemian, D, Dudukovic', MP. Effect of scale on liquid recirculation in bubble columns. Chem. Eng. Sci., Vol 49(24B), pp. 5637-5652, 1994.

Kumar, SB. Computed tomographic measurements of void fraction and modeling of the flow in bubble columns, Ph.D. Thesis, Florida Atlantic University, 1994.

Kumar, SB, Moslemian, D, Dudukovic', MP. Gas holdup measurements in bubble columns using computed tomography. AIChE J, Vol 43(6), pp. 1414-1425, 1997.

Larachi, F, Desvigne, D, Donnat, L, Schweich, D. Simulating the effects of liquid circulation in bubble columns with internals. Chemical Engineering Science, Vol 61(13), pp. 4195-4206, 2006.

Li, H. Heat transfer and hydrodynamics in a three-phase slurry bubble column. Thesis, PhD, University of Western Ontario, London, Ontario, 1998.

Lin, T-J, Tsuchiya, K, Fan, L-S. Bubble flow characteristics in bubble columns at elevated pressure and temperature. AIChE J, Vol 44(3), pp. 545-560, 1998.

Lefebvre, S, Guy, C. Characterization of bubble column hydrodynamics with local measurements. Chem Eng Sci, Vol 54, pp. 4895–902, 1999.

Luo, X, Lee, DJ, Lau, R, Yang, G, Fan, L-S. Maximum stable bubble size and gas holdup in high-pressure slurry bubble columns. AIChE J, Vol 45(4), pp. 655-680, 1999.

Menzel, T, in der Weide, T, Staudacher, O, Wein, O, Onken, U. Reynolds shear stress for modeling of bubble column reactors. Ind. Eng. Chem. Res., Vol 29, pp. 988-994, 1990.

Mudde, RF, Groen, JS, Van Den Akker, HEA. Liquid velocity field in a bubble column: LDA experiments. Chem. Eng. Sci., Vol 52(21/22), pp. 4217-4224, 1997.

O'Sullivan, JA, Benac, J. Alternating minimization algorithms for transmission tomography. Medical Imaging, IEEE Transaction on, Vol 26(3), pp. 283-297, 2007.

Ong, B. Experimental investigation of bubble column hydrodynamics - Effect of elevated pressure and superficial gas velocity. D. Sc. Thesis. Department of Chemical Engineering, Washington University, St. Louis, MO, USA, 2003.

Oyevaar, MH, De la Rie, T, Van der Sluijs, CL, Westerterp, KR. Interfacial areas and gas holdups in bubble columns and packed bubble columns at elevated pressures. Chem. Eng. Process., Vol 26, pp. 1-14, 1989.

Pino LZ, Solari RB, Siuier S, Estevez LA, Yepez MM, Saez AE. Effect of operating conditions on gas holdup in slurry bubble columns with a foaming liquid. Chem Eng Commun, Vol 117, pp. 367–82, 1992.

Prakash, A, Margaritis, A, Li, H, Bergougnou, MA. Hydrodynamics and local heat transfer measurements in a bubble column with suspension of yeast. Biochemical Engineering Journal, Vol 9, pp. 155-163, 2001.

Prakash, A, Margaritis, A, Saunders, RC, Vijayan, S. Ammonia removal at high concentrations by the cyanobacterium plectonema boryanum in aphotobioreactor system. Canadian Journal of Chemical Engineering, Vol 77, pp. 99-106, 1999.

Pradhan, A, Parichia, A, De, P. Gas hold-up in non-Newtonian solutions in a bubble column with internals. The Canadian Journal of Chemical Engineering, Vol 71, pp. 468-471, 1993.

Rados, N. Slurry bubble column hydrodynamics. D. Sc. Thesis. Department of Chemical Engineering, Washington University, St. Louis, MO, USA, 2003.

Rampure, MR, Buwa, VV, Ranade, VV. Modelling of gas–liquid/ gas– liquid–solid flows in bubble columns: Experiments and CFD simulations. The Canadian Journal of Chemical Engineering, Vol 81, pp. 692-706, 2003.

Reilly, IG, Scott, DS, De Bruijn, TJW, MacIntyre, D. The role of gas phase momentum in determining gas holdup and hydrodynamic flow regimes in bubble column operation. Can. J. Chem. Eng., Vol 72, p. 3, 1994.

Roy NK, Guha DK, Rao MN. Fractional gas holdup in two-phase and three-phase batch-fluidized bubble-bed and foam-systems. Indian Chem Eng, pp. 27–31, 1963.

Roy, S. Quantification of two-phase flow in liquid-solid risers. D.Sc. Thesis, Washington University, St. Louis, MO, 2001.

Saxena, SC, Rao, NS, Saxena, AC. Estimation of heat transfer coefficient for immersed surfaces in bubble columns involving fine powders. Powder Technology, Vol 63(2), pp. 197-202, 1990.

Saxena, SC, Rao, NS, Thimmapuram, PR. Gas phase holdup in slurry bubble columns for two- and three-phase systems. Chemical Engineering Journal, Vol 49(3), pp. 151-159, 1992.

Saxena, SC. A novel heat exchanger design for slurry bubble columns. Transp. Phenom. Therm. Eng., Proc. Int. Symp., Vol 6, pp. 896-901, 1993.

Saxena, SC, Rao, NS. Estimation of gas holdup in a slurry bubble column with internals: Nitrogen–therminol–magnetite system. Powder Technology, Vol 75, pp. 153–158, 1993.

Saxena, SC. Bubble column reactors and Fischer-Tropsch synthesis. Catal. Rev.-Sci.Eng., Vol 37(2), pp. 227-309, 1995.

Schluter, S, Steiff, A, Weinspach, P-M. Heat transfer in two- and three-phase bubble column reactors with internals. Chemical Engineering and Processing, Vol 34(3), pp. 157-172, 1995.

Shah, YT, Ratway, CA, Mcilvried, HG. Back-mixing characteristics of a bubble column with vertically suspended tubes. Transactions of the Institution of Chemical Engineers, Vol 56(2), pp. 107-112, 1978.

Shah, YT, Kelkar, BG, Godbole, SP, Deckwer, WD. Design parameters estimations for bubble column reactors. AIChE J, Vol 28(3), p. 353, 1982.

Shaikh, A, Al-Dahhan, M. Characterization of the hydrodynamic flow regime in bubble columns via computed tomography. Flow Measurement and Instrumentation, Vol 16(2-3), pp. 91-98, 2005.

Shaikh, A, Al-Dahhan, MH. A review on flow regime transition in bubble columns. International Journal of Chemical Reactor Engineering, Vol 5, p. 155, 2007.

Shaikh, A. Bubble and slurry bubble column reactors for syngas to liquid fuel conversion: Mixing, flow regime transition, and scale-up, D.Sc. Thesis, Washington University in St. Louis, Saint Louis, MO, USA, 2007.

van Baten, JM, Krishna, R. CFD simulations of a bubble column operating in the homogeneous and heterogeneous flow regimes. Chemical Engineering and Technology, Vol 25, pp. 1081-1086, 2002.

Varma R, Al-Dahhan M. Effect of sparger design on hydrodynamics of a gas recirculation anaerobic bioreactor. Biotechnology and Bioengineering, Vol 98(6), pp. 1146-1160, 2007.

Varma R, Bhusarapu S, O'Sullivan JA, Al-Dahhan MH. A comparison of alternating minimization and expectation maximization algorithms for single source gamma ray tomography. Measurement Science & Technology, Vol 19(1):015506, 14pp, 2008.

Varma R. Characterization of anaerobic bioreactors for bioenergy generation using a novel tomography technique, Ph.D. Thesis, Washington University in St. Louis, Saint Louis, Mo, USA, 2008.

Vial, C, Camarasa, E, Poncin, S, Wild, G, Midoux, N, Bouillard, J. Study of hydrodynamic behavior in bubble columns and external loop airlift reactors through analysis of pressure fluctuations. Chem. Eng. Sci., Vol 55, pp. 2957-2973, 2000.

Wang S, Arimatsu Y, Koumatsu K, Furumato K, Yoshimato M, Fukunaga K, et al. Gas holdup, liquid circulating velocity and mass transfer properties in a mini-scale external loop airlift bubble column, 2003. Where did you find this? The journal information is missing.

Wilkinson, PM, Spek, AP, Van Dierendonck, LL. Design parameters estimation for scale-up of high-pressure bubble columns. AIChE J, Vol 38(4), pp. 544-554, 1992.

Wu, C. Heat transfer and bubble dynamics in slurry bubble columns for Fischer-Tropsch clean alternative energy. Ph.D. Thesis, Washington University in St. Louis, Saint Louis, MO, USA, 2007.

Wu, Y, Al-Dahhan, MH. Prediction of axial liquid velocity profile in bubble columns. Chem. Eng. Sci., Vol 56, pp. 1127-1130, 2001.

Wu, Y, Ong, BC, Al-Dahhan, MH. Predictions of radial gas holdup profiles in bubble column reactors. Chemical Engineering Science, Vol 56(3), pp. 1207-1210, 2001.

Wu, C, Suddard, K, Al-Dahhan, M. Bubble dynamics investigation in a slurry bubble column, Title of journal? Vol 54(5), pp. 1203-1212, 2008.

Xue, J. Bubble velocity, size, and interfacial area measurements in bubble columns. D.Sc. Thesis, Washington University, St. Louis, MO, 2004.

Xue, J, Al-Dahhan, M, Dudukovic, MP, Mudde, RF. Bubble velocity, size, and interfacial area measurements in a bubble column by four-point optical probe. AIChE J, Vol 54(2), pp. 350-363, 2008.

Xue, J, Al-Dahhan, M, Dudukovic, MP, Mudde, RF. Bubble dynamics measurements using four-point optical probe. The Canadian Journal of Chemical Engineering, Vol 81, pp. 1-7, 2003.

Yamashita F. Effects of vertical pipe and rod internals on gas holdup in bubble columns. Journal of Chemical Engineering of Japan, Vol 20(2), pp. 204-206, 1987.

Youssef, AA, Al-Dahhan, MH. Impact of internals on the gas holdup and bubble properties of a bubble column. Industrial and Engineering Chemistry Research. Vol 48, pp. 8007-8013, 2009.

Youssef, AA. Fluid dynamics and bubble columns with internals. Ph.D. Thesis, Washington University in St. Louis, Saint Louis, Mo, USA, 2010.

Zahradnik, J, Kastanek, F, Kratochvil, J. 1982. Hydrodynamics and mass transfer in uniformly aerated bubble column reactors. Collection Czechoslovak Chem. Commun., Vol 47, p. 262, 1982.

Zehner, P. Momentum, mass, and heat transfer in bubble columns. Flow model of bubble columns and liquid velocity. Institution of Chemical Engineers Symposium Series, Vol 26(22-35), pp. 347-351, 1982.

VITA

Mohammed Khloofah Al Mesfer was born in Abha, Saudi Arabia, on July 12, 1977. He received his B.S. and M.S. in Chemical Engineering in May 2000 and May 2006, respectively, from King Saud University, Riyadh, Saudi Arabia. He worked in the education field for almost nine years before joining the Missouri University of Science and Technology, Rolla, Missouri, USA, where he earned his Ph.D. in Chemical Engineering in May 2013.

Mohammed Al Mesfer has been a member of the American Institute of Chemical Engineers since 2009. He has attended several conferences related to his research interests and published two conference papers; additionally, three journal papers have been submitted and currently are in process. His research interests involve hydrodynamics in multiphase systems.